08/09/2024
University of Wales Trinity Saint David - School of Engineering.

Measurement and Analysis of Rider Input and Motorcycle Response in High-Performance Environments

Master's Project (ACFA7003)

2023 - 2024

Figure 1: UWTSD's RS660 Measurement Platform & RS660.

Ilias Gideon Iatrakis (2011922)

Supervisor: Andrew Harrison

Declaration Sheet

This work has not previously been accepted in substance for any degree and is not being concurrently submitted in candidature for any degree.

Signed: *Iatrakis Gideon Ilias* Date: *08/09/2024*

This thesis is the result of my own investigations, except where otherwise stated. Where correction services have been used the extent and nature of the correction is clearly marked in a footnote(s). Other sources are acknowledged by the Harvard citation style giving explicit references. A bibliography is appended.

Signed: *Iatrakis Gideon Ilias* Date: *08/09/2024*

I hereby give consent for my thesis, if accepted, to be available for photocopying and for inter-library loan, and for the title and summary to be made available to outside organisations.

Signed: *Iatrakis Gideon Ilias* Date: *08/09/2024*

I hereby give consent for my thesis, if accepted, to be available for deposit in the University’s digital repository.

Signed: *Iatrakis Gideon Ilias* Date: *08/09/2024*

Acknowledgements

I would like the following people:

- lecturer and thesis supervisor, Andrew Harrison, for his unwavering support and invaluable guidance throughout the course of this project. His assistance has been instrumental in its successful completion.

- I would like to express my deep gratitude to Dr. Owen Williams, Director of Motorcycle Engineering, for his continuous guidance and support, both technical and personal, over the past years. Since joining the university as a 17-year-old, his mentorship has been invaluable in my development.

- I would like to particularly thank my parents, Carine Valkeneers and Evaggelos Iatrakis, for their unwavering support and tireless efforts in helping me throughout my academic and personal journey. Offering me many opportunities and freedom to develop my young self. Their guidance, encouragement, and sacrifice have been invaluable to me throughout my studies and upbringing.

- My classmate and friend Jacob Quarry for the help, ideas, elevating work spirits and good company throughout our time here at UWTSD.

- All the workshop technicians in the UWTSD Engineering department for the continuous technical support and help throughout the project in order to realise this.

- My friends Benjamin Hilton, Brody Crockford, Lewis Cox, Michael Charity, Max McGowanBunting, Dylan Arthur, Evan Arthur for the help, good times and a lot of fun at all times.

- Sophia-Anna Chardavoine for her unwavering love, support and assistance in my academic and personal life, even from afar.

- Werner Daemen, BMW Motorrad EWC & IDM Team Manager, for providing me with the invaluable opportunity to work and learn at a professional motorsport level. His support, guidance, and technical resources over the past year have been instrumental, and I am grateful for the chance to be part of such an enjoyable and high-performing team.

Abstract

This thesis presents the development and validation of a novel rider input measurement platform designed to capture and analyse key rider inputs, including handlebar forces, footpeg inputs, and steering torque, to better understand rider and motorcycle behaviour in high-performance settings. The project aimed to provide insights into the relationship between rider inputs and motorcycle response, enabling a comparison of how different riders apply forces and control their motorcycles during high-speed riding.

The study builds on the foundational work by (Przibylla 2020) and confirms several of his findings, particularly the transient effects influencing steering torque. However, this research also challenges traditional views, especially regarding the role of footpeg inputs in steering. The data confirms that counter-steering through the handlebars remains the primary input for directional changes, while footpeg forces are suspected to mainly serve to brace the rider's body during cornering and braking. The analysis revealed that experienced riders use their body weight and footpeg forces more effectively, optimising their performance by distributing weight efficiently and minimising upper body strain.

The platform was tested with riders of varying skill levels, highlighting the differences in their ability to manage steering torque, body positioning, and throttle and brake inputs. These findings suggest that the system can be a valuable tool for rider comparison and performance analysis, offering objective, quantitative data for improving riding techniques.

Despite some technical challenges, the platform demonstrated great potential for future rider analysis and training. Recommendations for further development include refining the system's data logging capabilities and expanding testing with a broader range of riders, including professional racers.

1 Contents

2 List of Figures

3 List of Tables

4 Introduction

This thesis presents the development of a rider input measurement system for motorcycles and explores its potential for enhancing the understanding of high-performance riding and rider inputs.

Motorcycles evoke a passion in many, offering a thrilling and sometimes daunting experience that stimulates the senses. For enthusiasts, high-performance track riding is more than just a hobby; it's a pursuit of speed, skill, and precision. For some, it's a profession focused on pushing the limits of both rider and machine. The development of motorcycles and the quest for increased speed and control is a field of constant evolution, driven by both technological advancements and the quest to understand motorcycle dynamics more deeply.

Motorcycle dynamics, while a subject of research for decades, remain complex and often misunderstood. Unlike the automotive world, where vehicle dynamics are extensively studied, motorcycles present unique challenges due to their freedom of movement and the significant influence of the rider (Cossalter 2006). Despite this, the basic principles of motorcycle dynamics have been established through the work of pioneers in the field. However, the subtleties of rider input and its effects on motorcycle behaviour, particularly at the highest levels of performance, are less well understood.

Riding schools and coaches have long focused on improving rider technique, and while the basics of riding techniques for going fast can be taught, there remains a small percentage of elite riders—often referred to as "aliens"—who seem to transcend conventional understanding. These riders can extract performance from their machines that others cannot, often through techniques that are difficult to quantify or replicate (Bom 2024).

In motorcycle racing, data systems have become increasingly sophisticated, monitoring an array of parameters to understand what the motorcycle is doing at every point on the track (Spalding 2010). However, there remains a gap in understanding exactly how rider inputs lead to these outcomes. While throttle, braking, and clutch usage are monitored, the mechanics behind steering and other critical inputs are less often measured and analysed.

This thesis aims to lay the groundwork for further research into rider inputs by developing a system that can measure how riders use their bodies to influence motorcycle performance. The goal is to provide insights that can help riders improve their technique, identify areas where they can extract more from their machines, and understand the differences between top riders and those who are nearly as fast but not quite at the same level.

A key motivation for this project is the need to validate common beliefs about motorcycle riding techniques, such as the idea that riders can steer at high speed using pressure on the footpegs (Bradley 2014; Moss 2019). The proposed measurement system seeks to provide concrete data to either support or refute such claims.

The author's passion for motorcycles, racing, and working with highly skilled riders is a driving force behind this project. This work is part of a larger effort to improve motorcycle performance, rider training, and ultimately, contribute to the advancement of the sport.

Fundamentally, there is limited research and literature available on motorcycle dynamics. The motorcycle industry is relatively small and niche compared to others, and the complexity of motorcycle dynamics presents unique challenges. These include the high degree of movement freedom, the significant influence of the rider on the bike's behaviour, and the lack of comparable research in other industries, especially when compared to cars, where dynamics and driver interaction are far less complex (Sharp et al. 2004).

The field of motorcycle dynamics and rider input has been explored in recent research, with significant contributions such as (Przibylla 2018) development of a steering torque measurement platform, and their subsequent analysis in 2020 on the physically applied steering torque (Przibylla 2020). These studies identified and assessed factors controlling dynamic behaviour and steering performance. (Bartolozzi et al. 2023b) introduced comprehensive input measurements using handlebars and Inertial Measurements in controlled tests to develop a steering torque model. (Bartolozzi et al. 2023a)continued this exploration by integrating input measurements from handlebars, footpegs, and seat to investigate the influence of different riding styles on motorcycle response, concluding that steering torque / countersteering is the primary steering input, whereas applying pressure on footpegs or shifting weight over the saddle has minimal effect.

The working hypothesis is that while riders are taught various body movements influence motorcycle steering, the effective control still primarily involves counter steering through the handlebars, potentially aided by different muscular engagements or body movements to facilitate this action. Along with the aim to investigate if systems like the proposed measurement system can be used to improve rider training, development.

5 Literature Review

5.1 Overview

The study of single-track vehicle dynamics dates back to the invention of the first bicycle in the 19th century. Comprehensive historical overviews of the literature on this subject are provided by (Schwab and Meijaard 2013) and (Kooijman and Schwab 2011), (Sharp 1978; Sharp 1985) offers motorcycle-specific reviews, albeit somewhat dated, that cover the prevailing dynamics theories and mathematical modelling capabilities of the time. These works discuss general steering behaviour, oscillatory disturbances observed at certain speeds and excitation frequencies in straight-line running, as well as the impact of motorcycle design and technology.

A more recent and comprehensive review of single-track vehicle modelling techniques and control considerations is presented by (Limebeer and Sharp 2006). Both authors have significantly contributed to the understanding of motorcycle dynamics through numerous publications, including (Sharp 1971; Sharp 1994; Limebeer et al. 2001; Sharp 2001; Sharp and Limebeer 2001; Sharp et al. 2004; Sharp 2010), which primarily focus on modelling motorcycle stability and control.

Another key source is the work by (Weir et al. 1979), which provides an in-depth presentation of the mathematical models and derivations foundational to the investigation of capsize, weave, and wobble modes, along with considerations of rider control and their implications for motorcycle handling.

5.2 Model Developments

Over the years, numerous theoretical models of bicycle and motorcycle dynamics have been developed at various universities, including those by (Koenen 1983; Giles 1985; Styles 2004; Rowell 2007; Ooms 2011). Key references in current literature include the books by (Foale 2002)and (Cossalter 2006). The latter, authored by one of the most prominent figures in motorcycle dynamics, Professor Vittore Cossalter, who held a chair in vehicle dynamics at the University of Padova, has been particularly influential. Much of the recent and significant research in this field has originated from his consortium at the University of Padova.

Examples of work include the development of sophisticated modelling techniques that leverage advanced computational methods and incorporate unique and complex multibody codes to simulate motorcycle dynamics. Notable examples include studies by (Cossalter et al. 1999; Cossalter and Lot 2002; Cossalter et al. 2004; Massaro and Lot 2007; Cossalter et al. 2011a; Massaro et al. 2012; Massaro et al. 2013). The multibody models developed at the University of Padova have also led to the creation of lap time simulators, such as 'FastBike,' presented by (Cossalter et al. 2003).

These simulators predict the fastest lap times a specific motorcycle model can achieve under predefined conditions by defining an ideal path within adjustable limits and computing its dynamic behaviour through multiple iterations. Such simulations are invaluable for assessing various design and setup configurations to achieve optimal performance, as demonstrated by (Cossalter et al. 2008;

Cossalter et al. 2013). As a result, lap time simulators are increasingly utilised by manufacturers and motorsport teams competing at the World Championship level.

5.3 Handling Analysis

The physical steering input required from a rider for a given manoeuvre and its interaction with the motorcycle's dynamic response has long been of great interest to researchers, manufacturers, and road traffic safety organisations. Following fundamental research on single-track vehicles in steady turning by (Fu 1966) and the subsequent derivation of a formula to calculate steering torque by (Sharp 1971), the evaluation of motorcycle design based on manoeuvrability, handling performance, and the definition of ideal handling qualities has been extensively studied.

The first evaluations of transient-state handling characteristics and the influence of different riding techniques were conducted as early as the mid-1970s. These studies employed datalogging and steering torque measurements on instrumented motorcycles during simple manoeuvres, such as lane changes and slalom tests. Early works by (Taguchi 1975) and (Rice 1979) reported experimentally acquired results, while a more comprehensive report for the U.S. Department of Transportation's National Highway Traffic Safety Administration (DOT) by (Rice and Kunkel 1976) also included simulated data. (Weir and Zellner 1978) took a similar approach, comparing recorded measurements to the results obtained from a linearised mathematical model. Their extensive investigations into motorcycle stability and the effects of design alterations, along with steering torque measurements, led to further reports for the DOT by (Weir et al. 1979) and considerations regarding handling test procedures by (Weir and Zellner 1980).

Practical research in this area was also conducted for Japanese motorcycle manufacturers by (Aoki 1980; Sugizaki and Hasegawa 1988; Kuroiwa et al. 1995). More recently, using much more advanced sensory equipment than was available in earlier studies, experimental transient-state validations of analytical transfer functions derived from (Sharp 1971) mathematical model and a computational multibody model by (Cossalter and Lot 2002) were performed at the University of Padova. These validations involved slalom manoeuvres at different speeds and cone spacings, as presented by (Biral et al. 2003). The authors reported a "fair to good agreement" between the calculated transfer functions from physical steering inputs and the resulting motorcycle response behaviour with the computed model predictions.

(Sharp 1971)' original equations of motion were later revised to include additional factors and improve accuracy, as seen in works by (Sharp 1994; Ueda 2004). Other mathematical models exploring rider-applied steering torque have also been developed, such as the analytical approach by (Cossalter et al. 1999) which describes the individual components of total steering torque in steady-state cornering. The nature of this overall steering torque and its constituents was further investigated, and the results were experimentally validated using data from multiple reference motorcycles in turns of varying radii and at different cornering speeds by (Cossalter et al. 2007; Cossalter et al. 2011b).

(Przibylla 2018) at the University of Wales Trinity Saint David developed a steering torque measurement platform, with subsequent analysis in 2020 on the physically applied steering torque and the transient effects that influence the steering torque of the rider (Przibylla 2020). These studies were fundamental in identifying and assessing factors controlling dynamic behaviour and steering performance during track riding, also confirming the relationship between counter steering and motorcycle response. The collected data was then used in order to further develop the equations derived by (Cossalter et al. 1999) for estimating steering torque. (Bartolozzi et al. 2023b) introduced input measurements using handlebars and Inertial Measurement Unit (IMU) recordings in controlled tests to develop a steering torque model. (Bartolozzi et al. 2023b) continued this exploration by integrating input measurements from handlebars, footpegs, and seat to investigate the influence of different riding styles on motorcycle response during controlled tests and manoeuvres, concluding that steering torque is the primary steering input, whereas applying pressure on footpegs or shifting weight over the saddle has minimal effect in exciting a motorcycle response and steering.

Despite extensive studies, there remains ambiguity in the racing community—including riders, engineers, and coaches—about the effective methods of steering a motorcycle. Conventional wisdom and prior research suggest that motorcycles are primarily controlled through the application of torque at the handlebars (Cossalter 2006). However, training methods still advocate for alternative steering methods, such as applying force on the footpegs or using body weight shifts, which have not proven effective as standalone steering techniques ((Bartolozzi et al. 2023a; Harrison 2023; Daemen 2024). This research aims to dissect these conventional teachings under dynamic, high-performance conditions to explore how the riders body might be utilised differently in motorcycle steering and to determine if alternative effective methods exist.

Countersteering can be described very simply as push right, go right, and push left, go left, at higher speeds. At lower speeds, below 15-19mph, depending on the motorcycle and it's rotating mass, gyroscopic effects. The motorcycle rides more like a bicycle, where the front tire is pointed in the direction desired to go(Parks 2015).

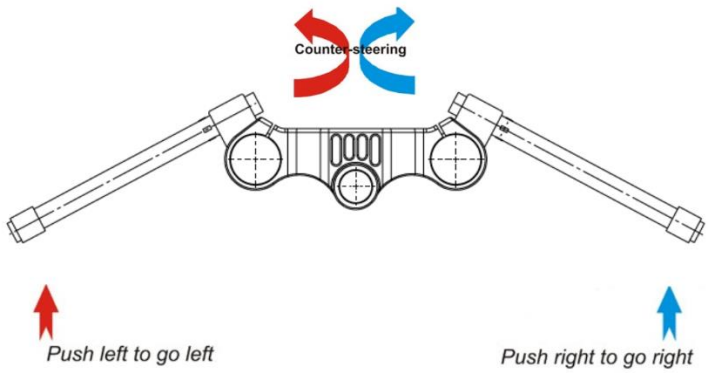

Figure 2: Countersteering Visual Representation.

Steering torque is the torque that is acting around the front assembly of a motorcycle and its steering head, where the magnitude of the torque that is applied

by the rider is equal to the resultant of all moments that are generated by the forces which are acting on the front section with either misaligning or aligning influence on the steering (Cossalter 2006). The centrifugal force of the front section, the lateral force on the front wheel and the gyroscopic effect of the front wheel are having an aligning influence for example, whilst the weight force of the front section, the normal load on the front wheel and the twisting torque of the front tire have a misaligning influence, as shown in Figure 3 below (Cossalter 2006).

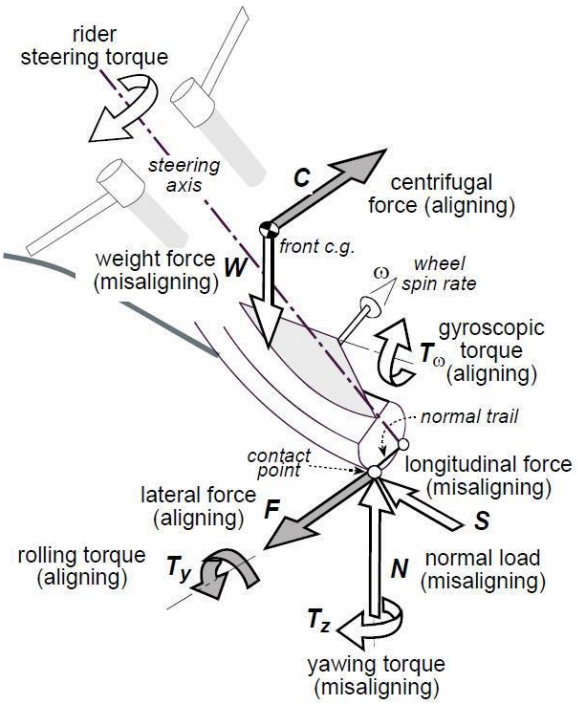

Figure 3: Equilibrium of the front frame. (Cossalter, et al., 2010)

6 Methodology

Figure 4: Measurement Platform and Roadgoing RS660 (left) & UWTSD's RS660 Trofeo (right).

The Aprilia RS660 is the motorcycle chosen for the current project and as a platform for the measurement equipment and testing. The 660cc parallel twin, is one of the leading mid-range Sportbikes currently on the market, both as a road bike and race bike. With an outstanding weight/ power ratio at 153kg, with 105hp and 67Nm, an excellent adjustable electronics package including Anti-wheelie Control, cornering - ABS, Traction control, Engine brake and a high performance geometry package. The RS660 Trofeo includes Andreani front fork cartridges, An Öhlins AP948 racing rear shock absorber, Racing rearsets, clip-ons, triple clamp, An SC project racing exhaust, racing air filter, for high performance on track (Aprilia 2024). The author's personal roadgoing version is also available to the University at the time of the project, with racing triple clamps, suspension, clip-ons, rearsets, exhaust, race mapping in order to allow calibration of the measurement system and data recording on the road. The rear sets and clip-ons allow the possibility to swap the sensor equipped bars, footpegs between the race and road motorcycles in order to decrease cost of sensors and ease of measurement.

The Aprilia RS660 is a centrepiece of the University of Wales Trinity Saint David's motorcycle engineering department, with two being raced, the Trofeo serving as the focus of multiple ongoing and future engineering projects. The extensive measurements and research surrounding the RS660 will provide a wealth of knowledge and data, making it an ideal platform for continued work at the University of Wales Trinity Saint David (UWTSD) and this project.

The rider can control a motorcycle by physically applying a force to the handlebar that generates a steering torque, by operating the throttle or the brakes of the motorcycle, which causes it to accelerate, maintain its speed or decelerate, as well as changing their body position on the motorcycle (Cossalter 2006).

While steering torque is the primary input for controlling a motorcycle, rider body movements serve as a secondary control input. These movements cause only small accelerations of the vehicle frame, with limited effects on the motorcycle's moment of inertia and the combined center of gravity, particularly when the vehicle's mass is significantly greater than the rider's mass. Additionally, the frequency range of handlebar control is much higher than that of body control, allowing the rider to adjust steering torque far more quickly than they can shift their body on the seat (Cossalter et al. 2007).

A rider can apply force, pressure, balance, and support their body using the handlebars, footpegs, seat, and sides of the tank. The author's goal is to record these pressures and input forces in all areas to better understand how riders control the motorcycle. Due to time constraints and the early stage of this research, the work builds upon previous measurements conducted at the university by (Przibylla 2018), which focused on handlebar input measured on circuit. This project expands on that foundation by developing a more robust system for the RS660, incorporating footpeg input measurements, and laying the groundwork for seat pressure measurements.

The following will describe the methodology and realisation of the measurement system to date.

6.1 Data Logging System

A 'Stick Logger V3' Data Logger from (2D Debus & Diebold Meßsysteme GmbH 2024) has been used to record the necessary parameters. This logger system integrates with the Aprilia RS660's Controller Area Network (CAN), enabling the measurement of internal data streams from the motorcycle's built-in sensors. Initially, these CAN channels provide raw data without specific meaning. However, through extensive testing, Andrew Harrison, Head of Race Engineering and lecturer at the university, has successfully mapped these CAN channels to critical parameters, allowing for the recording and analysis of Engine Speed, Wheel Speeds, Throttle Grip Position, Gear Position, and Coolant Temperature.

In addition to these values, the 2D Stick Logger is capable of accurately measuring three-axis acceleration, GPS location, GPS velocity, and lean angle, with the option to connect up to four external analog channels.

Bespoke mounts have been used to install external Suspension Position Potentiometers (Figure 5) and a steering angle sensor. On the RS660 Trofeo, an external front brake pressure sensor has been added to allow precise measurement. However, on the roadgoing RS660, the ABS unit remains installed, enabling the reading of brake pressure exerted. Unfortunately, this channel only indicates brake activation during riding, while it provides varying pressure values during bench testing. This limitation is accepted due to time and cost constraints regarding the installation of additional external brake pressure sensors. Despite this, the dataset remains useful by identifying when the rider is using the brakes.

The rider measurement system will be connected to the Stick Logger via CAN-Hub Connectors, this system will be discussed in the following section.

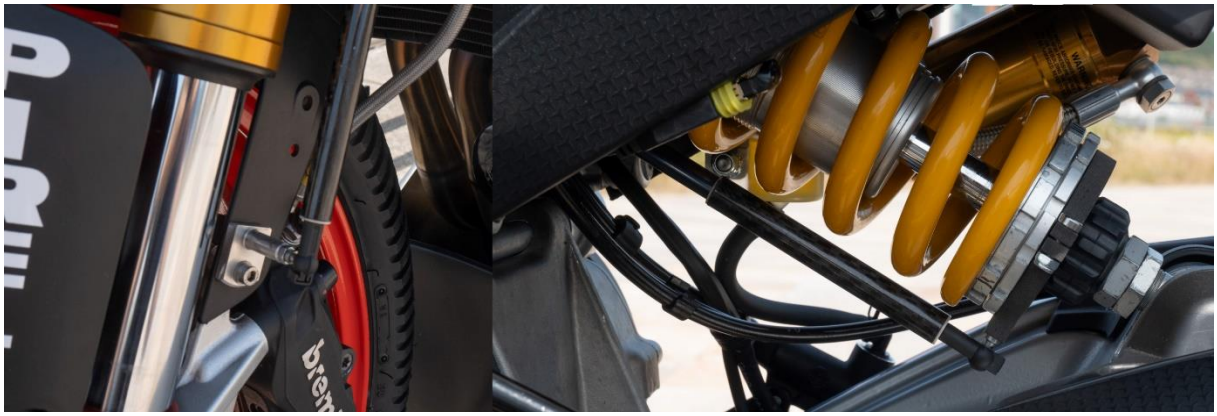

Figure 5: Suspension Position Potentiometers Mounted on the Aprilia RS660.

6.2 Rider Input Measurement System

The physical rider inputs are chosen to be measured using strain gauges positioned on the handlebars and footpegs, along with pressure strips beneath the seat and pressure pads on the tank. However, due to time and cost constraints, and the limitation of the data logger accepting only four analog channels, additional CAN hubs could not be purchased. Given the importance of the suspension potentiometers and steering angle sensor, for accurately determining the motorcycle's position and dynamic attitude, only one analog signal channel was available. Consequently, while the pressure strips were explored for feasibility and proof of concept, they were not integrated into the final system. The tank pads were also not used but remain available for future work and exploration.

The following section will describe the development of the force input measurement system on the handlebars and footpegs, and provide a brief overview of the use of pressure strips beneath the seat.

Figure 6: The RS660 Rider Input Measurement Platform along with the aftermarket and custom sensors.

6.2.1 Top Clamp Design and machining

To accommodate the strain gauges on the handlebars and footpegs, racing rearsets were installed to provide the fixed footpegs necessary for accurate measurement and track riding. Racing clip-on handlebars were also installed to create additional space on the handlebars and to ensure a aggressive riding position on the track. Since the RS660 requires a different top clamp to mount clip-on handlebars, the author designed a custom top clamp, which was 3D prototyped and CNC (Computer Numerical Control) machined in-house at the university by Wales Centre for Advanced Batch Manufacturing (CBM Wales) (Figure 7).

Figure 7: CAD Drawing to Finished Top Clamp.

6.2.2 Handlebar Strain Gauge Application

The following outlines the method used for installing strain gauges on each handlebar. Appendix 9.1 provides research on steering torque measurement techniques and explains the rationale for using strain gauges in the current measurement system.

The strain gauges were installed in the area of the handlebars where the most space is available, near the clip-ons. The centre of the 8mm long strain gauges were positioned 226mm from the end of the handlebar tube (Figure 8). Four strain gauges were positioned exactly 90° apart from each other on each handlebar tube to create two measurement axes.

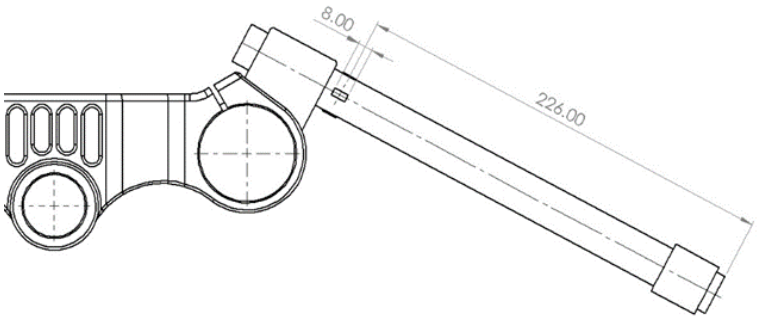

Figure 8: Graphical depiction of strain gauge placement on one handlebar.

To bond the strain gauges to the handlebar surface, the anodising was first removed, and the surface was prepared by sanding with 400-grit sandpaper, as recommended by Micro-Measurements (Vishay Measurements Group 2011). The strain gauges were then securely bonded to the handlebars using cold-curing, one-part Loctite SG401 adhesive (Loctite 2014).

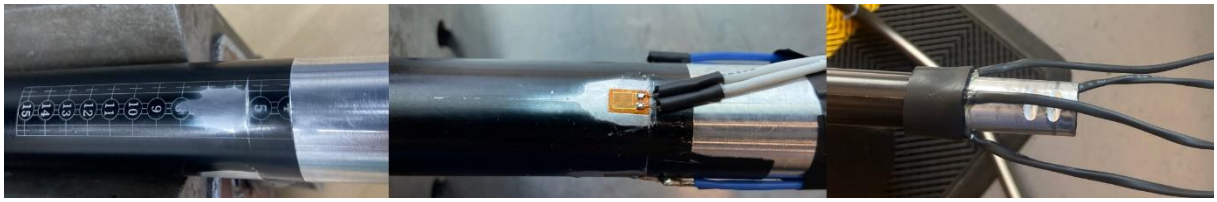

Figure 9: Prepared area (left) - Bonded and Soldered Strain Gauge (Middle) – Strain Gauges Sealed and Wires Heat shrunk (Right).

The strain gauges, each with a static resistance of 350Ω, were wired into four Wheatstone bridges, with each strain gauge pair forming one bridge. 120Ω resistors were used as dummy resistors in the strain gauge bridges. Binder connectors were utilised to allow direct connection of each strain gauge pair—Wheatstone bridge—to the 2D strain gauge amplifier module.

To protect the delicate strain gauges, they were sealed with adhesive-lined heat shrink tubing (Figure 9). Additionally, custom covers were designed and SLS 3D printed to safeguard against impact and other external factors. The wiring was heat-shrunk and carefully routed through the motorcycle to the data logger located beneath the seat.

Figure 10: View of the motorcycle cockpit as in use, with strain gauges and wiring protected and sealed.

6.2.3 Footpeg Strain Gauge Application

The strain gauges on the footpegs were installed using a method similar to that used on the handlebars. Readily available aluminium racing footpegs were selected for this purpose. The strain gauges were placed on the inside of the footpegs, where, as previously determined, there is minimal pressure or contact from the rider's foot. A recess was machined into the footpegs to protect the strain gauges and minimize their impact on the footpegs' structural integrity.

Due to the small diameter of the footpegs, four 5mm-wide flats were milled (Figure 11), each offset by 90°, to accommodate the strain gauges without excessive bending. The centres of the 8mm-long strain gauges were positioned 240mm from the motorcycle’s symmetry plane. To insulate and seal the strain gauges, adhesive-lined heat shrink tubing was applied. The wires were neatly insulated using heat shrink and routed behind the rearsets through the frame, leading to fly leads that formed the Wheatstone bridges. These were then connected to the 2D amplifier module and logger located below the seat. Additionally, custom covers were designed and SLS 3D printed to protect the strain gauges from the rider’s feet (Figure 12).

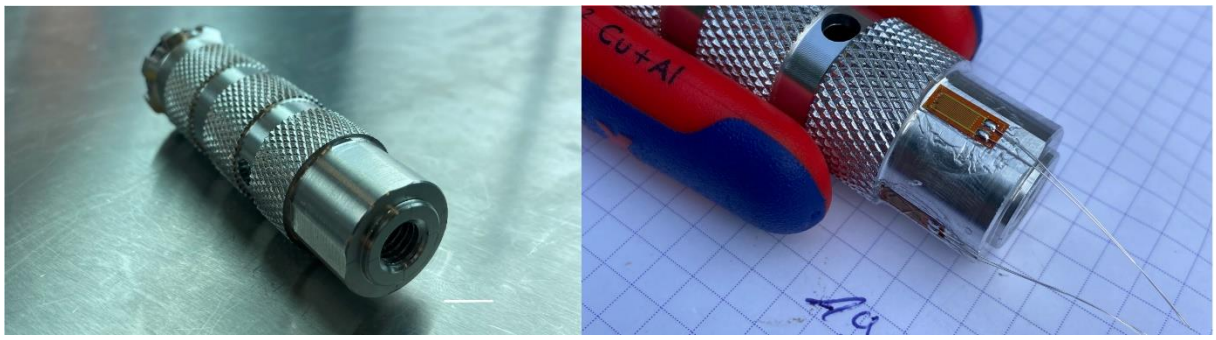

Figure 11: Footpeg with recess and flats machined (Left) - Strain gauges bonded (Right).

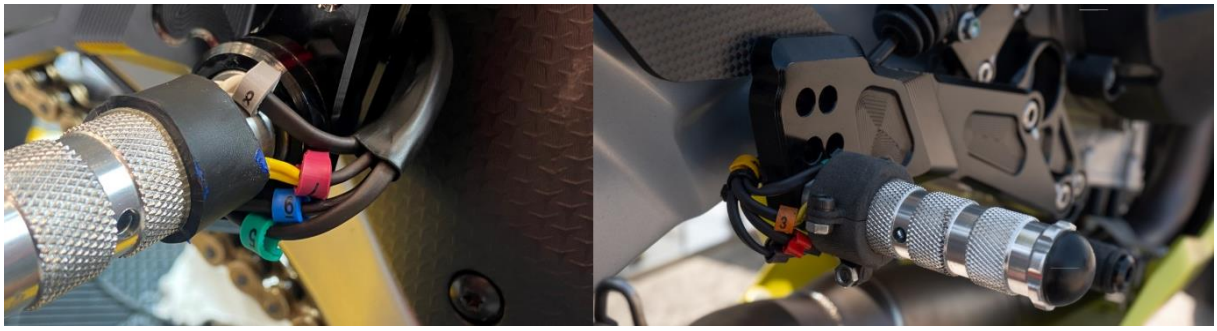

Figure 12: Strain gauges sealed (Left) and as in use with 3D printed protectors (Right).

None of the riders reported any interference or impact from the measurement system during use.

6.2.4 Seat pressure strips

Pressure strips were explored as a potential method for measuring weight distribution across the seat from left to right. The strips were bonded to the subframe using double-sided adhesive, positioned beneath two support points where the seat rests on either side of the subframe (Figure 13). These pressure strips were wired as analog inputs to the 2D logger for proof of concept, though they could not be used during actual measurements due to the previously mentioned limitation on available analog inputs.

The pressure strips demonstrated variation in response to changes in weight distribution between the left and right sides, confirming their feasibility for this application. However, full pressure distribution pads would provide more comprehensive data, though they are costly and may not offer significantly more information. For use with the racing seat unit on track, an additional part would need to be fabricated and bonded to the seat unit, as the support points differ from those of the stock seat unit.

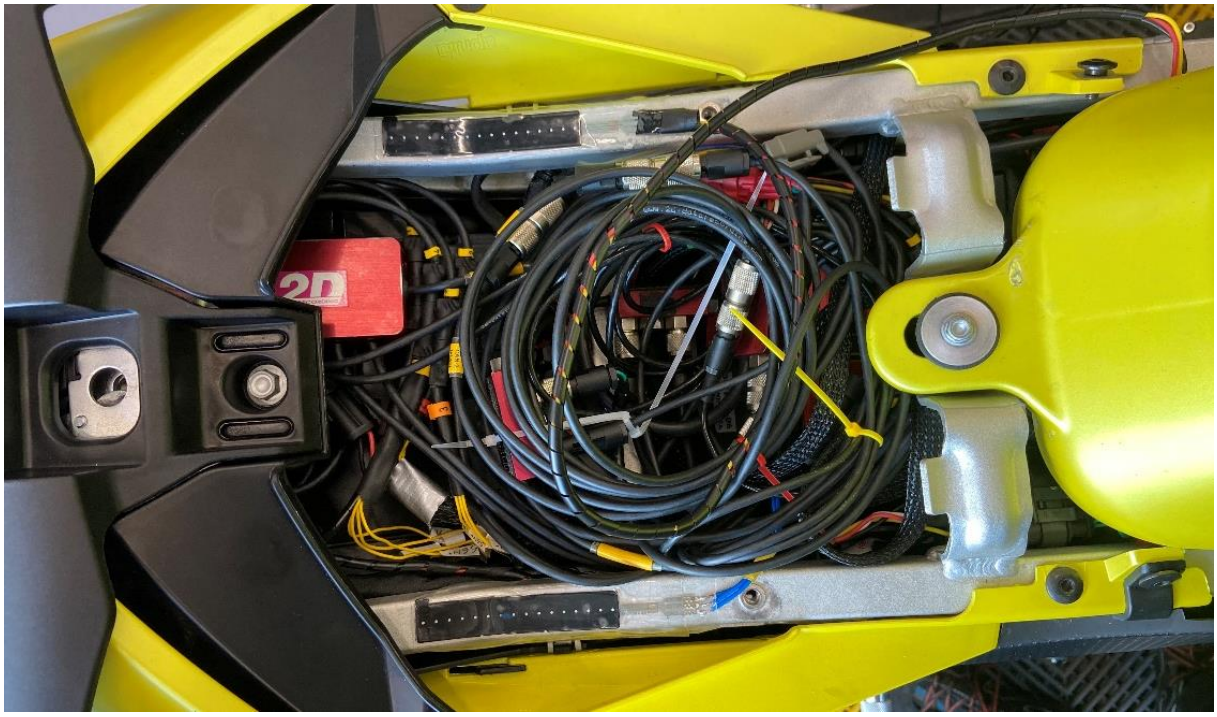

Figure 13: Pressure strips located below stock seat resting points.

6.2.5 Handlebar Force Input Calibration

In order to calculate the input force on the handlebars after measurement, calibration was carried out using calibrated weights in order to relate the measured raw strain gauge output values to a input force on the handlebars.

(Przibylla 2018) previously assumed the steering force input by the rider to be uniformly distributed over the handlebar grip, during his handlebar force input measurements.

The author, from experience in racing has noticed the handlebar grips on racing bikes seem to wear down around the outer area of the handlebar. Giving indication to believe the highest amount of force is executed there.

Figure 14 displays racing motorcycle handlebar grips, showing significant wear around the outer area. This wear is suspected due to concentrated pressure from the rider's hand and has developed after only four rounds of use. These grips are from different riders in the BMW Motorrad Alpha Van Zon IDM Superbikes team (MRP Racing 2024). On the right, the left handlebar grip of eight time MotoGP world champion Marc Marquez is depicted with the same wear (RedBull 2016).

Figure 14: Wear on outer area of handlebar grips. Champion Alpha Van Zon IDM SBK Team (Left & Right) - Honda HRC MotoGP (Right)

Due to a lack of literature specifically to this subject of pressure concentration on the handlebar grips, work in different areas has been explored to help confirm this or point towards correctness of this assumption.

Amateur and experienced bicyclists commonly experience sensory and motor impairments of the hands due to pressure and fatigue during cycling(Slane et al. 2011). A condition termed Cyclist’s palsy often presents numbness and/ or paraesthesia in the outer area of the hand palm (fifth and ulnar aspect of the fourth finger, sometimes accompanied by weakness in the abductors or adductors (lower muscles) of these fingers. (Slane et al. 2011), have conducted measurements using a high resolution pressure mat to record hand pressure on bicycle bars in order to compare this pressure without gloves, compared to different types of gloves. The research showed a focus on the outer area of the palm (Ulnar nerve, hypothenar area). The findings show the hand pressure and loading patterns seen on the hand induce ulnar nerve damage if maintained for long periods. This article shows a visual representation of where the pressure on

the hand is focused (Figure 15), supporting the suspicion of the most pressure being put on the outer area of the motorcycle handlebar grip, through the hypothenar.

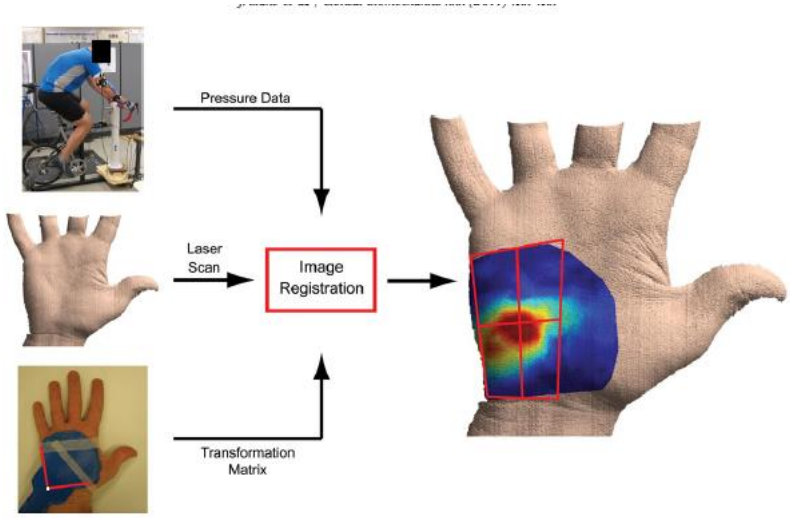

Figure 15: Cycling Handlebar Palm Pressure Distribution. (Slane J. Et al,. 2011)

(Chuckpaiwong and Harnroongroj 2009) show research where measurements have been conducted in order to measure the pressure distribution over the hand palm during a push-up exercise. Using 10 individuals, each executing push ups in five different hand positions. The palm was divided into five anatomic regions, viz. thenar, lunate, hypothenar, metacarpals and fingers. Statistical comparison between the measured pressure on the five positions of the hand was executed. A distribution of the mean peak pressure of the lunate and hypothenar areas were relatively higher than the other areas in both standby and full-elbow flexion positions. Different arm positioning showed to decrease pressure in the lunate areas. Though the hypothenar area showed the highest pressure throughout the different hand positions, when compared to the other areas of the hand. This is also the area which is suspected to be used the most to perform pressure on the motorcycle handlebars

From the previous, a 25mm wide area, positioned 5mm from the edge of the handlebar grip, has been defined as the “force input area” and used for calibration of the strain gauge measurements.

For calibration, various weights were suspended using a strap that matched the width of the "force input area" and placed on the defined pressure input area. This setup was used to establish a relationship between the changes in raw strain gauge readings and the applied force in this specific area. The strain gauges have a linear relationship between changes in resistance (V_out) and changes in strain (National Instruments 2016), as confirmed by the calibration measurements.

(Przibylla 2018) determined the Young's modulus by measuring and loading the bare handlebar tube to calculate the Uniformly Distributed Load (UDL) on the handlebar grip based on the measured strain. However, this approach was not adopted, as components such as switchgear, grips, and clutch and brake levers

are assumed to alter the effective Young's modulus of the assembly compared to the bare aluminium tube. Consequently, this method was deemed inaccurate for force calculations in this specific application.

Calibration measurements were conducted with all components installed as they would be during actual riding. Measurements were taken along both axes on the handlebars, using a footpeg stand to elevate the strap and ensure that the "pulling" force was aligned perpendicularly to the steering stem, a combination of the methods used by (Przibylla 2018; Wahl et al. 2020) (Figure 16).

Figure 16: Handlebar Calibration using weights - X-axis (Left) - Y axis (Right).

The raw digit values from the strain gauges were read using the 2D WinARace24 interface (Figure 17) when connected to the logger. The strain gauge readings were captured under both unloaded and loaded conditions with the weights. The weight of the strap and the weights themselves were measured using an accurate scale. These digit values were recorded under different loading conditions in Excel, allowing for the calculation of the weight required per digit change. The consistency of these values across different weights confirmed the linearity of the resistance change in relation to strain in the strain gauges. With these constants, the input force can be accurately calculated in 2D using the CalcTool.

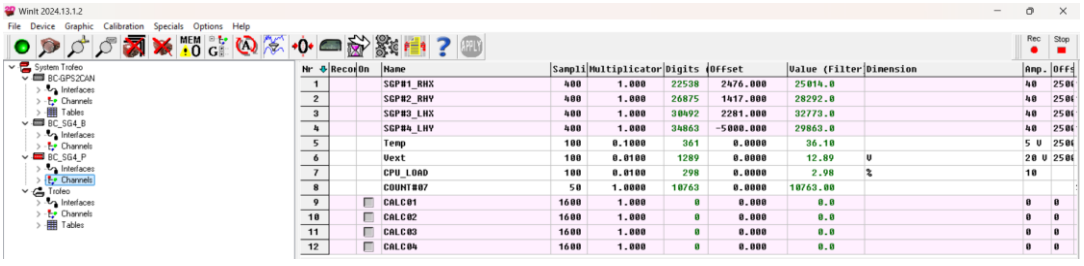

Figure 17: 2D WinARace Logger Communication interface. (2D Debus & Diebold Meßsysteme GmbH, 2024)

To further refine the calibration, it is important to note that the channel range of each strain gauge bridge within the amplification module extends from 0 to 65,535 digits. The supply voltage can be adjusted to zero the signal from each bridge or introduce an offset if needed (2D Debus & Diebold Mebsysteme GMBH 2014). Since

the strain gauges measure strain in both positive and negative directions (i.e., compressive and tensile strain), the supply voltage in millivolts is adjusted so that each strain gauge pair, when unloaded, has a signal output of 32,768 digits, centered within the range. However, due to system variations, these values do not consistently remain exactly at 32,768 digits when unloaded. To ensure accurate calculations, the change in digits from the unloaded state is calculated from the last recorded value of each strain gauge channel. This change in digits is then used to calculate the corresponding input force.

Table 1: Strain Gauge Couple measurement orientation & Handlebar Force Calibration Constants.

Handlebars		Handlebar Force Calculation constants	
Strain Gauge couple	Measurement Direction		Constant (g/ digit)
#1	X - RHS	Horizontal	50.932
#2	Y - RHS	Vertical	54.086
#3	X -LHS		
#4	Y - LHS		

(Przibylla 2018) previously highlighted the importance of accounting for strain caused by pulling the front brake and clutch levers. However, due to the current placement of the strain gauges, pulling these levers does not induce any measurable strain in the handlebars as detected by the strain gauges. This has been confirmed by using a G-clamp to simulate force applied solely to the levers without any pushing or pulling force from a rider.

Figure 18: Validating strain measured by pulling force on levers.

6.2.6 Footpeg Force Calibration

In order to calculate the input force on the footpegs, a similar technique to the handlebar calibration has been applied. Visual footage of experienced/ professional motorcycle racers show their feet are usually positioned with the Balls of their feet on the outside of the footpeg, especially on the inside of corners. This is expected to come down to the fact of how positioning the feet like this allows the rider to position their legs as good as possible in the corner, being able to move around the end and the top of the footpeg being the most effective/ accurate, being able to position the ankle, knee as freely as possible, when compared to the middle or back of foot (Baz 2021; Guintoli 2023)

Figure 19: Riders with the Ball of their foot on the footpeg. Ilya Mikhalchik (Left) - Ilias Iatrakis (Middle) - Jeremy Guarnoni (Right) (BMW Motorrad, 2024, 2023)

In cornering, some riders position their outside foot more relaxed, with the middle of their foot placed on the footpeg (Herrin 2019). The riders also have to shift to the middle of their foot to be able to reach the shift lever and rear brake lever.

(Guintoli 2023), says pushing through your legs can take load of the hands/ arms as they're a lot stronger compared to the upper body. He also recommends moving the foot forward as late or as close to the turn as possible. This is because during braking, the earlier you shift your foot, the more deceleration forces you must counteract with your leg, requiring more energy.

Figure 20: Pro Rider Boot Wear. (Herrin J. 2019)

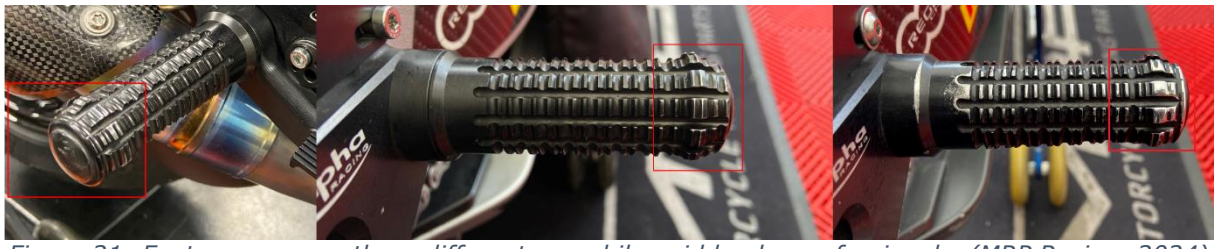

Figure 21: Footpeg wear on three different superbikes ridden by professionals. (MRP Racing, 2024)

As previously discussed, in a similar manner to the handlebars, a force input area has been defined on the footpegs on which the rider generally places his feet during high performance riding. The footpeg strain gauge couples were calibrated Using a range of weights with the exact know mass, hung by the footpegs, as installed and used on the motorcycle, the exact change in digits related to force input on this area can be determined for calculations, in the same way as done on the handlebars.

Due to some issues regarding installation and not being able to order the required strain gauges, the footpeg on the left and right are fitted with different strain gauges, thus the variation in resistance related to strain is different from each other. This can be accounted for in the force calculation by using the measured weight/ digit constants for each side. Figure 22 shows the weight hung from the outer edge of the footpeg on the instrumented RS660.

Figure 22: Footpeg Calibration Weight loading.

No difference in strain was found in the y and x axis between a single footpeg due to the symmetry of the footpeg. Table 2 shows the measured and calculated constants to relate measured strain to input force.

Table 2: Footpeg Force Calibration Constant.

Footpeg Force Calculation constants	
	Constant (g/ digit)
Left	35.182
Right	43.189

6.3 Handlebar Force and Steering Torque Calculations

The following section presents the calculations and formulas used to determine the forces and steering torque measured by the handlebar strain gauge pairs, along with the accompanying 2D CalcTool code.

The "horizontal" strain gauge pair is positioned perpendicular to the steering stem, allowing it to measure strain directly in the same plane as the steering torque. Therefore, the strain measured by this pair can be directly used to calculate steering torque without needing further direction resolution.

As previously noted, the last recorded value in each dataset is established as the zero reference point, from which the change in digital readings due to applied loads is calculated:

$$Digit\ Change\ from\ Unloaded = Instantaneous\ Digits\ Value - Zero\ Value$$

Using the measured force constant, the digit change amplitude can be related to an input force on each handlebar, this calculation is executed for both axis on each handlebar:

$$Force\ Input\ _{One\ Handlebar} = Digit\ Change\ from\ Unloaded\ \times Defined\ Force\ Constant\ (Kg)$$

Summing the calculated input forces for each axis on both handlebars yields the total input force for each respective axis:

$$Force\ Input\ X_{Total} = Force\ Input\ X\ _{Left} + \ Force\ Input\ X_{Right}\ (Kg)$$
$$Force\ Input\ Y_{Total} = Force\ Input\ Y\ _{Left} + \ Force\ Input\ Y_{Right}\ (Kg)$$

The steering input force is calculated based on the defined "force input area". To determine the steering torque generated by the combined input force on both handlebars, this force is resolved into its component acting at a 90° angle to a calculated torque radius around the steering stem.

To achieve this, SolidWorks was utilised to accurately define the distances and angles between the steering assembly components, including the handlebars, clip-ons, and top clamp. The top clamp model of the RS660, which was designed by the author, served as a reference. Precise measurements of the clip-ons and handlebars relative to the top clamp and front forks were taken to replicate the steering assembly as installed on the motorcycle. Using the SolidWorks drawing, the 'torque radius' around the steering stem was measured at the center of the defined force input area on the handlebars. Additionally, the angle between the input force and the force acting perpendicular to this radius was determined using the SolidWorks Drawing function (Figure 23).

These measured values were then used to calculate the steering torque generated by each handlebar, and subsequently, the combined steering torque.

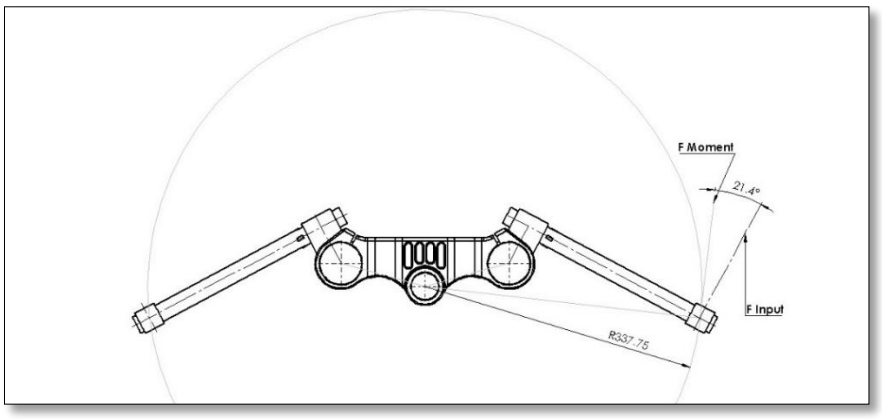

Figure 23: SolidWorks Drawing of Steering Assembly on the Measurement Platform.

$$F_{Moment} = \frac{F_{Input} \times 9.81}{Cos(21.4°)} \ (N)$$

$$T_{Steering\ 1\ Bar} = F_{Moment} \times Radius\ to\ steering\ Axis\ (Nm)$$

$$T_{Steering} = T_{Steering\ LHS} + T_{Steering\ RHS}\ (Nm)$$

The strain gauge pairs were wired so that a positive digit change on the X-axis of the right handlebar corresponds to pushing forward on the bar, while a positive change on the left handlebar corresponds to pulling back. In the Y direction, a positive digit change occurs on both handlebars for upward forces. This wiring simplifies the calculation of steering torque.

This setup ensures that a positive (or negative) digit change on the X-axis for both handlebars contributes to torque in the same direction around the steering stem. Similarly, in the Y direction, a force in the same direction (upward or downward) on both handlebars results in the same direction of digit change. This configuration prevents the steering torque calculation from canceling out when forces on each handlebar have different signs.

A positive digit change indicates a positive input force, which corresponds to a positive steering torque. As a result, positive forces consistently produce steering torque in one direction. Specifically, positive steering torque indicates counterclockwise rotation of the handlebars, while negative torque indicates clockwise rotation, a method also used by (Bartolozzi et al. 2023a).

According to (Parks 2015), the most efficient steering technique involves using the inside arm to apply the steering torque by executing the pushing force. This is recommended because it is challenging for both arms to apply reverse inputs on opposite ends of the handlebars in precise unison while allowing enough 'give' in the steering assembly for the trail and gyroscopic precession to function effectively. In his Total Control Advanced Riding Clinics, Parks has observed that one common hindrance in riders maintaining a tight line is that both arms are fighting for control of the steering. He found that once riders stop wrestling with the handlebars using both arms, the motorcycle becomes a much more efficient turning machine. Freed from the conflicting inputs, the bike is able to turn more smoothly and quickly at the given speed, allowing it to perform as it was

engineered to do. Professional car racers are found to do a similar thing, especially when racing in the rain. By having one hand dominate the steering, they can allow the vehicle to do whatever self-correcting 'wiggling' motion it needs to do as it struggles in the wet. A pulling motion on the bar also requires the forearm to tense in order for the hand to grip, which could lead to armpump (Cohen 2001).

For rider analysis, a push percentage is calculated to quantify the proportion of steering torque generated by pushing compared to pulling. The following outlines the calculations used to determine this percentage. The CalcTool automatically identifies the inside bar by using an IF function, which determines the sign of the total steering torque, and subsequently calculates the correct push percentage.

$$Steering\ Torque_{\ Push\ Percentage} = \frac{T_{Steering\ Inside\ Bar}}{T_{Steering\ Total}} \times 100\ (\%)$$

Figure 24 shows the 2D calculation file used to calculate the above mentioned values for the measured datasets.

```
[SG Bars Aug 24]

; Taking the absolute value of Raw Measured digits for ease of calculation.
SGB#1_RHX_Abs = Abs(#SGB#1_RHX)
SGB#2_RHY_Abs = Abs(#SGB#2_RHY)
SGB#3_LHX_Abs = Abs(#SGB#3_LHX)
SGB#4_LHY_Abs = Abs(#SGB#4_LHY)

[Force Calc Bars]

;Creates constant of the first value measured in the data Set, which is the zero position of the digits from which force is calculated.
C1 = LastValue(#SGB#1_RHX_Abs)
C2 = LastValue(#SGB#2_RHY_Abs)
C3 = LastValue(#SGB#3_LHX_Abs)
C4 = LastValue(#SGB#4_LHY_Abs)

;Calculate Digit Difference From 0
;Calculated Difference from starting value, which can be related to force on handlebars

C5 = -(#C1,#SGB#1_RHX_Abs) ; Because SGB_RHX_Raw measurement < 0, positive force makes absolute value smaller.
C6 = -(#SGB#2_RHY_Abs,#C2)
C7 = -(#SGB#3_LHX_Abs,#C3)
C8 = -(#SGB#4_LHY_Abs,#C4)


 ; Constants, force per digit in KG

Kg_Digits_Horizontal = Const(0.051)
Kg_Digits_Vertical = Const(0.054)

;Force Calc Bars in kg
;Calculates force by the digit change from zero times the determined force constant.
Force_SGB#1_RHX = *(#C5,#Kg_Digits_Horizontal)
Force_SGB#2_RHY = *(#C6,#Kg_Digits_Vertical)
Force_SGB#3_LHX = *(#C7,#Kg_Digits_Horizontal)
Force_SGB#4_LHY = *(#C8,#Kg_Digits_Vertical)

;Adding the LHS force to the RHS force gives the total force in each axis (in kg).
Force_SGB_Tot_Y = +(#Force_SGB#1_RHX,#Force_SGB#3_LHX)
Force_SGB_Tot_X = +(#Force_SGB#2_RHY,#Force_SGB#4_LHY)


;Fmoment calc for bars to offset angle.
Cos_21_4Deg = Const(0.931055816)

; Converting handlebar force from Kg to N

C9 =*(#Force_SGB#1_RHX,9.81)
C10 = *(##Force_SGB#3_LHX, 9.81)

; Calculates Force 90° around determined moment radius (in N).
F_Moment_RHX = /(#C9,#Cos_21_4Deg)
F_Moment_LHX = /(#C10,#Cos_21_4Deg)

;Radius where steering torque is calculated (in m)

Radius_Force_Application = Const(0.33775)

;Steering Torque Calc each side in Nm
T_Steering_RHX = *(#F_Moment_RHX,#Radius_Force_Application)
T_Steering_LHX = *(#F_Moment_LHX,#Radius_Force_Application)

;Steering Torque Total
T_Steering = +(#T_Steering_RHX,#T_Steering_LHX)

;Absolutes for ratio calc

T_Steering_RHX_Abs = Abs(#T_Steering_RHX)
T_Steering_LHX_Abs = Abs(#T_Steering_LHX)
T_Steering_Abs = +(#T_Steering_LHX_Abs,#T_Steering_RHX_Abs)


;Push/Pull Ratio in order to determine how much of total steering torque is done by pushing Or pulling.
C11 = /(#T_Steering_RHX_Abs,#T_Steering_Abs) ;Ratio of total steering torque executed by RHS
C12 = /(#T_Steering_LHX_Abs,#T_Steering_Abs) ;Ratio of total steering torque executed by LHS

;Converting ratio to percentage.
Percentage_T_Steering_RHX = *(#C11,100)
Percentage_T_Steering_LHX = *(#C12,100)

;Push percentage - gives percentage of the pushing force on the inside.
Push_Percentage= If(#T_Steering,>,0,#Percentage_T_Steering_RHX,#Percentage_T_Steering_LHX)
```

Figure 24: Steering Torque Calculation CalcTool Code.

6.4 Footpeg Force Input Calculation

The following outlines the calculations used to determine the input force on the footpegs. These calculations were performed using the 2D CalcTool, which computes the forces resulting from the strain measured by the strain gauges at each instantaneous measurement in the dataset.

For both footpegs, a vertical force input directed towards the floor results in a positive force, while a horizontal force directed towards the rear of the bike also yields a positive force, as forces in the opposite directions are not typically expected. This convention is applied consistently to both footpegs.

As with the handlebars, the last value in each dataset is taken as the zero point for unloaded conditions, accounting for potential minor variations in unloaded digit values between datasets due to influences within the data acquisition system. From this zero point, any change in measured digit value indicates a change in load, which can be related to an input force using the measured force constants.

$$Digit\ Change\ from\ Unloaded = Instantaneous\ Digits\ Value - Zero\ Value$$

$$Force\ Input_{One\ footpeg} = \ Digit\ Change\ from\ Unloaded\ \times Defined\ Force\ Constant\ (Kg)$$

Summing the calculated input forces for each axis on both footpegs provides the total input force for each respective axis.

$$Force\ Input\ X_{Total} = Force\ Input\ X_{\ Left} + \ Force\ Input\ X_{Right}\ (Kg)$$
$$Force\ Input\ Y_{Total} = Force\ Input\ Y_{\ Left} + \ Force\ Input\ Y_{Right}\ (Kg)$$

The total Y input force can be used to measure how much of the rider's body mass is supported by the footpegs.

For analysis purposes, a "rolling torque" relative to the motorcycle's symmetry plane is calculated to determine if any motorcycle response can be linked to footpeg force input. This concept will be expanded upon in subsequent sections. A rolling torque is calculated for the left side and right side. In order to match the sign of rolling torque, to the steering torque, the left footpeg will be denoted to create a negative rolling torque, initiating towards a left turn, while the right footpeg will be calculated to create a positive rolling torque, initiating towards a right turn.

$$Rolling\ Torque_{One\ Side} = (Force\ Input\ Y_{One\ side} \times 9.81)\ \times Centre\ Distance\ (Nm)$$

Figure 25 shows the 2D Calctool Code used in order to calculate this.

```
;Find starting point digits value (Unloaded)
C1 = LastValue(#SGP#1_RHX33)
C2 = LastValue(#SGP#2_RHY34)
C3 = LastValue(#SGP#3_LHX30)
C4 = LastValue(#SGP#4_LHY32)

; Force Constants (kg/digit)
Force_Per_Digit_RHS = Const(0.0432)
Force_Per_Digit_LHS = Const(0.0352)

;Change in Digits from unloaded
Digit_Change_SGP#1_RHX = -(#SGP#1_RHX33,#C1)
Digit_Change_SGP#2_RHY = -(#SGP#2_RHY34,#C2)
Digit_Change_SGP#3_LHX = -(#SGP#3_LHX30,#C3)
Digit_Change_SGP#4_LHY = -(#SGP#4_LHY32,#C4)

;Force Calc  (Change in digits x Force constant) (kg)
Force_SGP_RHX = *(#Force_Per_Digit_RHS,#Digit_Change_SGP#1_RHX)
Force_SGP_RHY = *(#Force_Per_Digit_RHS,#Digit_Change_SGP#2_RHY)
Force_SGP_LHX = *(#Force_Per_Digit_LHS,#Digit_Change_SGP#3_LHX)
Force_SGP_LHY = *(#Force_Per_Digit_LHS,#Digit_Change_SGP#4_LHY)

;Total Force on footpegs(kg)
F_Tot_Pegs_Y =  +(#Force_SGP_RHY,#Force_SGP_LHY)
F_Tot_Pegs_X =  +(#Force_SGP_RHX,#Force_SGP_LHX)

;Rolling Torque in Nm
C5 = Const(0.240) ; X distance from end of footpeg to symmetry plane of bike (m)
C6 = *(#Force_SGP_RHY, 9.81) ;Convert kg to N
C7 = *(#Force_SGP_LHY, 9.81) ;Convert kg to N

T_Rolling_Right = *(#C6, #C5) ; T = Force x Distance
C8 = *(#C7, #C5)
T_Rolling_Left= *(#C8, -1)    ; Reverse sign to match steering torque
T_Rolling_Tot = +(#T_Rolling_Right,#T_Rolling_Left) ; Combined rolling torque from both footpegs
```

Figure 25: Footpeg Calculation CalcTool Code.

6.5 Steering Torque Approximation

The following outlines the calculation of a theoretical steering torque derived from the dynamic behaviour of the motorcycle, specifically focusing on roll and roll rate. This calculation is intended for validation and comparison with the measured values.

As highlighted in the literature review, highly accurate models, such as those presented by (Przibylla 2020), have demonstrated strong agreement with experimentally measured data. However, due to the scope and complexity of implementing these models being beyond the objectives of the current project, a simplified mathematical model has been employed to serve as a proof of concept for the measured data and measurement system.

Following formula describes the resulting gyroscopic torque that causes the lean of the motorcycle and is fundamentally understood as the core process for the steering of a motorcycle from the perspective of the rider in terms of influencing the control and handling of the motorcycle (Williams 2023).

$$G_m = I_f \omega_f \dot{\delta} \cos \varepsilon$$

Where:

$G_m = Calculated\ steer\ torque\ from\ Gyroscopic\ moment$
$I_f = Moment\ of\ Inertia\ Front\ Wheel\ (kgm^2)$
$\omega_f = Wheel\ Velocity\ (rad/sec)$
$\dot{\delta} = Roll\ Rate\ (rad/\sec)$
$\varepsilon = Rake\ Angle\ (°)$

The previous formula is applied in the 2D CalcTool software to calculate the theoretical steering torque required, based on the measured data. This calculated torque can then be compared to the measured steering torque values.

The wheel velocity and roll rate are directly measured in the 2D data, of which the instantaneous values are used. The rake angle, which varies with suspension movement in both the front and rear, is calculated using functions generated by the chassis geometry program (MotoSpec 2024). This code provides the precise rake angle at each moment in the data, based on suspension travel, lean angle and the specific motorcycle setup. Figure 28 shows the RS660's chassis setup as ridden during the tests.

The moment of inertia (MOI) of the wheels was determined through measurements conducted by the author on the wheels installed on the RS660. To ensure accuracy, three different methods were employed:

Wheel Balancer Method: A weight was attached to the wheel on a balancer, applying a fixed force. The MOI was calculated based on the time it took for the weight to fall a specified distance.

Rolling Slope Method: The wheel was rolled down a slope, and the time taken to travel a certain distance was measured.

Trifilar Pendulum Method: The MOI was measured using a trifilar pendulum, with a data logger attached to the pendulum capturing the decaying oscillations from a given angle input.

The results of these methods are presented in Table 3. Among these, the trifilar pendulum method was ultimately used for calculation, as it is an industry standard and produced the most consistent results, minimising manual measurement errors (Hou et al. 2009).

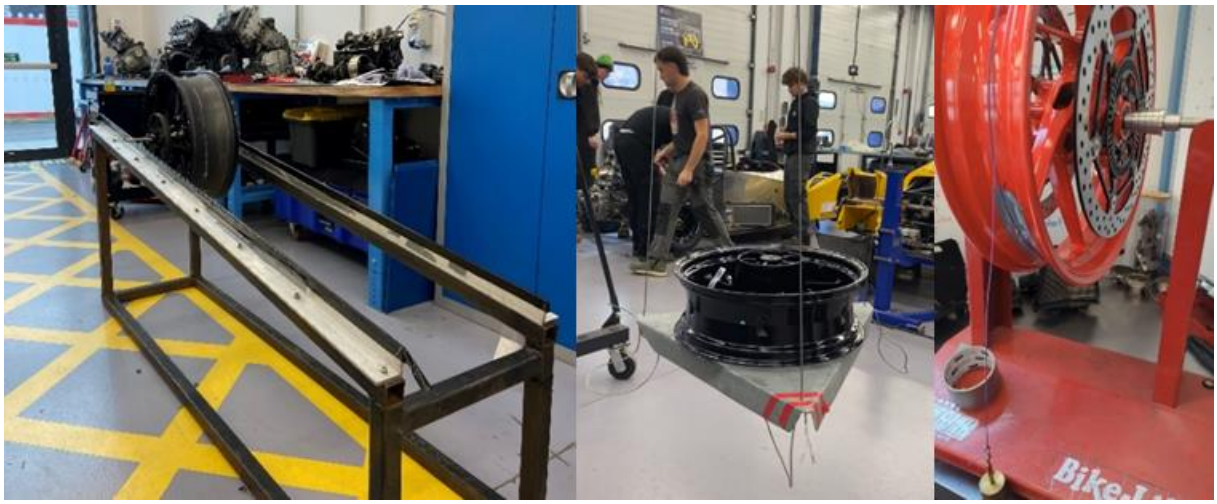

Figure 26: Wheel Moment of Inertia Measurements.

Table 3: Wheel Moment of Inertia results.

Average MOI						
	Front Wheel w/Tyre	**Rear Wheel w/Tyre**	**Front Wheel w/o Tyre**	**Rear Wheel w/o Tyre**	**BMW carbon rim**	**Verification weight**
Balancer	0.386	0.581	0.161	0.153	0.069	0.095
Ramp	0.325	0.627	0.108	0.074	0.054	0.068
Pendulum	0.483	0.689	0.166	0.169	0.095	0.115

```
[Steering torque calculated ]

C1 = Const(0.48)   ; Front Wheel MOI (kgm^2)
C2 = Const(24.1)  ; Headstock Angle when static(degrees)
C3 = dcos(#MotoSPEC_Rake2Dcalc) ; Cosine of headstock angle

C4 = /(#V_Front,3.6) ; Front wheel velocity from km/h to m/s
C5 = /(#V_Rear,3.6) ; Rear wheel velocity from km/h to m/s
C6 = Const(0.296) ; Front wheel radius (m)
C7 = Const (0.318) ; Rear wheel radius (m)
C8 = /(#C4,#C6) ; Front wheel angular velocity (rad/s)
C9 = /(#C5,#C7) ; Rear wheel angular velocity (rad/s)


C10 = *(#Banking_GPS,@DEG2RAD) ; Roll angle from Degrees to Radians (Lean angle)
Roll_Rate_Radians = Derivate(#C10) ;Roll rate in rad/s


C13 = *(#C1,#C8) ; MOI times Front wheel angular velocity
C14 = *(#C13,#Roll_Rate_Rad) ; MOI * Front wheel Angular velocity * roll rate
C15 = *(#C14,#C3) ; calculated steering angle -> MOI * Front wheel angular velocity* Roll Rate* Cos headstock angle (Nm)
T_Steering_Calculated = *(#C15,-1) ; reversing sign on calculated steering torque to match measured
T_Steering_Calculated = Set(Dim='Nm') ;Set Unit for calculated Steering Torque
```

Figure 27: 2D CalcTool Code for calculating approximated Steering Torque.

MotoSPEC CHASSIS PROGRAM	1 Aprilia RS 660 2024	
FRONT SETTINGS		
Yoke Offset (mm)	28.0	
Steering Axis Angle (degrees)	0.00	deg
Steering Axis Offset (mm)	0.0	mm
Fork Position (mm)	5.0	
Fork Name	Stock	
Damping Setting (REFERENCE ONLY)		
Comp | Reb Clicks (REFERENCE ONLY)		
Spring Rate L/R (N/mm)	9.00	9.00
Spring Preload L/R (mm)	5.0	5.0
Oil Level L/R (mm) or Oil Volume (cc)	170.0	170.0
Topout Spring Rate L/R (N/mm)	4.0	4.0
Topout Spring Effective Length L/R (mm)	40.0	40.0
REAR SETTINGS		
Swingarm Length (mm)	545.0	
Shock Clevis Ride Height Adjustment (mm)	0.0	
Shock Name	Stock	
Shock Length (mm)	306.0	
Damping Setting (REFERENCE ONLY)		
Comp | Reb Clicks (REFERENCE ONLY)		
Spring Rate (N/mm) or Rear Multi-Rate Spring Selection	130.0	
Spring Preload (mm)	7.0	
Topout Spring Rate (N/mm)	0.0	
Topout Spring Effective Length (mm)	0.0	
Swingarm Pivot (positive to rear | positive up, mm)	0.0	0.0
Rocker Name		
Linkarm Length (mm)	0.00	
TIRES		
Front Tire Name	KR448F 120/7	
Rear Tire Name	KR451 180/65	
SPROCKETS		
Front | Rear	16	43
Final Ratio	2.688	

Figure 28: RS660 Chassis Setup as Ridden. (MotoSpec, 2024)

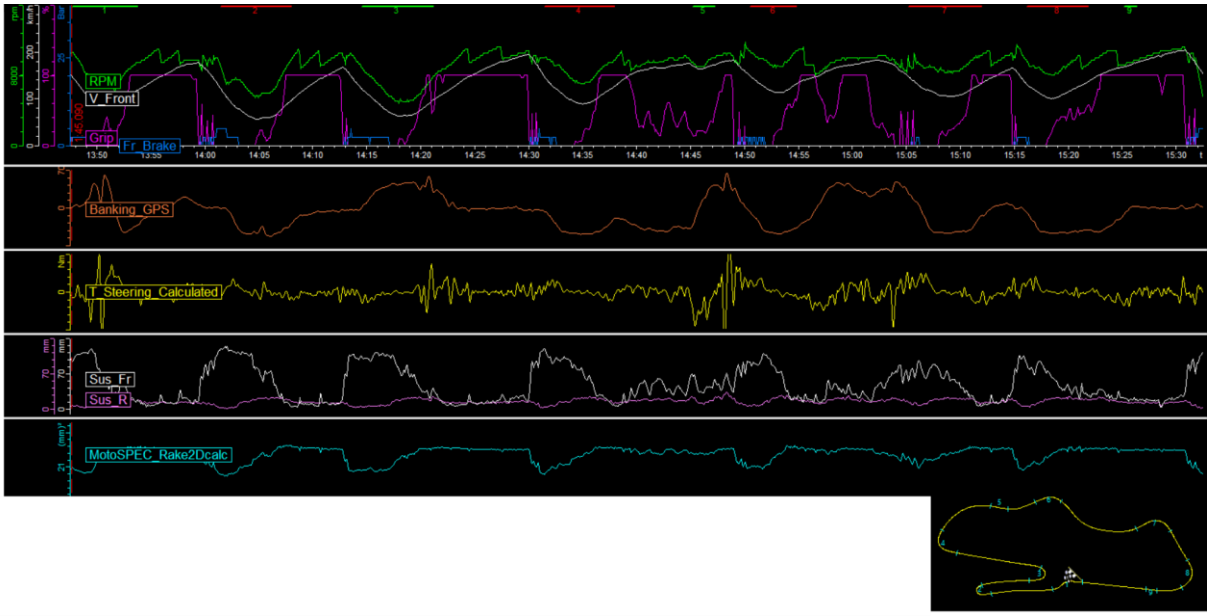

Figure 29: Calculated Steering Torque and Rake Angle throughout a lap around Donington.

6.6 Data Collection

This section outlines the data collection process for this work, emphasising the systematic approach to ensuring accurate and reliable measurements. All riders involved in the measurements had previous motorcycle riding experience, which was essential for obtaining meaningful data. The RS660 measurement platform was built from new and consistently prepared and checked to ensure correct technical functioning under the high loads experienced during track riding. All necessary safety considerations and risk assessments were conducted as required.

Given the focus on developing a system for rider input measurement, analysis, and improvement, the need for robust data was paramount. The author, having raced on track for the past eight years, leveraged this experience to effectively test and refine the measurement platform, which was crucial to achieving the project's current scale. The riders throughout the following analysis will be referred to as Rider 1 and Rider 2, with Rider 1 having eight years of track riding experience and having raced for five at years national club level with Podium results. Rider 2 has 20 years of road riding experience, with very limited track riding experience.

Throughout the project, bench testing was conducted to test, calibrate, and validate the system. However, bench testing alone does not confirm a system's viability under real-world track conditions.

The road-going RS660 was converted into a track-spec measurement platform, equipped with race fairings, Rearsets and Clip-On handlebars, Bespoke Top Clamp, Race Suspension, Race Exhaust, Race ECU Map, slick tires, rain light, and custom-made handlebar controls for on-track testing and measurement.

Figure 30: RS660 Measurement Platform in Track Specification.

Figure 31: Rider 1 riding the Measurement Platform at Snetterton Circuit.

The first on-track test was carried out by rider 1 at Snetterton Circuit to evaluate the CAN logging system and suspension potentiometers after the track conversion. Following this, a test day at Pembrey Circuit was conducted to specifically assess the handlebar input measurement system. These tests provided valuable insights into the system's performance under track conditions.

Following the completion of the footpeg strain gauge input measurement system, a race weekend at Cadwell Park was planned to record data for analysis. However, this event revealed an issue where the two strain gauge amplifier modules interfered with each other, rendering the data unusable.

Figure 32: Rider 1 riding the Measurement Platform at Cadwell Park.

After identifying and resolving the interference issue, the RS660 was converted back to road specification. This allowed the system to be tested on the road by UWTSD Workshop Lead and Chief Test Rider, confirming the system's full integrity and calibration before further track testing.

Figure 33: Onboard GoPro Footage from UWTSD Chief Test Rider Road Riding the Measurement Platform.

The final test day was conducted at Donington Park, where the RS660 measurement platform was ridden by Rider 1 and Rider 2. This test was instrumental in collecting the final data used for analysis in this report.

7 Discussion

While steering torque is the primary input for motorcycle control, the rider's body movements serve as a secondary input. These movements cause only minor accelerations of the vehicle frame and result in limited changes to the motorcycle's moment of inertia and the combined centre of gravity, particularly when the vehicle mass is significantly greater than the rider mass. Additionally, the frequency range of handlebar control is significantly higher than that of body control, allowing the rider to adjust steering torque more rapidly than they can shift their body position on the seat (Cossalter et al. 2007).

However, the rider can still transfer body weight toward the turn centre to reduce the centrifugal effect on the motorcycle, thereby reducing the roll angle required to maintain cornering equilibrium for a given turning radius at a specific velocity. Furthermore, shifting the upper body and leg creates an aerodynamic yawing moment that aids in entering and negotiating a turn (Cossalter 2006). This technique of shifting the motorcycle-rider system's centre of gravity toward the inside of the turn involves both leg movement and body repositioning in the saddle. By doing so, the rider can achieve higher cornering speeds at any given roll angle compared to a rider who does not shift their body inwards, thus increasing maximum velocity through a turn. Conversely, achieving the same cornering speeds with less roll angle enhances the rider's safety margin, allowing for further trajectory adjustments if necessary.

The following section will discuss the dynamics of counter steering by handlebar based input on the recorded data. (Przibylla 2020) has previously conducted an in-depth investigation into riding dynamics and steering phenomena on track, with his work being fully accessible to the author. (Przibylla 2020) also performed measurements around the Donington GP track to illustrate certain phenomena described in motorcycle dynamics. This section will review these same phenomena to, first, confirm the foundational work previously established and, second, validate the current work as a basis for further analysis. The current findings will also be compared with the estimated steering torque to enhance the analysis.

Figure 34: Rider 1 riding the Measurement Platform at Donington Park.

7.1 Steering Input Validation

The following will go through looking at the transient effects that influence the rider's steering torque in order to validate the previous novel work executed by (Przibylla 2020).

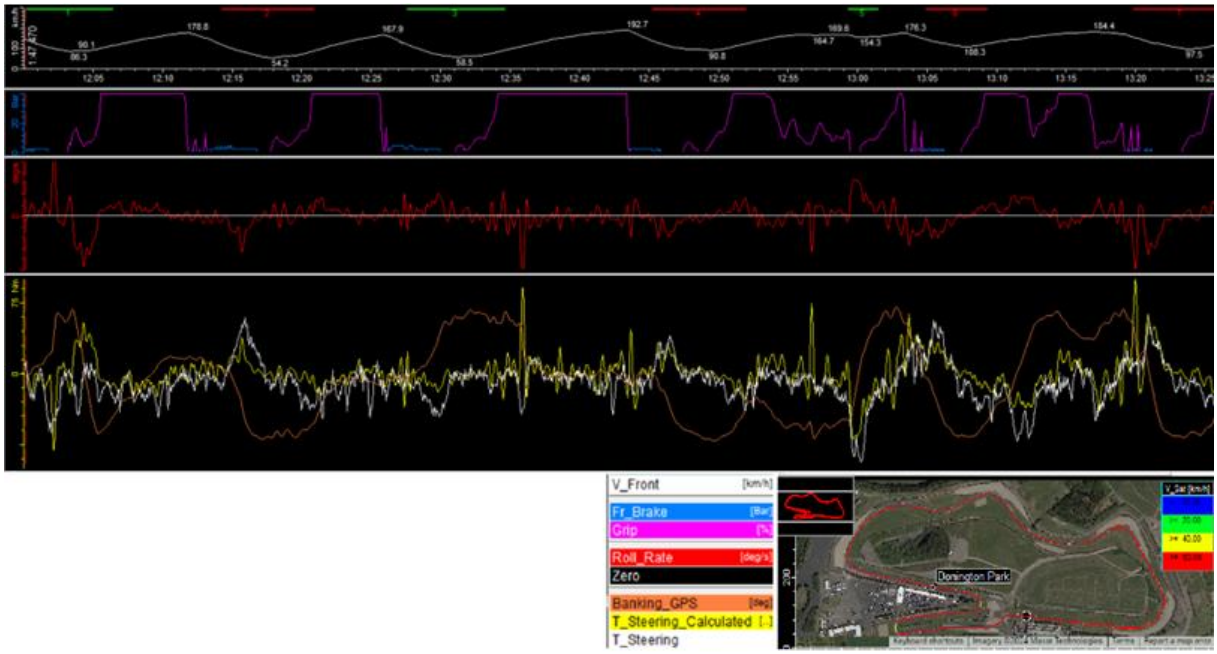

Figure 35: Complete lap of Donington Park with Steering Torque measurements.

Figure 35 shown above shows a complete lap around Donington Park, the bottom area shows the calculated steering torque and the measured steering torque. It is visible that the general trend and magnitude of the calculated values and measured values are similar to some degree. Though velocity changes with regards to the longitudinal forces that arise at the front and rear contact patch during acceleration and braking also control the steering input that is required of the rider due to a coupling between in-plane and out-of-plane dynamics, which significantly affects motorcycle behavior (Cossalter et al. 2011a). For which the calculation model doesn't account, the following will discuss some of the major limitations and differences involved.

Unless the motorcycle is perfectly upright, applying the front brake generates a braking force between the front tire and the road surface, which creates a misaligning torque around the steering axis. This torque causes the motorcycle to reduce its roll angle unless the rider compensates by applying a resistive steering torque to counteract this effect (Cossalter et al. 2011a).

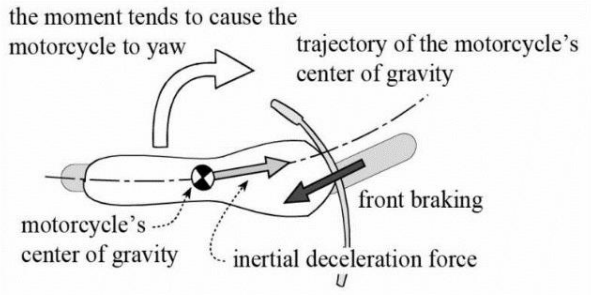

Figure 36: Graphical representation of the yawing effect during hard braking. (Cossalter 2006)

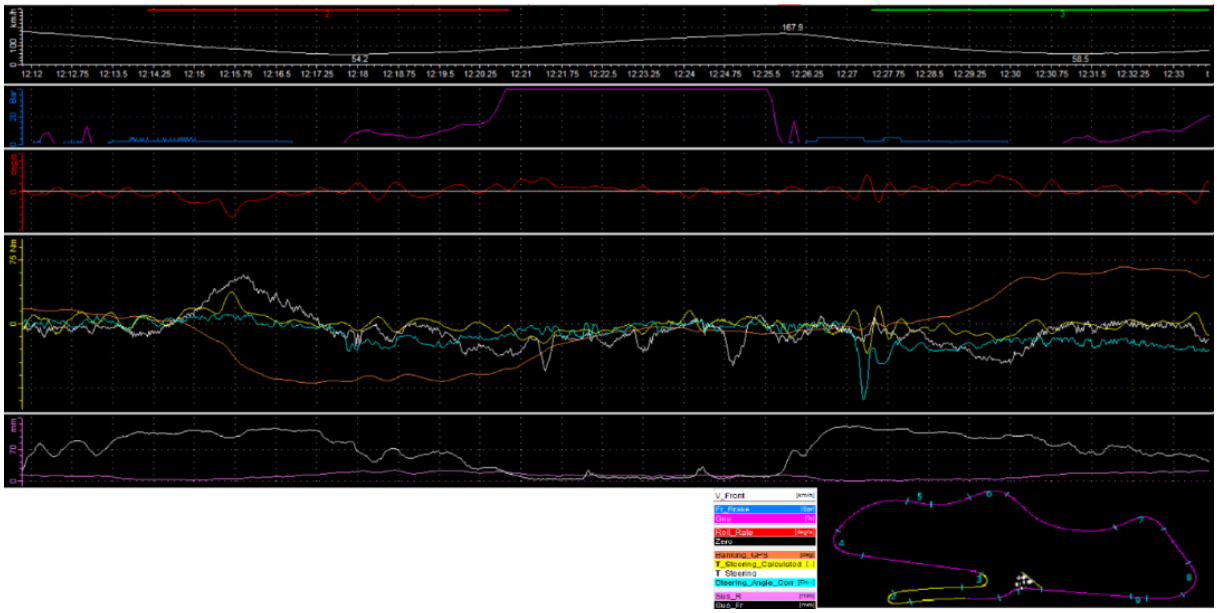

Figure 37: Enlarged section from 'Melbourne Hairpin' to 'Goddards'.

Figure 37 shows an enlarged section of the previously presented data set recorded at donington park, covering the section highlighted in yellow on the track map, focusing on the braking sections coming into 'Melbourne Hairpin' (T11) and 'Goddards' (T12).

The blue trace in the second area of the 2D Analyzer software shows when the front brake is actived, unfortunately brake pressure wasn't recorded, though braking behaviour can be derived from the front suspension trace in the bottom area.

Between minutes 12:15 to 12:17.25 and 12:28.5 to 12:30, the data channels plotted in the fourth section indicate that during braking, the measured steering torque magnitude exceeds the calculated steering torque. This difference highlights the previously mentioned misaligning effect on the front wheel caused by using the front brake, which opposes the rider's counter-steering effort and necessitates a higher steering torque input to maintain the desired roll rate.

Between 12:27 and 12:28.5, another instance of braking effectively acting as a steering input occurs. If the motorcycle is not perfectly upright—especially during a sudden, hard application of the front brake—weight on the rear wheel diminishes nearly to zero due to load transfer from deceleration. The braking force at the front

contact patch, combined with the inertial force acting at the center of gravity, generates a moment that causes the motorcycle to yaw (as shown in Figure 36). The data in the fifth section shows that the rear suspension is fully extended, and the rear wheel loses contact with the ground, leading to a loss of grip. The rapid change in steering angle and roll rate, without a corresponding significant increase in measured steering torque compared to the calculated value, suggests that the rear of the motorcycle is sliding out and yawing around the steering stem. Once the rear wheel regains traction, the steering angle stabilises again. (Przibylla 2020) has shown the same behaviour around these specific parts of the track.

Figure 38: Toprak Razgatioglu Demonstrating the diminished rear loading and controlling the yawing motion during hard braking. (Paddock-GP, 2024)

Whilst the point of rear wheel lift-off from the ground ultimately limits the amount of front braking that can be utilised (Cossalter 2006; Przibylla 2020), the positive rotation of the chassis around the front frame places the motorcycle differently on the road, implying that it has already accomplished some part of the yaw motion that is required to make the turn. When comparing the entry into both the highlighted corners, which are of similar characteristic, tight hairpins, with hard braking, the entry roll rate is similar to eachother, though the second approach shows less physical effort (steering torque) is required to create the desired change in roll angle. However, the psychological effort and technique that could be required to accurately modulate the braking pressure and control the yawing moment may be higher. Within the available grip limit, the rear brake can be used to stabilise the motorcycle. The rear braking force generates a torque that helps to align the motorcycle, counteracting the yawing moment produced by the front braking force, as illustrated in Figure 39 (Cossalter 2006). This explains why riders find engine braking beneficial on the track and often express dissatisfaction when there is too little of it, as the stabilising and decelerating effects are diminished. The introduction of electronically adjustable engine braking allows engineers to tailor the amount of negative force generated by engine braking to suit the riders preferences and optimise performance. Figure 40 shows an example of motorsport

electronics packages where the braking force generated by the engine brake can be adjusted by lean angle, gear, and even corner by corner (BMW Motorrad 2022).

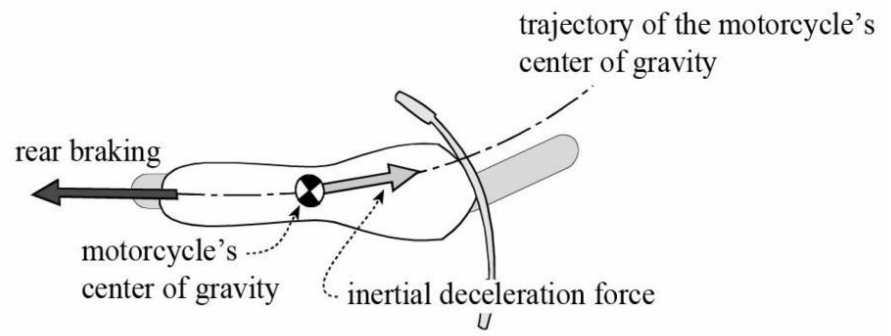

Figure 39: Graphical representation of the aligning moment induced by the rear braking force. (Cossalter, 2006)

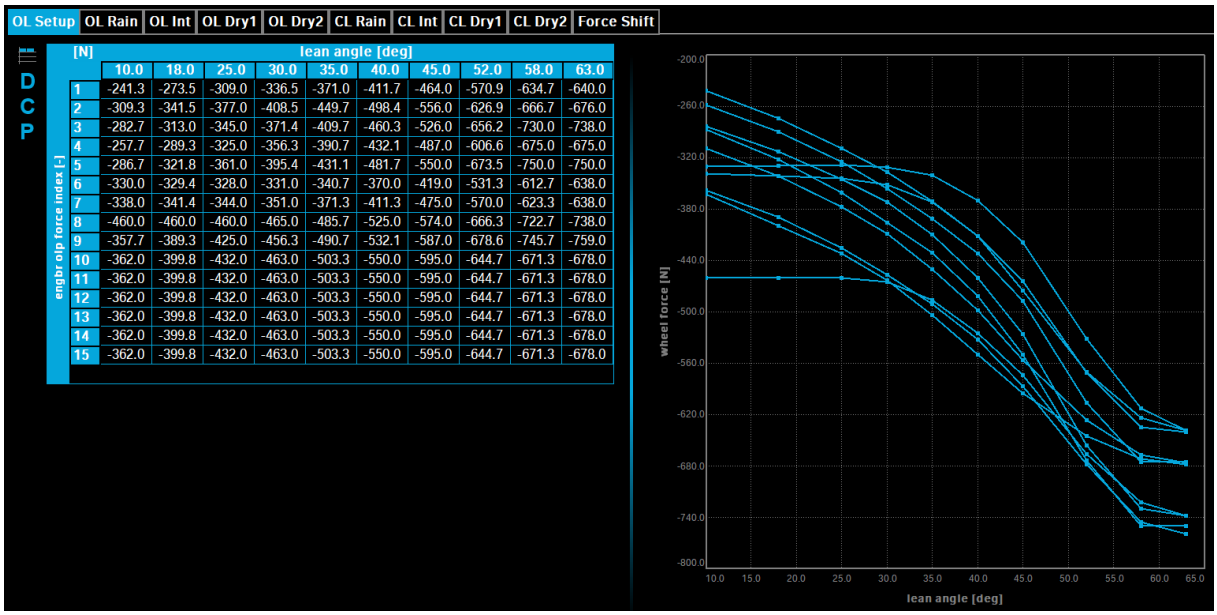

	10.0	18.0	25.0	30.0	35.0	40.0	45.0	52.0	58.0	63.0
1	-241.3	-273.5	-309.0	-336.5	-371.0	-411.7	-464.0	-570.9	-634.7	-640.0
2	-309.3	-341.5	-377.0	-408.5	-449.7	-498.4	-556.0	-626.9	-666.7	-676.0
3	-282.7	-313.0	-345.0	-371.4	-409.7	-460.3	-526.0	-656.2	-730.0	-738.0
4	-257.7	-289.3	-325.0	-356.3	-390.7	-432.1	-487.0	-606.6	-675.0	-675.0
5	-286.7	-321.8	-361.0	-395.4	-431.1	-481.7	-550.0	-673.5	-750.0	-750.0
6	-330.0	-329.4	-328.0	-331.0	-340.7	-370.0	-419.0	-531.3	-612.7	-638.0
7	-338.0	-341.4	-344.0	-351.0	-371.3	-411.3	-475.0	-570.0	-623.3	-638.0
8	-460.0	-460.0	-460.0	-465.0	-485.7	-525.0	-574.0	-666.3	-722.7	-738.0
9	-357.7	-389.3	-425.0	-456.3	-490.7	-532.1	-587.0	-678.6	-745.7	-759.0
10	-362.0	-399.8	-432.0	-463.0	-503.3	-550.0	-595.0	-644.7	-671.3	-678.0
11	-362.0	-399.8	-432.0	-463.0	-503.3	-550.0	-595.0	-644.7	-671.3	-678.0
12	-362.0	-399.8	-432.0	-463.0	-503.3	-550.0	-595.0	-644.7	-671.3	-678.0
13	-362.0	-399.8	-432.0	-463.0	-503.3	-550.0	-595.0	-644.7	-671.3	-678.0
14	-362.0	-399.8	-432.0	-463.0	-503.3	-550.0	-595.0	-644.7	-671.3	-678.0
15	-362.0	-399.8	-432.0	-463.0	-503.3	-550.0	-595.0	-644.7	-671.3	-678.0

Figure 40: Engine Braking Force over Lean Angle and it's adjustability. (BMW M Race Calibration, 2022)

Thus, it can be seen that the proper use of the front and rear brakes, as well as engine braking, has a stabilising effect on the motorcycle. Previous observations indicate that longitudinal accelerations can be considered additional steering control inputs. Theoretically, when a motorcycle travels at a constant speed through a turn, it maintains a constant circular path unless the rider adjusts the motorcycle's attitude. In a steady-state turn, this implies that no significant steering torque or inputs are needed to follow the path. Figure 41 illustrates an example of this mid-corner behavior, where neither brakes nor throttle are applied, and the roll angle remains steady, resulting in near-zero steering torque.

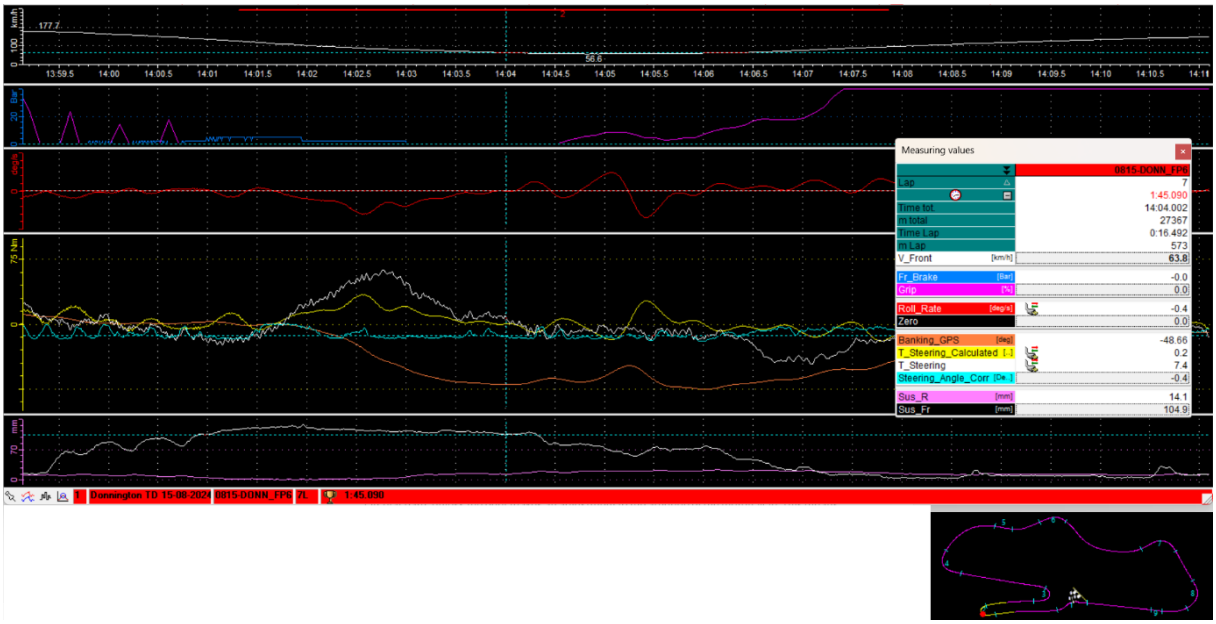

Figure 41: Melbourne Loop Mid Corner Highlight.

Applying a negative steering torque increases the roll angle and tightens the path, while applying a positive steering torque decreases the roll angle and widens the path. However, depending on its velocity, the motorcycle may follow the same path despite carrying a different roll angle, meaning that the path can also be adjusted by accelerating or decelerating.

The previously discussed dataset shows that decelerating by applying the front brakes can create a misaligning torque that the rider must resist to prevent a sudden change in roll angle. In contrast, applying the rear brake does not directly generate an equivalent torque around the steering axis since the braking force acts at the rear contact patch. Instead, rear braking may contribute to the overall steering torque by generating a moment that increases the normal force on the front contact patch, similar to load transfer. However, any additional steering torque from this increased normal force is likely counteracted by the steering torque generated from the corresponding increase in lateral force at the front contact patch, as observed with front brake application (Cossalter et al. 2011a).

Thus, the motorcycle's path through a turn can be tightened by applying the rear brake, but without the need to counteract an increasing steering torque. This allows the front frame assembly to self-adjust and restore cornering equilibrium.

An example of how - the previously mentioned misaligning effect of using the front brake while leaning - can assist the rider in standing the motorcycle back up is illustrated in Figure 42. this figure shows a sequence from the exit of Old Hairpin (T4) through Sharkey’s Bridge (T5 & T6) into McLean’s (T7). In this sequence, the rider exits a fast right-hander and continues through two long left-handers, staying on the throttle, under continued lean angle, until McLean’s, reaching speeds of up to 182 km/h on the RS660. At the point where the rider applies the brakes, the motorcycle is leaned over at a -48° roll angle. Between time marks 13:19.5 and 13:20.5, the data shows that the steering torque applied by the rider is lower than the calculated torque based on the roll rate. This confirms the effect of the misaligning torque caused by applying the front brake while leaning, which reduces the roll angle (Przibylla 2020). As the motorcycle approaches the upright position

and braking pressure decreases, the required steering effort to adjust the roll angle aligns more closely with the calculated values.

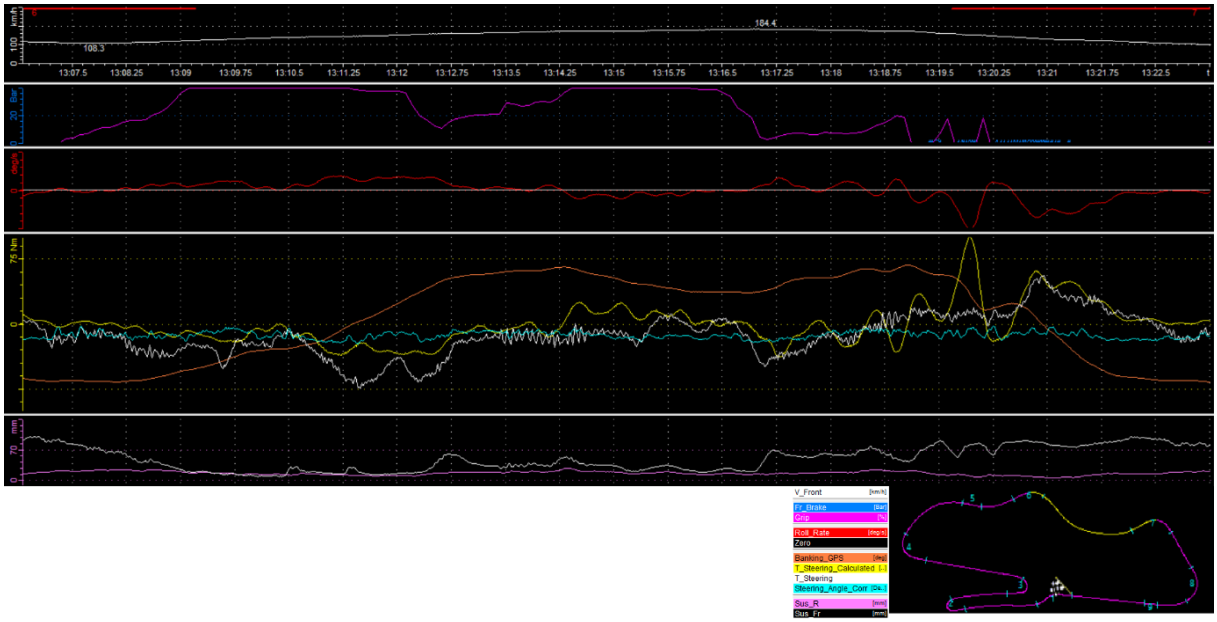

Figure 42: 'Old Hairpin' to 'McLeans'.

Another motorcycle control phenomenon commonly observed among skilled riders, and supported by previous studies (Przibylla 2020), is that applying throttle—thereby generating a driving force at the rear—can be used to decrease the yaw angle, widen the path, and reduce the roll rate. Between time mark 13:05.25 to 13:13.5, the measurements show (Figure 42) a suspicion towards this phenomenon, as the rider needs to apply an increased steering torque to counteract the reduced roll angle and widening path when accelerating, to maintain a tighter line. Between 13:14.25 and 13:15.75, as the roll angle decreases and the path widens toward the outside of the track while the rider remains on the throttle, the steering input is lower than the calculated amount related to the change in roll angle, further confirming this effect.

Riders have reported that an identical motorcycle, when lowered by a certain amount in both the front and rear suspension, with a lower center of gravity, tends to run wide more easily and picks up more quickly when getting on the throttle, compared to a higher bike. Conversely, a higher bike feels more challenging to pick up and switch direction, but it also offers greater stability in long corners when on the throttle (Harrison 2023). Although this phenomenon has not been precisely defined, it is suspected that a higher center of gravity increases the influence of the weight force (m*g) during cornering. The moment generated to the contact patch is greater with a higher center of gravity compared to a lower one with the same weight force. This means that more effort is required to counteract this force when picking the bike up, whether by applying throttle or manually changing direction, such as in a chicane.

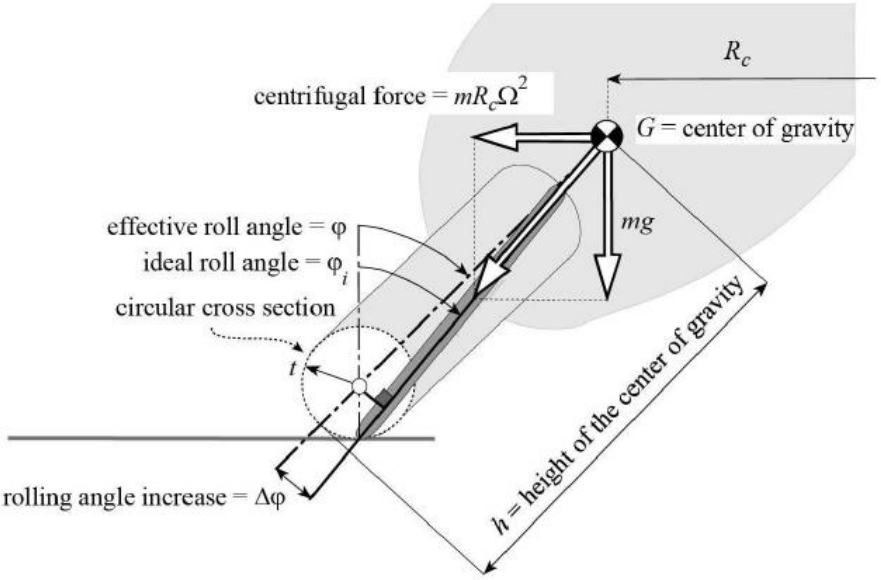

Figure 43: Steady Turning Motorcycle equipped with real tires (Cossalter, 2006)

Using the MotoSpec calculation function, the sixth area shows the ground trail at each point in the dataset. A sequence between Redgate (T1) and Coppice (T8) is displayed below (Figure 44), with the cursor placed at a point where the rider significantly closes the throttle in this fast corner (T5) to able to aim the bike better. The data shows that as the throttle is applied and acceleration occurs, load transfer reduces the load on the front, extending the suspension and increasing the ground trail value. This increase in ground trail enhances the aligning effect, pulling the front frame more in line with the rear frame, which is suspected to aim the front wheel further towards the outside, widening the path and decreasing the roll angle.

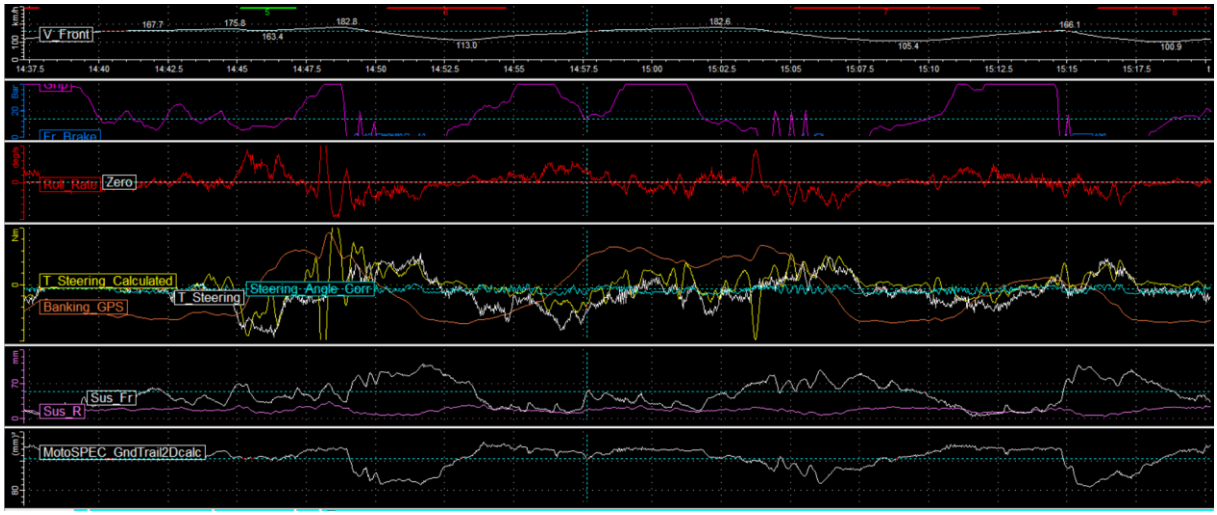

Figure 44: Sequence between Redgate (T1) and Coppice (T8) highlighting ground trail through Starkey's Bridge (T5).

The previous section of the discussion provided a comparison at the same parts around Donington Part with (Przibylla 2020)'work, investigating and validating certain phenomena related to steering and handlebar force input measurements. The following section will explore new insights regarding the forces applied to the footpegs during riding and analyse findings from the recorded data.

7.2 Footpeg Input Analysis

The following part will discuss some findings regarding footpeg loading and measurements conducted during this project, as previously mentioned, no true analysis of footpeg loading has been done or no records of high performance recordings regarding this have been found, thus the following part will be adding to knowledge and discussing findings from the current measurements.

A validation of the measurement system's integrity was demonstrated through a weight measurement. As Rider 1 exited the pit lane and lifted their lower body completely off the seat to check for oncoming riders, the footpegs recorded a total weight of 75kg, with an additional 3kg combined load on the handlebars. This totals 78kg, which matches the rider's weight including riding gear, confirming the accuracy of the force input calibrations.

Figure 46 shows an example of the riders standing up to look over their shoulders in order to exit pitlane.

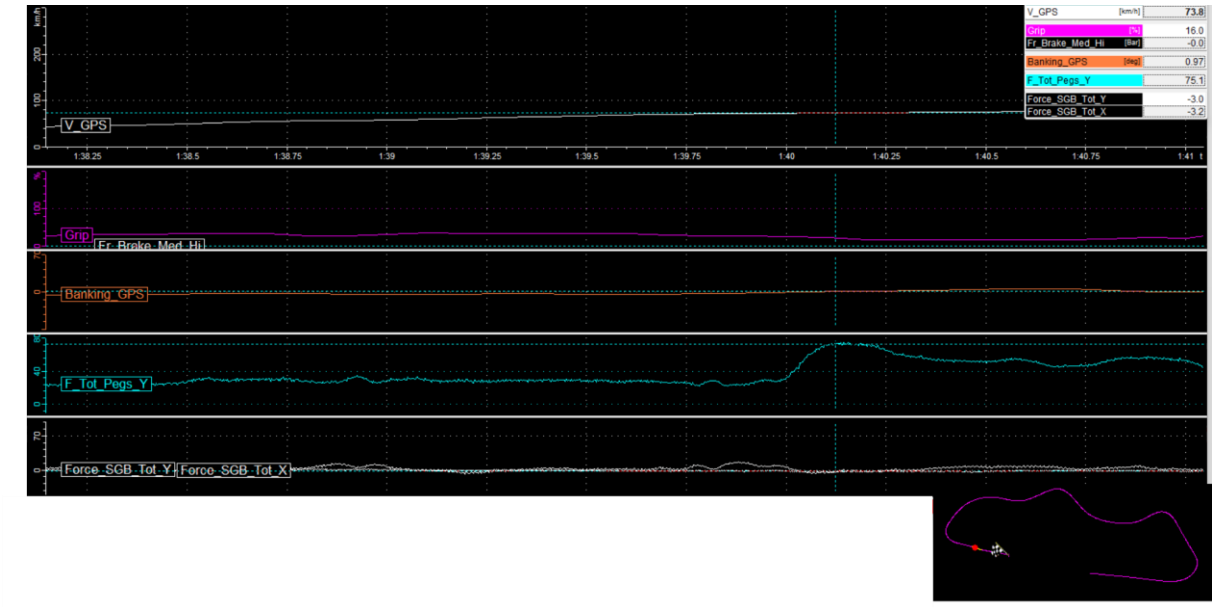

Figure 45: Track Exit weight validation.

Figure 46: Riders standing up, looking over to exit pitlane.

As previously mentioned, a total rolling torque is calculated, indicating on what footpeg the most force is input and what rolling torque compared to the symmetry plane of the motorcycle is generated.

Figure 47 shows a complete lap around the Donnington GP circuit, Area 6 displays the calculated resulting rolling torque from both footpeg torques, the results indicate that during cornering, a rolling torque is generated towards the inside of the corner, every corner. Indicating that the most force/ weight is supported by the inside footpeg, contrary to some beleifs (Life at Lean 2024). On the straight, the resulting rolling torque is around zero, indicating there is a balance between input on the two footpegs.

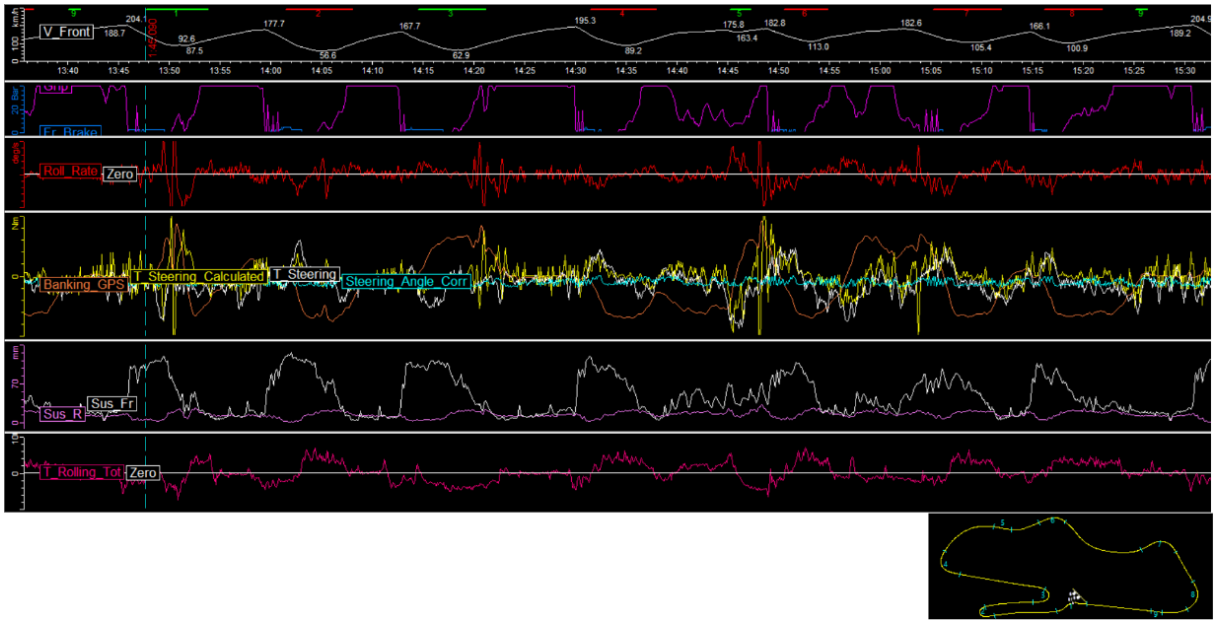

Figure 47: Full lap displaying Resulting Rolling torque from both footpegs.

As higher level riders prepare for braking to go into a corner, the rider moves his body to the inside of the corner on the straight in order to properly position their body and brace for the braking with their legs, and also not to have to move their

body during braking and upset stability and their body during braking. Figure 48 shows a zoomed part of the approach to Redgate (T1) at Donnington, where the rider would be moving from the centre of the seat to the right of the seat. Where the pointer is positioned, it's visible that the throttle closes ever so slightly, a steering negative steering torque is generated, with a small response in roll angle change which corrects right before shutting the throttle and applying the brakes. It's visible that initially the rider applies force on the right footpeg, which is assumed to move the body over, then momentarily an increase of force on the left footpeg is measured, which matches with the rider's blip to downshift, these two peaks are assumed to be because of the pushing motion against the gear lever to downshift twice into the first corner.

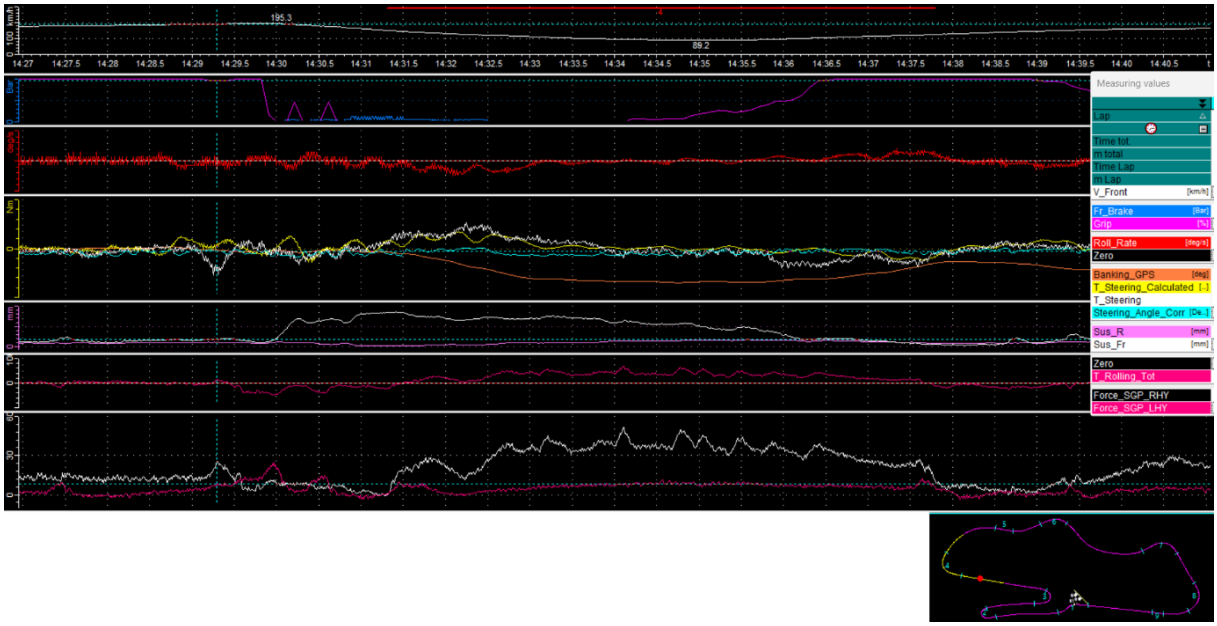

Figure 48: Entry into 'Redgate'.

Throughout the corner, the force on the left footpeg (outside leg) stays reasonably constant at around 8kg, while the inside footpeg shows the highest force, it also shows that the load is varying, indicating that the rider is moving or making adjustments throughout the long corner, adjusting his body, though only minor or no results in roll rate are seen, mid corner during the 'neutral phase', the steering torque is close to zero, the roll angle is constant, and the load on the inside footpeg is 50kg, with the left side at 9kg, totalling to 59kg of load on the footpegs, indicating that 75% of the rider's 78kg weight is supported by the footpegs. Towards the exit of the corner, the load varies and slowly diminishes towards 12-15kg, indicating the rider's legs are relaxed and his weight mostly supported by the seat, after corner exit the steering torque diminishes towards zero except for small steering torques in order to correct the riding line.

In the slowest corner, at 56 kph, it appears that the footpegs have little to no influence on the motorcycle's response, a finding consistent with the road riding test conducted at approximately 45 kph. It seems that when smaller peaks or

changes in roll angle occur, they often align with changes in steering torque, whether minor or significant. Although the rolling torque toward the inside varies, it does not consistently correspond with the motorcycle's response and often lags behind. The small increases or peaks in footpeg force are suspected to be a result of executing a steering torque, likely due to the rider bracing their body to exert the required steering force, with muscles positioning themselves to support the upper body during the maneuver.

The Combined Rolling Torque plotted over Roll Rate doesn’t really show a direct correlation to suspect that a rolling torque initiates a roll/ change in lean angle at speed.

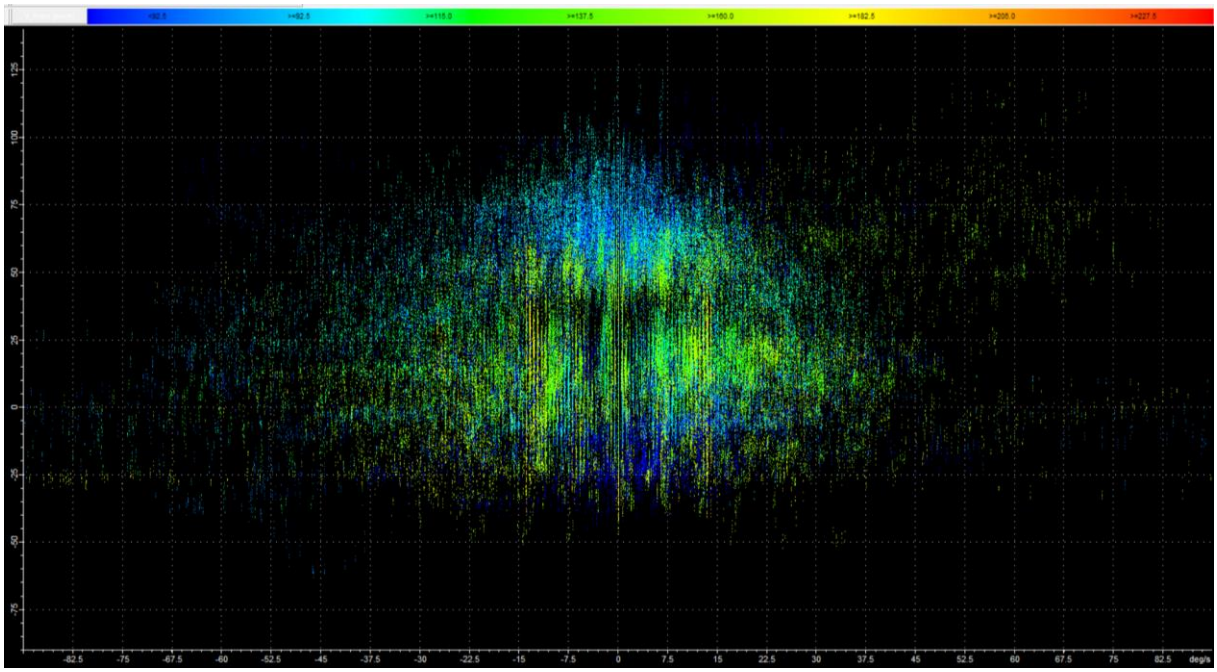

Figure 49: Combined Rolling Torque over Roll Rate over four laps.

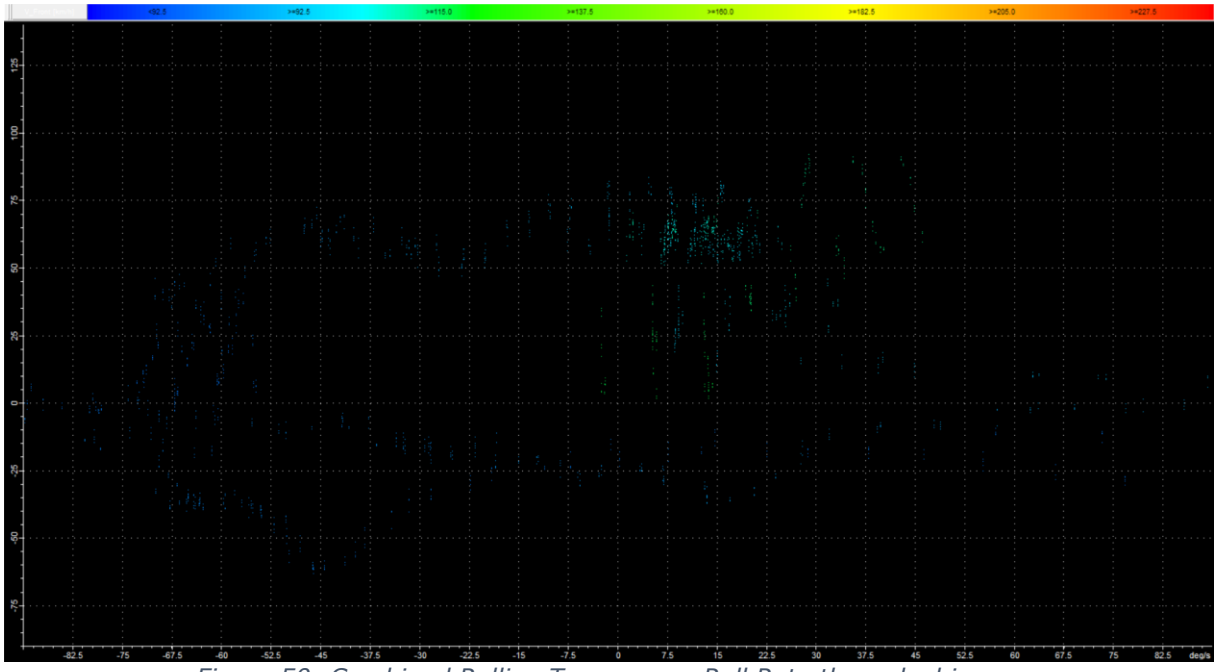

Figure 50: Combined Rolling Torque over Roll Rate through chicane.

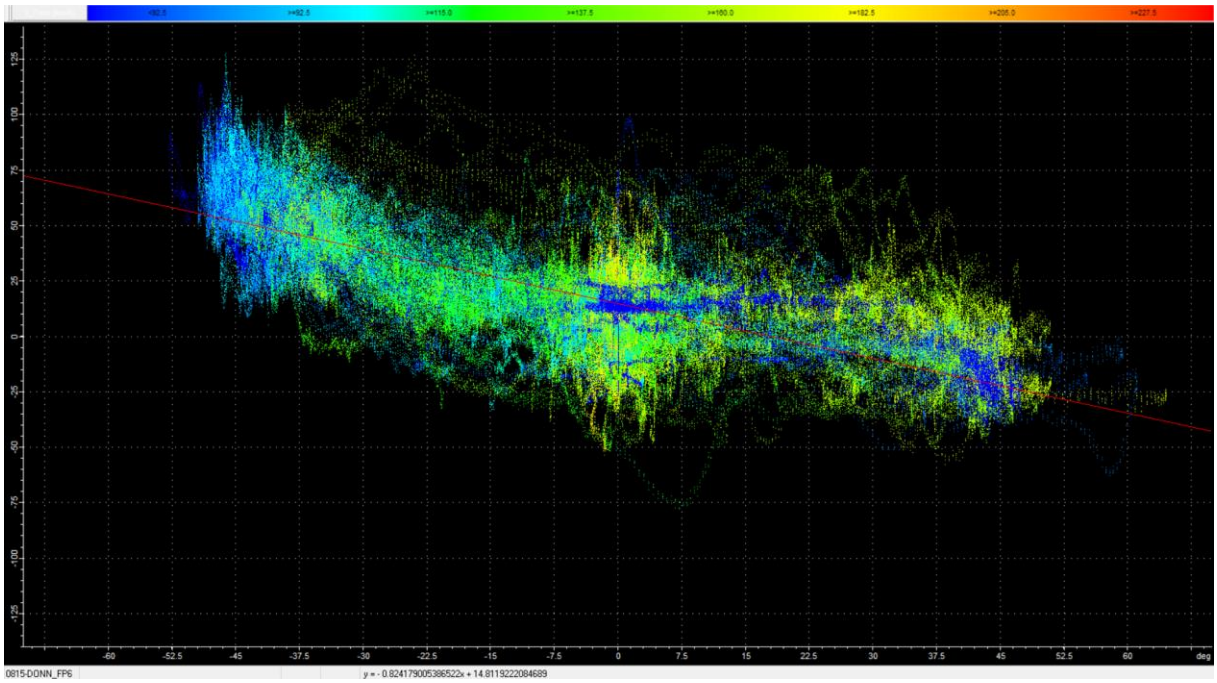

Figure 51: Combined Rolling Torque over Roll Angle all laps.

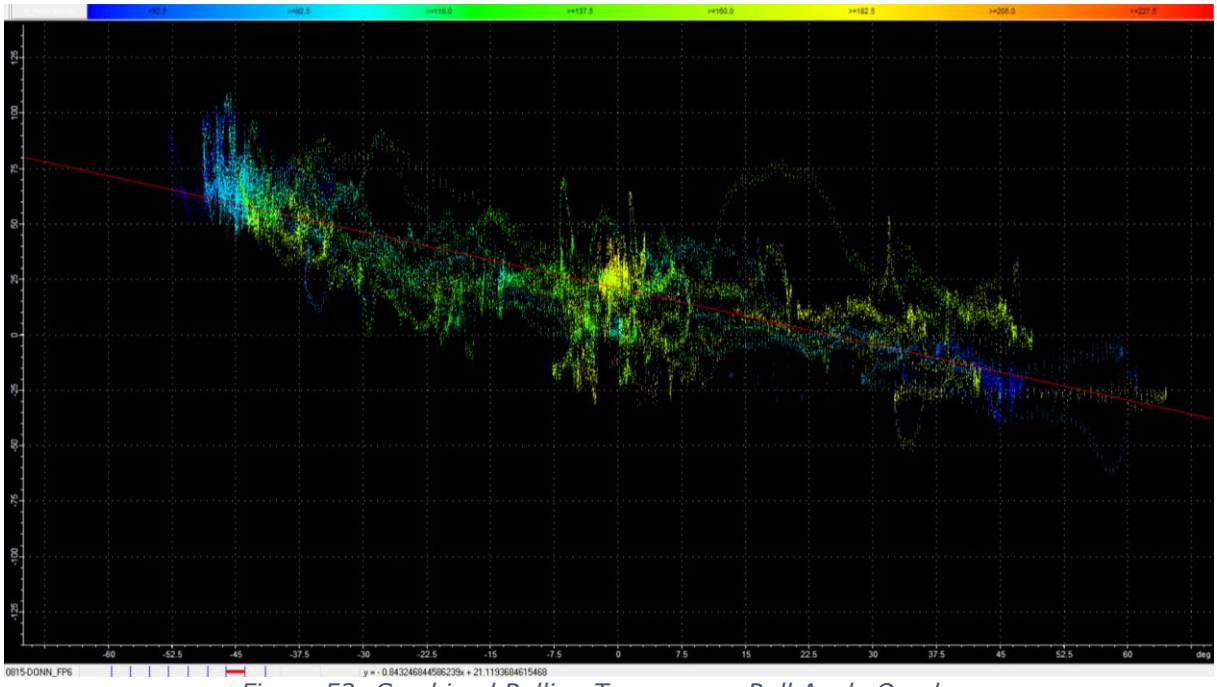

Figure 52: Combined Rolling Torque over Roll Angle One lap.

It can be observed that during right turns (negative roll angle), there are higher rolling torques, indicating more weight on the inner (right) footpeg compared to left turns. This is suspected because the track is predominantly right-hand cornered, with the right-hand corners being faster and longer. The only significant left-hand turns are Craner Curves, Starkey's Bridge, and the Esses (chicane). This pattern strongly suggests that the inner foot and the force on the inner footpeg consistently bear the most weight, and this supported weight increases with lean angle.

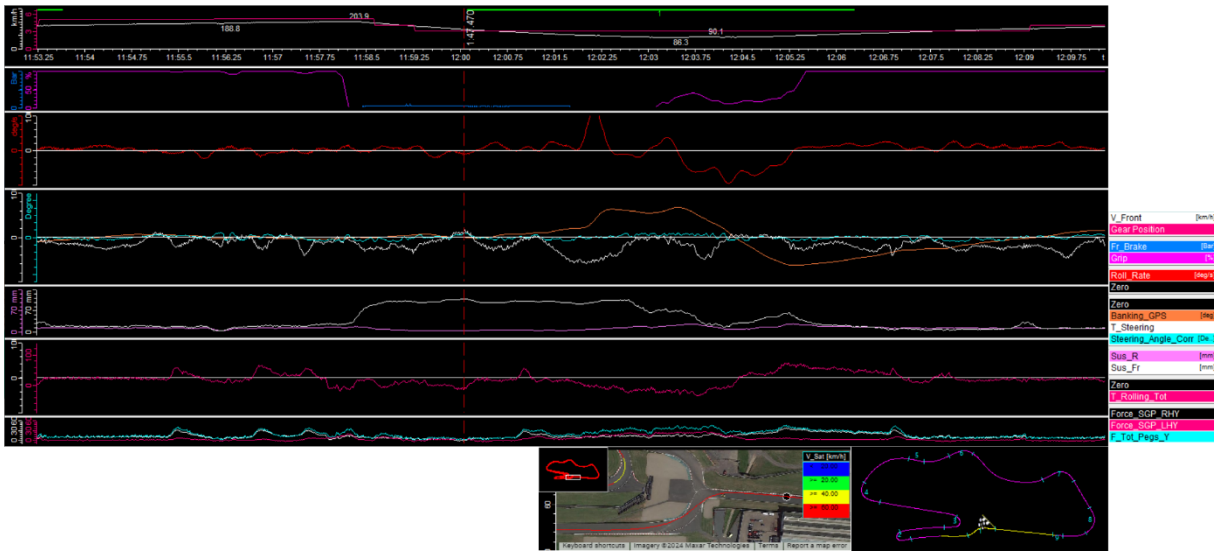

Figure 53: Chicane Analysis 'Esses'.

Figure 53 shows a segment between Starkey's Straight and the Esses (chicane, T9 & T10) at Donington Park GP.

On the initial approach along the straight, up to timepoint 11:56.25, the rider is seen making small adjustments in steering torque to transition the motorcycle from the left side of the track—following the exit from a right-hand corner—over to the right side in preparation for the chicane entry. At 11:56, a small peak in steering torque is observed, along with a drop in suspension travel and a slight shake in the steering angle. This suggests that the front wheel momentarily loses contact with the track due to a dip, reducing load and allowing the steering assembly to move slightly.

At 11:55.5, an increase in right footpeg force is detected. Video footage shows that at this point, the rider shifts his body from the right side of the seat towards the centre, as the roll angle approaches 0 degrees after exiting Coppice. Between 11:57 and 11:57.75, two peaks in right footpeg force are observed, along with smaller fluctuations on the left. The footage indicates that the rider appears hesitant in setting up his body for the corner, making two smaller adjustments rather than one decisive movement. This hesitation could be improved, as more direct movements typically result in less disruption to the motorcycle and increase rider confidence, ensuring they are fully prepared for the next manoeuvre.

Between 11:58.25 and 12:00, a negative steering torque is applied, though with minimal response in roll angle. The rider reported experiencing strong winds during braking in this section, which pushed him towards the outside (right). The data shows the effort required to counteract the wind by applying negative steering torque while braking with the body upright. The left footpeg bears the dominant force, counteracting the upper body's movement and the steering torque.

Just after 12:00, the rider initiates the roll into the corner with negative steering torque. At 12:01.00, the rider shifts his body towards the left once more, having not been fully prepared earlier. At this point, the steering torque diminishes before re-engaging, indicating that inadequate body positioning before braking and turn-

in can affect performance. The effort needed to reposition the body detracts from steering, potentially slowing the turn-in rate and unsettling the bike. If the rider had been properly braced beforehand, it is suspected that he could have turned in faster and carried more speed.

At 12:03, the steering torque decreases toward zero as the rider begins to apply throttle. More steering torque is then added to increase roll angle and correct the path, suggesting that the rider might not be moving fast enough or is lacking confidence to execute the turn more directly. As the throttle is applied, the footpeg forces indicate that the rider is gradually shifting his body rather than making a sudden movement. The diminishing lean angle with lower steering torque reflects the throttle's effect in lifting the bike. Just before 12:04.5, the lean angle shifts from positive to negative, and it is evident that the force primarily applied to the left footpeg during the left turn transitions to the right footpeg as the bike leans into the right corner.

Between 12:04.5 and 12:05.25, as the bike reaches the upright point, the rider eases off the throttle, and a near-zero positive steering torque is applied to maintain the bike’s roll to the right. This suggests that the momentum generated during the bike's pickup, combined with the high centre of gravity due to the rider's position and the forces pulling the bike down during the lean in, is sufficient to sustain the roll towards the right. As the rider then fully engages the throttle, a negative steering torque is applied to widen the line and follow the track’s left-cresting shape.

Figure 54: Chicane Sequence (MotoGP, 2016).

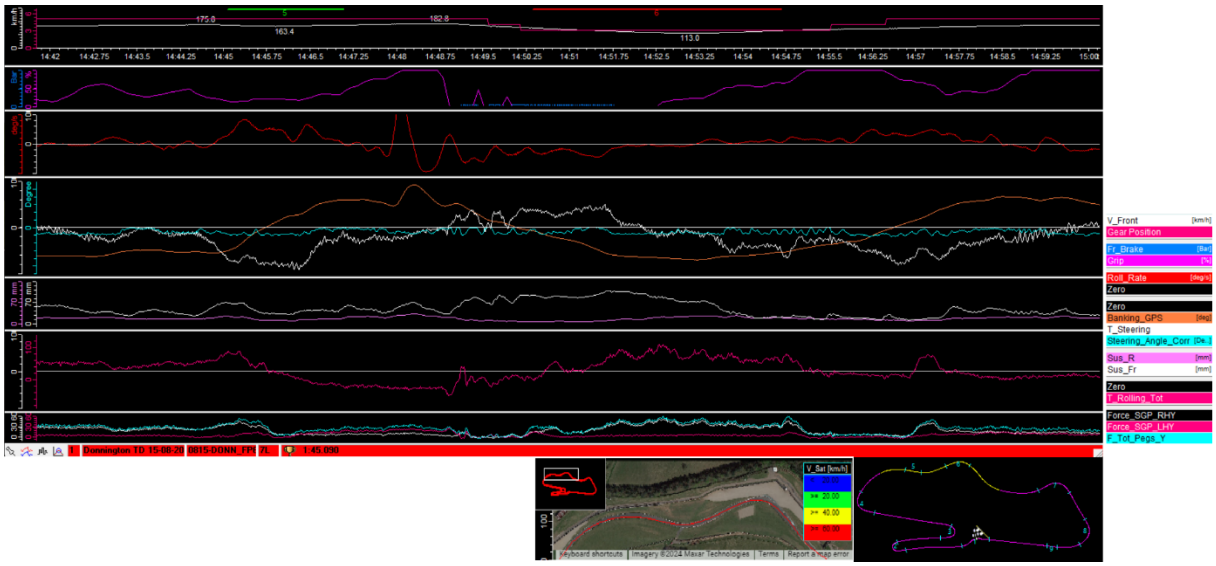

Figure 55: 'Hollywoods' to 'Starkey's Bridge'.

Figure 55 shows a segment between 'Hollywood's' (T2) and 'Starkey's Bridge' (T5) for further rider analysis using the current rider input measurement system.

The sequence begins with the rider leaned over to the right in corner 2, maintaining throttle and applying a negative steering torque to control the line. At 14:45, the rider applies a higher negative steering torque, reaching up to 90Nm, to flip the bike's roll angle to the left in this high-speed corner. The motorcycle is traveling at 175 km/h when the rider initiates the direction change, with the lowest speed during the transition being 163 km/h, hence the high steering torque required. As the roll angle switches at 14:45.5, indicating a change in direction, a peak in footpeg force is measured as the rider shifts his body.

At 14:49, as the rider closes the throttle, begins braking, and initiates the direction change to flip the bike from left to right, another peak in footpeg force is observed, corresponding to the rider shifting his body to the right. As the bike changes direction, the footpeg force transitions from the left to the right footpeg, indicating the force on the inside of the corner.

Between 14:49 and 14:50.25, it is apparent that when the rider blips the throttle to relieve load on the gearbox during downshifting, there is a corresponding reduction in steering torque and brake pressure. This alters the front suspension load, unsettling the bike and decreasing the roll-in rate, ultimately affecting performance. This suggests that, although throttle blipping may feel beneficial to the rider, it is dynamically less advantageous than using an automatic blipper. The rider may need to adapt to using the motorcycle's blipper for better performance.

As the rider gets back on the throttle, he controls the motorcycle's path and roll angle with a fluctuating negative steering torque while exiting the right-hander and gradually moving toward the fast left-hander. It is noticeable that the loading on the inside footpeg is inconsistent, with peaks occurring when additional corrections in steering torque are made. This indicates that the rider is bracing to

exert steering torque, which affects the dynamic response, aligning with the steering torque rather than the increase in footpeg force.

At 14:54.75, the rider shifts from the right side of the bike to the middle, as seen in the footpeg input and visual footage. At 14:57, the rider shifts over to the left. Each time the rider changes position, there is a reduction in steering torque, throttle, or both, demonstrating that minimising body movements allows for more effective steering and control inputs.

The previous analysis proves that the rider input system shows some beneficial insights into the rider's riding, in this case mainly body movement upsetting the motorcycle, reducing steering torque, efficiency of his manoeuvres, how his throttle blipping decreases steering torque, how moving over on the seat in some instances ends up decreasing throttle, the visual footage allowed analysis to see what occurrences seen on the data related to what the rider was doing body wise, while the seat pressure measurement system can add to this, there has still been some good analysis and improvements found from the footpeg input and handlebar input measurements.

As previously mentioned, part of the initiation to build this measurement system, was some common belief of that the rider inputting force on the footpegs resulted in a response or could steer the motorcycle. The rider himself has noticed before that if he'd focus on putting a force on the footpegs while riding, he could initiate a roll, though if he would try the same with his hands off the handlebars, this would not have a roll effect. Together with the previous data and analysis, it is suspected that the pressure on the footpeg helps bracing the body, or initiates a steering torque subconsciously in the way that the body needs to support the force input through his leg. As the data shows, the footpeg inputs don't seem to relate directly to a response in motorcycle roll rate or steering, they occur as when the steering torque increases or in a corner, but don't completely cross over with the response, showing that the motorcycle response, as suspected, mainly comes from counter steering, and not footpeg input. Though, the idea is expected to be usable for riders who might be tiring their upper body too much by not bracing their lower body for steering or are tight on the motorcycle. The system further developed promises some good insights in riding, especially when the possibility arises to put a 'really' good rider on it who can ride up to the limits of machinery.

7.3 Rider Training – Comparison

The following section will explore the feasibility of using the input measurement system for rider training and analysis. Rider 2, who has limited track riding experience, rode the instrumented RS660 on the same day as Rider 1, ensuring bike setup and conditions were identical, allowing for a direct comparison of rider inputs. While it is important to note that not every detail will be considered, given the significant gap in rider experience, the analysis will focus on the main differences and demonstrate the system's potential.

Figure 56: Rider 2 on the RS660 Measurement Platform at Donington Park

The lap time difference between Rider 1 and Rider 2 on the day was 15 seconds, with Rider 2 recording a 2m00s lap time compared to Rider 1's 1m45s. As expected, the key differences include lower corner speeds, later and more hesitant throttle application, earlier throttle release, and longer neutral phases—factors generally associated with less experienced riders. The following section will highlight key insights and demonstrate the usability of the system for rider analysis.

An initial comparison to further validate the integrity of the system is executed by comparing maximum loadings for both riders. With Rider 1 and rider 2 weighing in at 78kg and 96kg respectively wearing all gear as on the motorcycle.

The MinMax Table 4 generated by 2D for the complete session indicates that the maximum footpeg loading for both riders occurs when they shift their body across the seat. However, Rider 1 consistently relies more on his legs during these movements, with 85% of his body weight supported by the pegs, while Rider 2 applies a maximum of 79% of his weight to the pegs. This suggests that Rider 2 uses more of his arms and upper body to support his weight during these transitions.

The highest individual footpeg loading occurs during right-hand turns under lean angle. On average, Rider 1 places a higher percentage of his body weight on the inside peg, with 10% more compared to Rider 2's 30%. However, due to the weight difference between the two riders, Rider 2 ultimately applies more total weight to the inside peg, generating a significantly higher rolling torque through the footpegs. Despite this, no direct impact on the motorcycle's dynamic behaviour is suspected from the data.

Table 4: MinMax Table Steering torque, footpeg loading. Rider 1 (Top) - Rider 2 (Bottom)

Lap	Time	Meters	T_Steering			F_Tot_Pegs_Y			T_Rolling_Tot			Force_SGP_LHY			Force_SGP_RHY		
			MIN	MAX	AVG	MIN	MAX	AVG	MIN	MAX	AVG	MIN	MAX	AVG	MIN	MAX	AVG
0	2:48.080 min	2752	-114.0	69.7	-2.9	-9.6	75.1	19.5	-77.7	99.6	-1.0	-1.5	27.5	10.0	-10.4	58.4	9.5
1	1:49.280 min	3991	-116.9	69.3	-10.3	-9.6	62.6	19.3	-54.0	93.7	17.0	-5.1	27.9	6.1	-9.8	48.2	13.3
2	1:49.080 min	4007	-117.6	75.5	-11.4	-7.2	67.8	22.4	-40.2	109.1	27.8	-4.8	37.1	5.3	-3.1	54.1	17.1
3	1:49.910 min	3976	-114.0	80.4	-9.4	-2.0	65.8	24.0	-57.8	126.7	30.8	-5.0	31.8	5.4	-0.9	57.1	18.5
4	1:51.680 min	4023	-98.9	62.3	-9.8	-3.0	65.2	24.3	-45.4	121.2	24.9	-4.8	30.6	6.9	-1.6	54.7	17.5
5	1:52.010 min	3975	-117.4	68.6	-9.1	-3.2	62.4	22.5	-40.9	108.9	25.5	-5.0	24.5	5.8	-3.1	53.1	16.7
6	1:47.470 min	4009	-112.5	70.2	-9.8	-4.3	66.9	23.5	-43.7	127.5	26.6	-4.7	28.1	6.1	-3.4	59.7	17.4
7	1:45.090 min	4008	-106.9	75.0	-12.2	-4.7	61.8	23.3	-63.0	108.9	27.7	-5.1	28.7	5.8	-3.5	53.1	17.5
8	2:00.850 min	4022	-105.8	63.7	-6.6	-6.0	58.4	19.0	-50.8	95.3	19.2	-5.1	27.1	5.4	-2.9	42.3	13.6
9	1:29.800 min	1023	-74.2	55.0	-1.5	-3.8	48.0	9.7	-41.8	91.5	10.9	-4.3	29.0	2.5	-2.7	40.2	7.1
MIN			-117.6	55.0	-12.2	-9.6	48.0	9.7	-77.7	91.5	-1.0	-5.1	24.5	2.5	-10.4	40.2	7.1
MAX			-74.2	80.4	-1.5	-2.0	75.1	24.3	-40.2	127.5	30.8	-1.5	37.1	10.0	-0.9	59.7	18.5
AVG			-107.8	69.0	-8.3	-5.3	63.4	20.7	-51.5	108.2	20.9	-4.6	29.2	5.9	-4.2	52.1	14.8

Lap	Time	Meters	T_Steering			F_Tot_Pegs_Y			T_Rolling_Tot			Force_SGP_LHY			Force_SGP_RHY		
			MIN	MAX	AVG	MIN	MAX	AVG	MIN	MAX	AVG	MIN	MAX	AVG	MIN	MAX	AVG
0	1:11.890 min	1166	-96.0	39.0	-2.2	-2.3	82.0	31.4	-14.0	166.4	64.7	-6.4	22.4	2.0	-0.2	76.1	29.4
1	2:02.990 min	3957	-85.7	54.8	-6.5	-5.7	71.9	26.7	-41.9	169.3	56.8	-8.5	27.2	1.3	-2.9	71.9	25.4
2	2:01.640 min	3957	-97.8	51.7	-6.0	-5.4	76.1	30.3	-16.3	189.1	71.6	-9.2	25.3	-0.0	-1.1	75.8	30.4
3	2:00.240 min	3953	-89.5	51.5	-6.8	-2.5	79.3	32.8	-6.0	197.0	75.3	-11.2	20.9	0.4	2.8	79.3	32.4
4	8:02.760 min	2631	-78.8	40.3	-0.5	-7.1	82.1	6.6	-7.0	184.2	23.3	-12.1	27.4	-1.7	-2.5	78.3	8.2
MIN			-97.8	39.0	-6.8	-7.1	71.9	6.6	-41.9	166.4	23.3	-12.1	20.9	-1.7	-2.9	71.9	8.2
MAX			-78.8	54.8	-0.5	-2.3	82.1	32.8	-6.0	197.0	75.3	-6.4	27.4	2.0	2.8	79.3	32.4
AVG			-89.5	47.5	-4.4	-4.6	78.3	25.6	-17.0	181.2	58.3	-9.5	24.6	0.4	-0.8	76.3	25.2

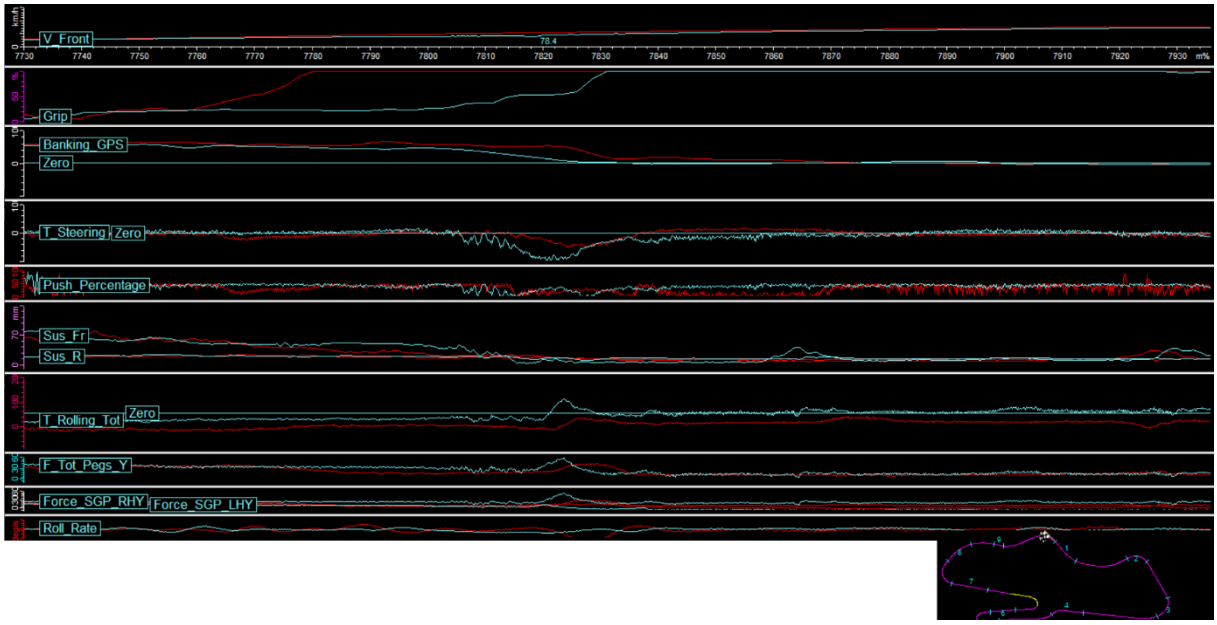

Figure 57:Rider comparison exit 'Goddards' .

Figure 57 presents a comparison at the exit of the final turn onto the main straight. As previously discussed, applying the throttle tends to widen the line and reduce the roll angle. Between 7800m and 7830m, it is evident that Rider 1 opens the throttle earlier and more aggressively, while Rider 2 is more hesitant. Consequently, Rider 2 must apply a higher steering torque to decrease the roll angle on exit, despite being at a lower speed and with a lower roll rate. This comparison reinforces the concept that throttle application can serve as a steering input on the motorcycle.

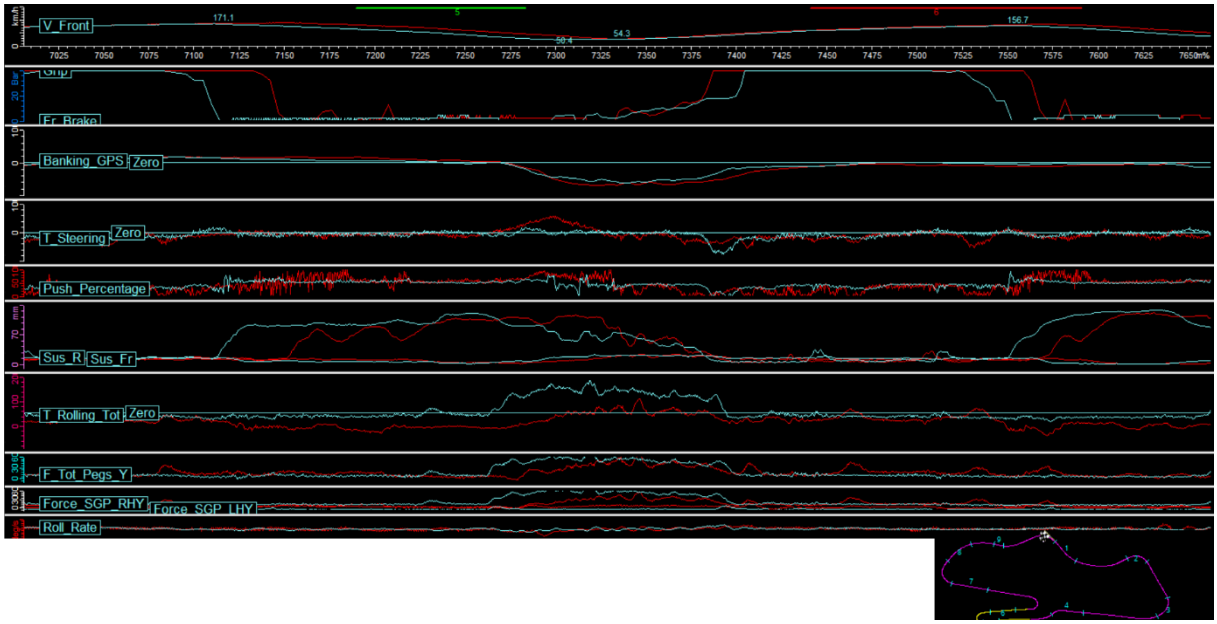

Figure 58: Rider Comparison 'Melbourne Loop'.

Figure 58 presents a comparison of the Melbourne Loop (T11) between Rider 2 and Rider 1. The entry shows a 50-meter difference in their braking points, with Rider 2 braking earlier and reaching his slowest speed of 50 km/h, while Rider 1 continues braking, reaching 80 km/h at the same point. It is evident that Rider 2 does not initiate a roll until he releases the brake, thereby minimising the misaligning effect induced by the front brakes during the roll action. Rider 2 generates only a small initial positive steering torque to begin the roll, after which the significantly higher rolling torque applied through the inside footpeg appears sufficient to overcome resistive forces and allow the motorcycle to continue rolling. At 7300 meters, Rider 2's steering torque is nearly zero, yet the roll angle continues to increase, fluctuating in response to the force on the inside footpeg. Although this occurs at lower speeds without braking, it demonstrates that Rider 2's increased rider mass (96 kg compared to the 153 kg motorcycle mass) can exert a more significant influence through the footpegs.

In contrast, Rider 1 brakes later and significantly harder, carrying his braking further into the turn. Upon entry, a negative rolling torque suggests an increased force on the outer footpeg. Footage and rider feedback suggest that this is to counteract the yawing motion caused by the near-zero load on the rear wheel, as Rider 1 reported the rear wheel lifting in this section. Due to the high level of

braking, Rider 1 requires a significant steering torque to turn the bike, managing the misaligning effect of the brakes and the increased speed during the turn-in manoeuvre. His lowest speed coincides with the highest lean angle, with Rider 1 traveling at 104 km/h at the turn-in point, compared to Rider 2's 67 km/h.

On the exit, Rider 2 appears more hesitant, getting on the throttle later, while Rider 1 applies the throttle earlier and requires less steering torque to decrease the roll angle.

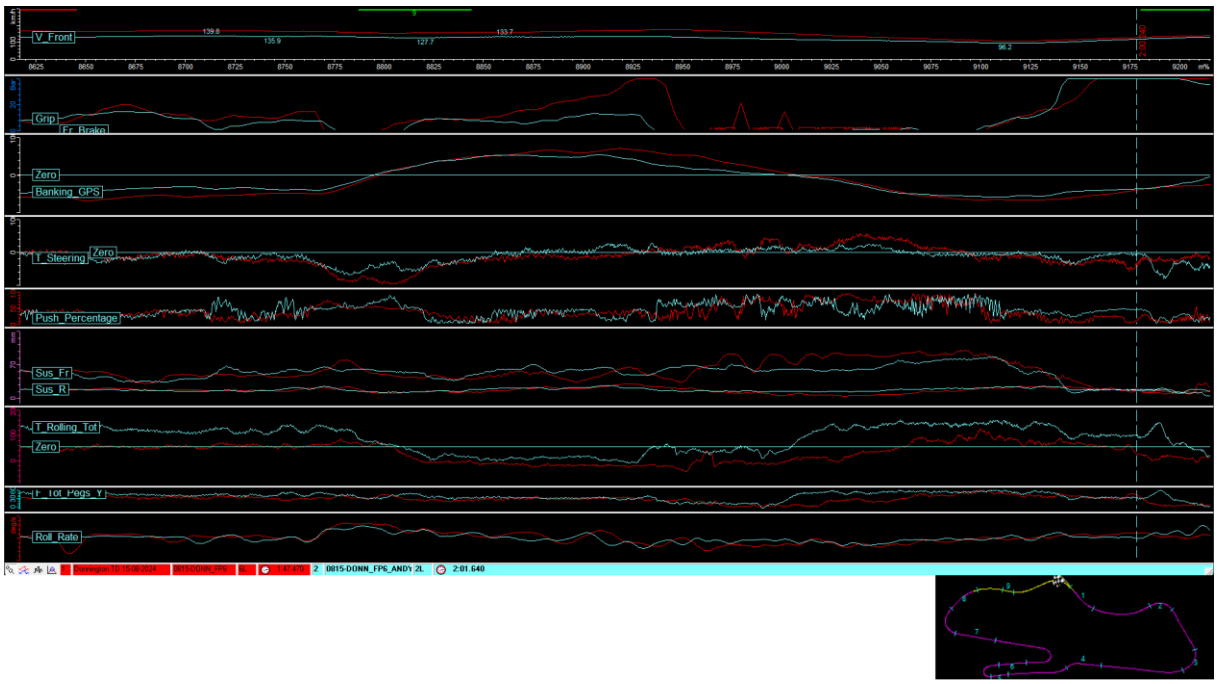

Figure 59: Rider Comparison 'Craner Curves' through 'Old Hairpin'.

Presented in Figure 59, is a comparison between Rider 1 and Rider 2 during a section between Craner Curves (T3) and Old Hairpin (T5). It is evident that through Craner Curves (8800m to 8925m), Rider 1 maintains significantly more throttle, achieving higher speeds and lean angles. In contrast, Rider 2 shuts off the throttle and relies solely on engine braking, while Rider 1 continues to accelerate and brake into the corner.

During the direction change between 8770m and 8820m, Rider 1 generates higher steering torque, resulting in a faster roll rate at higher speeds. For Rider 2, the roll angle is controlled primarily by his steering torque, with little influence from footpeg rolling torque, which is mainly related to pressure on the inside footpeg for bracing.

Throughout the remainder of the direction change and corner, Rider 1's steering torque remains higher to maintain his speed and line, while also counteracting braking forces—something Rider 2 does not need to account for.

Between 9000m and 9060m, Rider 1's footpeg rolling torque remains negative even as the roll angle changes direction, indicating he is applying pressure on the outer footpeg until braking ends and the pressure shifts to the inside footpeg. Rider

2’s footpeg pressure remains on the inside throughout, as he is not braking during this sequence. Rider 1’s use of outer footpeg pressure likely aids in stabilising his upper body during deceleration under lean, which is why more experienced riders can lift their inside leg off the footpeg during braking while maintaining control (Guintoli 2023).

Between 9025m and 9050m, as Rider 2 applies his highest steering torque to complete the roll-in manoeuvre near his maximum lean angle, his push percentage shows that only 30-60% of the steering torque is generated by the inside arm through pushing. The remaining percentage comes from pulling with the outside arm, which could lead to quicker fatigue and less efficient manoeuvres. In contrast, Rider 1 maintains a push percentage between 65-98%, indicating greater efficiency and experience, and demonstrating the effectiveness of this calculated value.

At 9190m, a peak in footpeg force and the video footage indicates where Rider 2 shifts his body weight. Simultaneously, he generates a peak in steering torque, which only causes a minor change in roll angle. This suggests that Rider 2 is using his arms and pulling on the handlebars to move his body around the motorcycle. This behaviour is observed at various exits around the circuit, causing a small shake in the front assembly around the steering stem, which may not be problematic at the moment but could lead to issues at higher speeds, accelerations, or over bumps.

Road Tests showed that Rider 1 could exert very minor changes in roll angle through the footpegs below 50kmh, the motorcycle reverts to ‘conventional steering’ at 34kmh and becomes unstable. Though further measurements are necessary with controlled tests to confirm the influence of footpeg input on roll changes, especially with heavier riders, though the author suspect from the previous measurements that footpeg inputs have no steering to minor input at higher speeds, especially not assumed at very high speeds and higher levels where the motorcycle’s get heavier and the riders get smaller and lighter.

This analysis, along with Rider 1’s earlier measurements, highlights the system is expected to be usable to monitor rider behaviour. While body movement is often pointed out by spotters on the track (Harrison 2023; Bom 2024), this data provides direct measurements that can be used to improve rider performance, efficiency, and ultimately, speed.

7.4 VI Grade Simulation

The multibody dynamics modelling software VI-Grade BikeRealTime was used with an RS660 model previously created by the author and classmate Jacob Quarry to simulate motorcycle behaviour around the Donnington GP circuit. This simulation was conducted to facilitate a comparison with the recorded data. The appendix provides the complete setup of the VI-Grade RS660 model, with all necessary measurements conducted in-house, including centre of gravity, suspension damper dyno testing, spring rate measurements, tire deflection and contact patch measurements, frame measurements, frontal area, and engine power measurements. The only exception was the engine component moments of inertia. A pre-existing track model of the Donnington GP circuit was employed, although the simulation has some limitations, such as the rider following the centreline of the track rather than the racing line observed in real environments. Creating a more accurate path using the measured data is possible but has not been implemented in the current work due to time constraints.

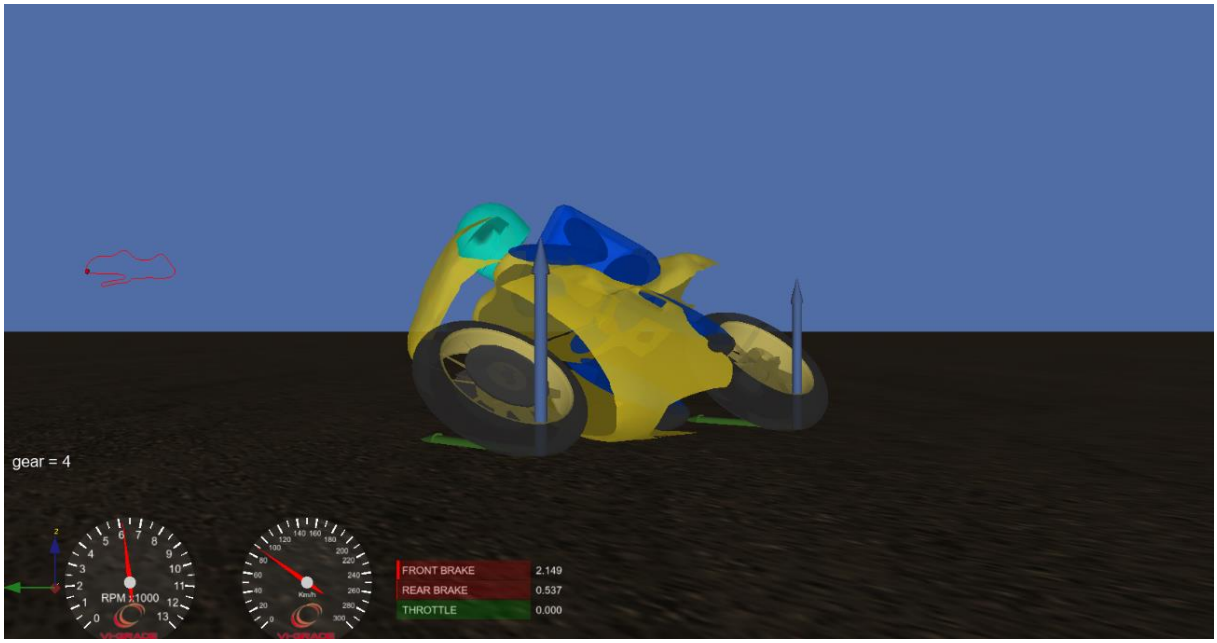

Figure 60: Screenshot of Simulated Animation in VI-Grade 'VI-Animator'.

Previous work using VI-Grade simulations has shown that comparing simulated data with measured lap data can reveal key insights into motorcycle performance and dynamic behaviour. While there were discrepancies, particularly in throttle response and suspension travel, the overall alignment in lean angles and velocity profiles confirmed the model's effectiveness, providing a solid foundation for further refinement and improvements (Iatrakis 2024).

In the current simulation of the Donnington GP track, the velocity profile compares to the real data (Figure 61) , although the differences in rider path and track modelling result in some discrepancies. The lean angle comparison (Figure 62)

reveals noticeable differences, with the model exhibiting a weaving pattern as it struggles to accurately follow the intended line. This limitation is particularly evident on the back straight, where the rider follows a weaving pattern, likely due to the simulation overcompensating during the transition from one side of the track to the other. This also affects the simulated steering torque (Figure 63), which differs from the rider's input. The simulated lap time was 1m48s, compared to the measured 1m45s, reflecting a 2.8% difference. Although the lap times are close, the method by which they are achieved is not entirely accurate.

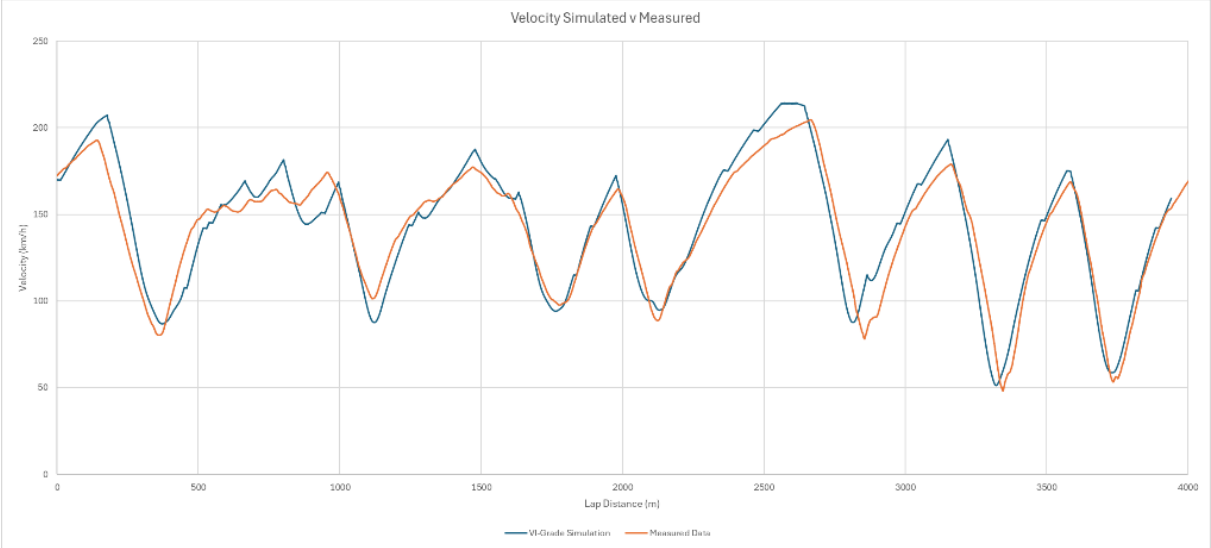

Figure 61: Velocity Comparison VI-Grade V Measured Data.

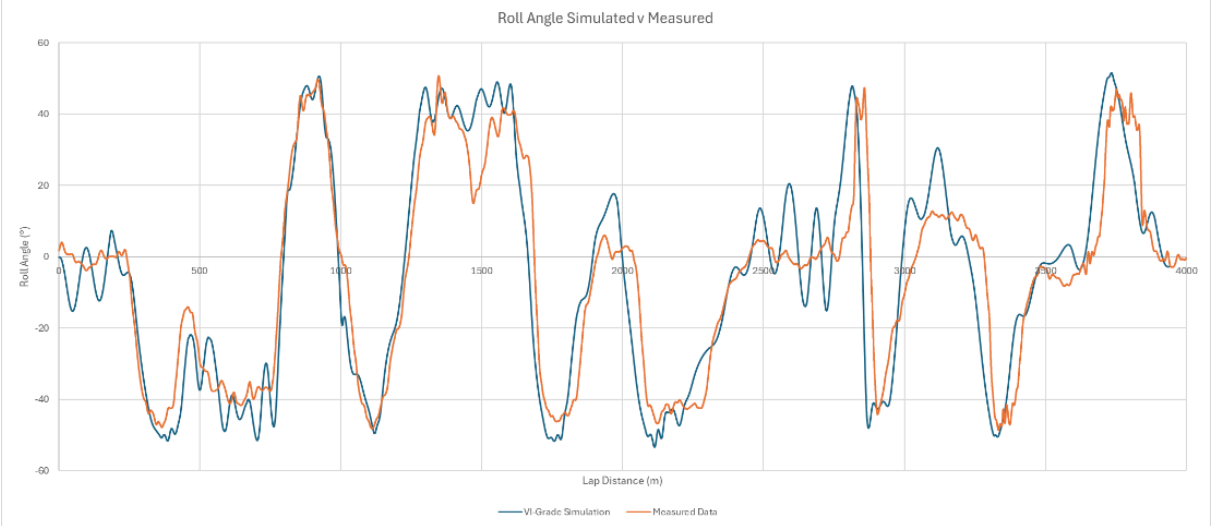

Figure 62: Roll Angle Comparison VI-Grade V Measured Data.

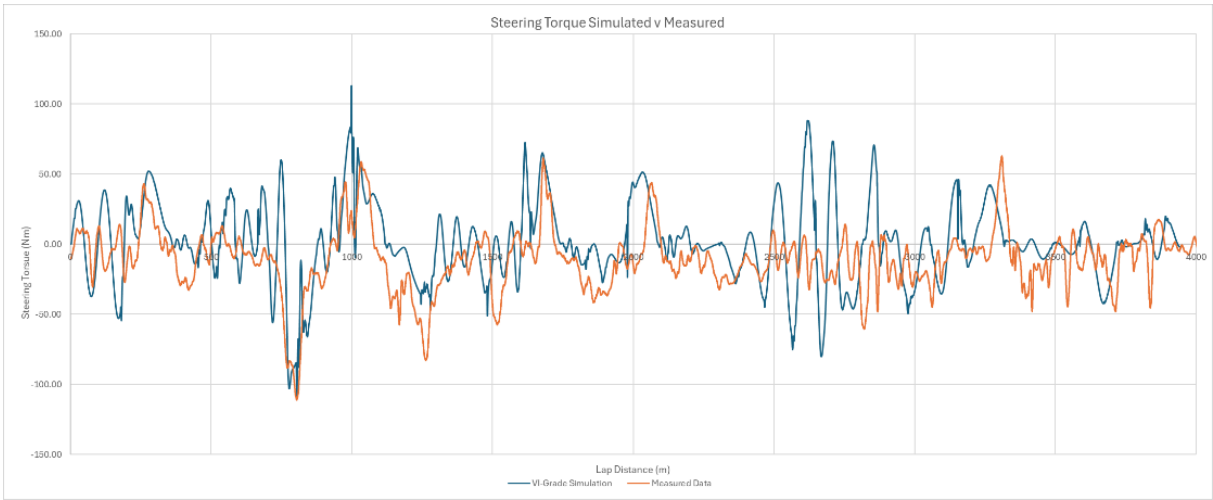

Figure 63: Steering Torque Comparison VI-Grade V Measured Data.

The recorded data from this project allowed for a comparison of steering torque behaviour with the simulated data. Despite being the highest quality motorcycle simulation software available, the VI-Grade model has inherent limitations that lead to overcompensation for certain corrections or unrealistic motorcycle behaviour. However, the simulated data shows a reasonable correlation with the measured data in areas where velocity, roll angle, and roll rate are similar. This suggests that, with further refinement of both the track model and the simulation model's performance, VI-Grade software could generate representative data useful for motorcycle development and baseline setup. With future work and planned controlled tests, such as slalom, which the software has preprogrammed simulations for, the software could be further validated with real data.

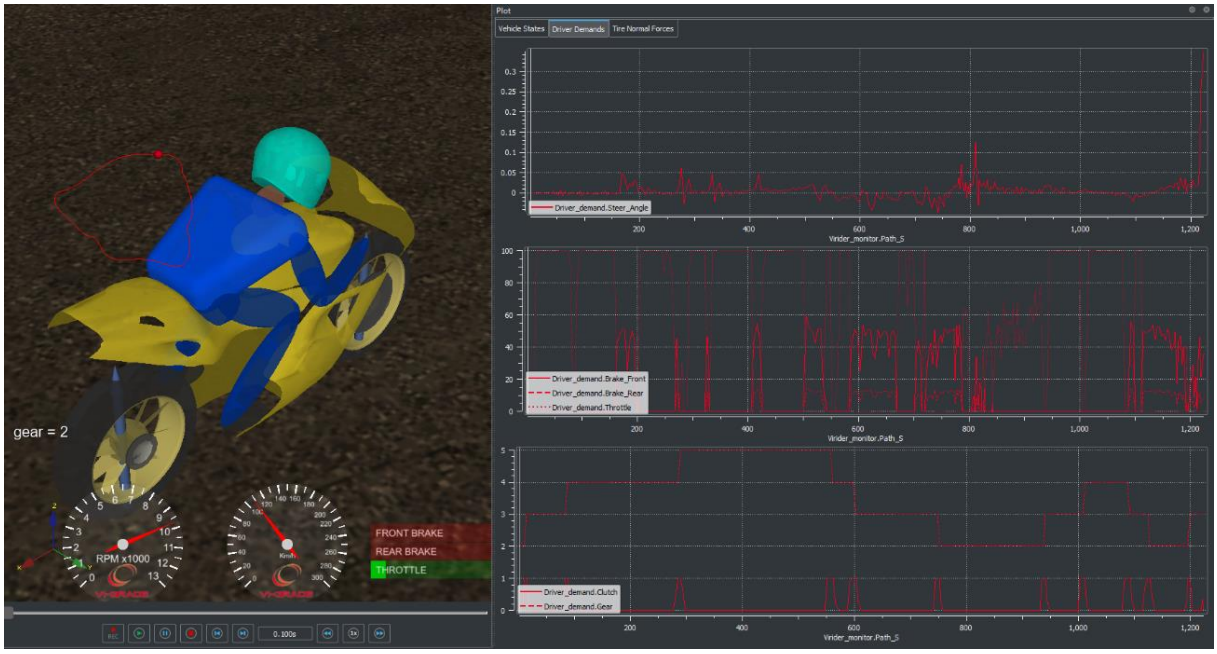

Figure 64: Screenshot of VI-Grade 'VI- Animator' and Data Plots.

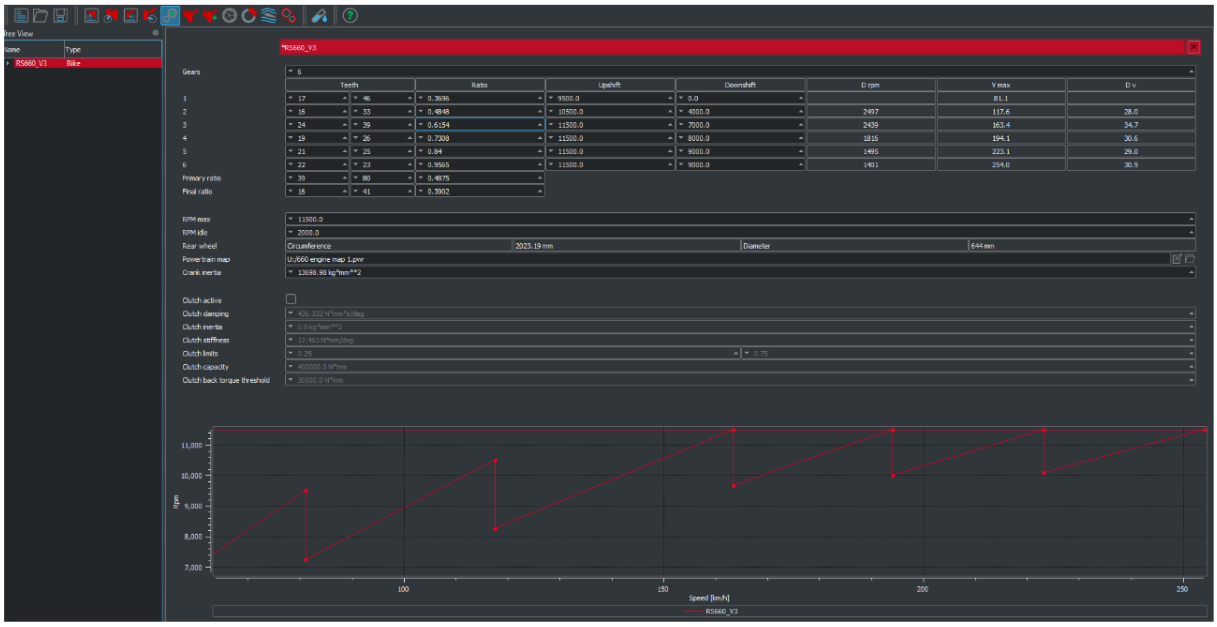

Figure 65: Example of setup page in VI-Grade - Powertrain Setup Page.

8 Further Work

Alongside further developing the Rider Input Measurement system to measure seat pressure, tank pressure, grip pressure in order to complete measurement of the rider inputs, a promising direction for further work involves incorporating electromyography (EMG) measurements, specifically surface electromyography (sEMG), to examine the muscle activity of riders, particularly in relation to the push vs. pull steering techniques. By comparing the muscle activation patterns during these two techniques, it is hypothesized that pulling on the handlebars and gripping the handlebars could place more strain on the forearms, potentially leading to forearm fatigue or "arm pump" (Cohen 2001; Marina et al. 2021). Conversely, pushing may reduce this strain, which could be crucial for improving rider endurance and reducing forearm pump.

(Torrado et al. 2021) conducted relevant research using sEMG to investigate muscle fatigue during motorcycle riding on track. In their study, muscle activation patterns were measured over three 30-minute sessions to assess how different muscles were engaged throughout the riding session. The sEMG signals were recorded unilaterally from key muscles, including the biceps brachii (BB), triceps brachii (TB), deltoid (DA, DP), flexor digitorum superficialis (FS), extensor carpi radialis (CR), extensor digitorum communis (ED), and pectoralis major (PM). Their findings showed that the pushing muscles, such as the triceps and deltoid, played a significant role, while the forearm extensor muscles (ED) were more fatigued compared to the flexors (FS and CR). Additionally, the chest and shoulder muscles (PM and DA) showed increased fatigue as the session progressed.

A limitation of (Torrado et al. 2021)'s study was that the measurements were only taken on the right arm, primarily engaged in braking and throttle control, potentially skewing the results. Measurements on the left arm, which is less

involved in these controls, could provide insights into differences in muscle activation that are unrelated to braking or throttle use. Additionally, the data was not linked to specific motorcycle actions like braking and throttle, limiting its utility in understanding how muscle fatigue correlates with specific riding inputs.

Building on this, the integration of sEMG measurements with the rider input measurement system developed in this project could provide a more comprehensive analysis of how rider inputs, such as steering torque and body movement, correspond to muscle fatigue. This would allow for direct comparisons between muscle effort and the physical forces exerted on the motorcycle, offering valuable insights into rider technique optimization. For example, if pulling on the handlebars places more strain on the forearm muscles compared to pushing, it could be beneficial to train riders to rely more on pushing for steering inputs, thereby reducing forearm fatigue and preventing arm pump. Additionally, this approach could help identify fatigue patterns and specific causes of performance decline, such as muscle overuse during prolonged riding.

Fatigue and Training Considerations

Previous studies, such as those by (Hirono et al. 2022), have shown that muscle fatigue occurs when muscles that are not well-conditioned face continuous strain, leading to swelling and decreased performance. Riders and trainers often debate the need to condition forearm muscles, with some opting not to train them to avoid increasing the risk of arm pump. However, it can be argued that well-conditioned muscles are better equipped to handle strain, reducing the likelihood of arm pump. This balance between muscle growth and endurance needs to be carefully managed, particularly in racing scenarios.

(Marina and Porta 2011) have examined rider fatigue during a 24-hour endurance race highlighted the decline in grip strength and forearm muscle efficiency over time, as measured by sEMG. This study demonstrated that as muscle fatigue set in, more effort was required to perform the same tasks, such as gripping the handlebars or braking. Shorter rest intervals, simulating race conditions, were recommended for future testing to more accurately capture the progression of muscle fatigue in motorcycle riders.

By combining the further developed force input measurement system with sEMG analysis, future work could focus on understanding how different riding techniques impact muscle strain and fatigue. In a combination with the current system to analyse how the amplitude of the rider’s input forces change over time and as the rider fatigues, this information could be valuable for designing targeted physical conditioning programs aimed at reducing fatigue and improving rider performance.

Controlled Tests

Controlled tests are planned for the future to further analyse transient effects and body usage in motorcycle control using the enhanced rider input measurement system. VI-Grade offers the ability to simulate pre-set slalom tests. Previous studies found in the literature (Cossalter et al. 2011a; Bartolozzi et al. 2023a) have utilized similar manoeuvres. Based on these references, the author has developed the following test plan to align with both previous experiments and the VI-Grade simulations.

Table 5: Controlled Test Manoeuvres.

Type	Geometry
Steady Corner	Centreline Radius 15m
Steady Corner	Centreline Radius 12.5m
Lane Change	3m x 14m
Lane Change	2.75m x 5.5m
Slalom	Cone spacing 7m
Slalom	Cone Spacing 14m

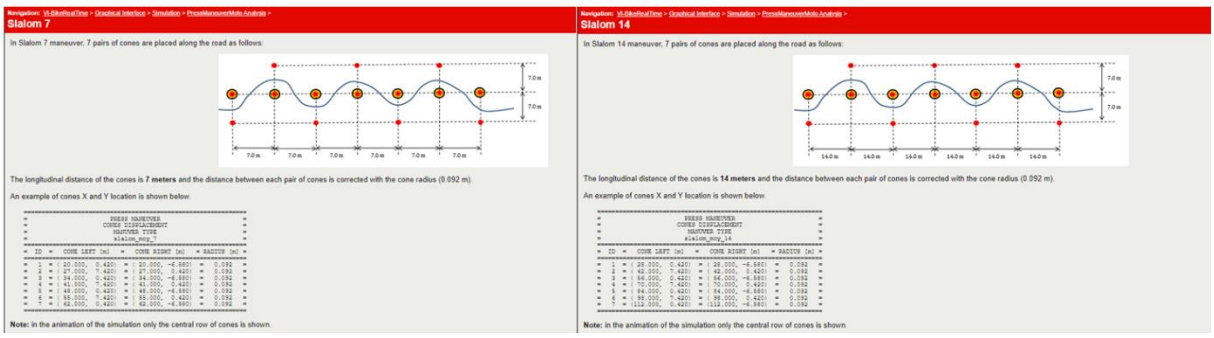

Figure 66: VI-BikeRealTime Slalom Manoeuvres.

Updated Footpeg Input Measurement System Integration

CAD drawings of the footpegs have been created to enhance the integration and robustness of the footpeg measurement system, improving both its appearance and functionality. These designs are intended for CNC machining as part of the continued development of the measurement system.

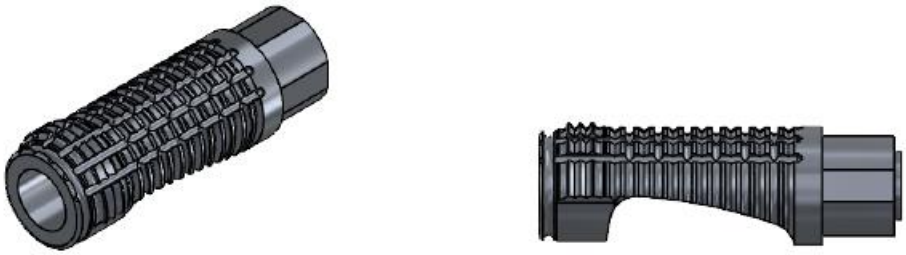

Figure 67: Footpeg Design for Updated Integration of Strain Gauges.

Conclusion

This project successfully created a novel rider input measurement platform that offers valuable insights into how riders interact with their motorcycles, particularly in high-performance environments. The system was developed to collect and analyse data on handlebar forces, footpeg inputs, and steering torque, leading to a more in-depth understanding of how rider movements impact motorcycle dynamics. While much of the foundational work by (Przibylla 2020) was validated, this research also presents challenges to some conventional beliefs in motorcycle racing.

One of the primary findings was the suspicion that counter-steering through the handlebars is the dominant input for changing direction. Although footpeg forces have been previously thought to influence steering, the data suggests their main role is in supporting the rider's body and aiding in manoeuvring, particularly during high-speed cornering and braking. Specifically, riders tend to use the outside footpeg to counteract the yawing motion caused by reduced rear-wheel load, while the inside footpeg stabilizes the rider's body mass during cornering without contributing directly to steering.

The analysis also revealed that experienced riders utilise their body weight and footpeg forces more effectively, particularly during transitions between turns and during braking. More skilled riders distribute their weight in ways that reduce upper body strain and improve overall stability. For instance, during braking, experienced riders shift their weight to the outside footpeg, helping to maintain the motorcycle's balance without disrupting its stability. This observation sheds light on why professional riders are able to take their inside leg off the peg during braking for enhanced stability and deceleration.

This study underscores significant differences in how riders with varying levels of experience apply steering torque and manage their body position. Advanced riders make smoother transitions between turns, optimise throttle and brake inputs, and handle the bike with greater efficiency. These findings highlight the value of the developed system as a tool for comparing rider performance, providing objective data that can help identify areas for improvement.

The results challenge traditional assumptions about the role of footpeg input in steering. While it was previously believed that footpeg forces could influence steering, the data allows to suspect that handlebar counter-steering remains the primary input for direction changes. Footpeg forces, although crucial for rider stability, do not directly steer the motorcycle. Instead, they help brace the rider's body during intense manoeuvres like high-speed cornering and braking. This supports the idea that body movements are less about controlling motorcycle roll or direction and more about maintaining rider stability.

Additionally, the system highlighted important distinctions between novice and elite riders. The experienced rider was found to be more efficient in applying steering torque and managing their body positions, especially during turns. Handling techniques, particularly in how riders manage throttle and braking inputs,

significantly impact performance and efficiency, as revealed through rider comparisons.

Despite some technical challenges, such as interference with strain gauge data, the platform's overall success demonstrates its potential for future rider analysis and training. It offers a promising tool that, with further refinement, can deliver precise feedback to riders, helping them enhance their techniques based on objective data.

Looking ahead, future work should aim to enhance the system's data logging capabilities, and test the platform with a broader range of riders, including professionals. Combining this data with simulation models could provide both riders and engineers with powerful insights to predict motorcycle behaviour under different conditions, enhancing performance optimization.

In conclusion, this project establishes a solid foundation for continued research into motorcycle dynamics and rider input. By capturing the intricate relationship between rider movements and motorcycle behaviour, this system offers valuable potential to improve rider performance, safety, and understanding of high-performance riding techniques.

2D Debus & Diebold Mebsysteme GMBH. 2014. *BC-SG4-0000 DataSheet*.
2D Debus & Diebold Meßsysteme GmbH. 2024. 2D Stick Logger V3 DataSheet.
Aoki, A. 1980. Experimental Study on Motorcycle Steering Performance. *SAE International*, p. 16.
Aprilia. 2024. *Aprilia RS660 Workshop Manual*.
Bartolozzi, M., Boubezoul, A., Bouaziz, S., Savino, G. and Espié, S. 2023a. Understanding the behaviour of motorcycle riders: An objective investigation of riding style and capability. *Transportation Research Interdisciplinary Perspectives* 22. doi: 10.1016/j.trip.2023.100971.
Bartolozzi, M., Savino, G. and Pierini, M. 2023b. Motorcycle steering torque estimation using a simplified front assembly model: experimental validation and manoeuvrability implications. *Vehicle System Dynamics* 62(3), pp. 759–784. doi: 10.1080/00423114.2023.2194542.
Baz, L. 2021. Feet position, Body Position, When to Downshift, and more - Youtube.
Biral, F., Bortoluzzi, D., Cossalter, V. and Da Lio, M. 2003. Experimental Study of Motorcycle Transfer Functions for Evaluating Handling. *Vehicle System Dynamics* 39, pp. 1–25.
BMW Motorrad. 2022. BMW M Race Calibration 2022 Software.
Bom, P. 2024. MotoGP - Everything's Connected.
Bradley, A. 2014. Pressuring the pegs - Riding skills series.
Chuckpaiwong, B. and Harnroongroj, T. 2009. Palmar Pressure Distribution during Push-Up Exercise. *Singapore Medical Journal*.
Cohen, J.L. 2001. Unravelling the Mysteries of ArmPump.
Cossalter, V. 2006. *Motorcycle Dynamics Second Edition*. 2nd ed. Padova.
Cossalter, V., Doria, A. and Lot, R. 1999. Steady Turning of Two-Wheeled Vehicles. *Vehicle System Dynamics* 31, pp. 157–181.
Cossalter, V., Doria, A., Lot, R. and Massaro, M. 2011a. The Effect of Rider's Passive Steering Impedance on Motorcycle Stability: Identification and Analysis. *Meccanica* 46, pp. 279–292.
Cossalter, V. and Lot, R. 2002. Multibody System Dynamics Simulations Based on the Natural Coordinates Approach. *Vehicle System Dynamics* 37, pp. 423–447.
Cossalter, V., Lot, R. and Maggio, F. 2003. A Multibody Code for Motorcycle Handling and Stability Analysis with Validation and Examples of Application. *SAE 2003-32-0035 JSAE 20034335*.
Cossalter, V., Lot, R. and Maggio, F. 2004. The Modal Analysis of a Motorcycle in Straight Running and on a Curve. *Meccanica* 39, p. 16.
Cossalter, V., Lot, R. and Massaro, M. 2011b. An Advanced Multibody Model for the Analysis of Motorcycle Dynamics. *Meccanica* 46, pp. 943–958.
Cossalter, V., Lot, R. and Peretto, M. 2007. Steady Turning of Motorcycles. *Proceedings of the Institution of Mechanical Engineers Part D Journal of Automobile Engineering* 221, pp. 1343–1356.
Cossalter, V., Lot, R. and Tavermini, D. 2013. Optimization of the Centre of Mass Position of a Racing Motorcycle in Dry and Wet Track by Means of the "Optimal Maneuver Method". *IEEE International Conference on Mechatronics .*
Cossalter, V., Massaro, M. and Peretto, M. 2008. Application of the "Optimal Maneuver Method" for Enhancing Racing Motorcycle Performance. *SAE International Journal of Passenger Cars - Mechanical Systems,* p. 9.
Costa L. 2017. *Modelling of the Powered Two-Wheelers dynamic behavior for accident reconstruction and incident detection.* Marseille.
Daemen, W. 2024. Statement World Endurance Team Boss.

Evertse. 2010. *Rider Analysis Using a fully instrumented motorcycle*.
Foale, T. 2002. *Motorcycle Handling and Chassis Design - The Art and Science.* Tony Foale Designs.
Fu, H. 1966. Fundamental Characteristics of Single-Track Vehicles in Steady Turning. *Bulletin of JSME* 9, pp. 284–293.
Giles, C.G. 1985. Motorcycle Steering Behaviour.
Guintoli, S. 2023. *Feet Position Tutorial/ Coaching*.
Harrison, A. 2023. Statement Rider Interviews.
Herrin, J. 2019. *Pro Racer Explains Proper Foot Positioning! Youtube*.
Hirono, T., Kunugi, S., Yoshimura, A. and Holobar, A. 2022. Acute changes in motor unit discharge property after concentric versus eccentric contraction exercise in knee extensor. *Journal of ElectroMyography and Kinesiolis*.
Hou, Z.C., Lu, Y. ning, Lao, Y. xin and Liu, D. 2009. A new trifilar pendulum approach to identify all inertia parameters of a rigid body or assembly. *Mechanism and Machine Theory* 44(6), pp. 1270–1280. doi: 10.1016/j.mechmachtheory.2008.07.004.
Iatrakis, I. 2024. VI-Grade RS660 Model Development.
Koenen, C. 1983. The Dynamics Behaviour of a Motorcycle when running straight ahead and when cornering. *Delft University Press*.
Kooijman, J.D.G. and Schwab, A.L. 2011. *A REVIEW ON HANDLING ASPECTS IN BICYCLE AND MOTORCYCLE CONTROL*.
Kuroiwa, O., Baba, M. and Nakata, N. 1995. *Study of Motorcycle Handling Characteristics and Rider Feeling During Lane Change.* Detroit, USA.
Life at Lean. 2024. Weighting the Pegs and Body Steering on a Motorcycle.
Limebeer, D.J.N. and Sharp, R.S. 2006. Bicycles, Motorcycles, and Models. IEEE Control Systems Magazine. pp. 34–61.
Limebeer, D.J.N., Sharp, R.S. and Evangelou, S. 2001. The stability of motorcycles under acceleration and braking. *Proceedings of the Institution of Mechanical Engineers, Part C: Journal of Mechanical Engineering Science* 215(9), pp. 1095–1110. doi: 10.1243/0954406011524450.
Loctite. 2014. Loctite SG401 Technical Data Sheet.
Marina, M. and Porta, J. 2011. Monitoring hand Flexor Fatigue in a 24-h motorcycle endurance race. *Journal of ElectroMyography and Kinesiology* 21(2).
Marina, M., Torrado, P. and Bescos, R. 2021. Recovery and Fatigure behavior of Forearm Muscles during a Repetitive Power Grip Gesture in Racing Motorcycle Riders. *Environmental Research and Public Health*.
Massaro, M., Cossalter, V. and Cusimano, G. 2013. The Effect of Inflation Pressure on the Tyre Properties and the Motorcycle Stability. *Proceedings of the Institution of Mechanical Engineers Part D Journal of Automobile Engineering.*, p. 15.
Massaro, M., Cossalter, V. and Lot, R. 2012. A Virtual Motorcycle Driver to Simulate Real Manoeuvres from Experimental Data. *Proceedings of the Institution of Mechanical Engineers Part D Journal of Automobile Engineering.*, p. 19.
Massaro, M. and Lot, R. 2007. Application of Laplace Transform Techniques to Non-Linear Control Optimization. *Multibody Dynamics*.
Moss, D. 2019. *Motorcycle Cornering: Brake then Gas then Turn - Youtube*.
MotoSpec. 2024. MotoSpec Chassis Software.
MRP Racing. 2024. MRP Racing IDM Team Handlebar Grips.
National Instruments. 2016. *Measuring Strain with Strain Gauges*.
NCTE. 2024. NCTE Internal Torque Sensors.
Ooms, W. 2011. *Motorcycle Modeling and Control*. Eindhoven, The Netherlands.

Parks, L. 2015. *Total Control - High Performance Street Riding Techniques*. Beverly, USA: Quarto Publishing Group USA Inc.
PicoAuto. 2023. *CAN Bus physical layer*.
Przibylla, A. 2018. Ducati Panigale 1199 S Dynamic Vehicle Response Measurement Platform.
Przibylla, A. 2020. *Practical and Analytical Investigation into Motorcycle Steering Dynamics and Rider Control*.
RedBull. 2016. *Marc Marquez HRC MotoGP Bike Close Up - https://www.redbull.com/int-en/motogp-motorcycle-close-up-photo-gallery*.
Rice, R.S. 1979. Rider Skill Influence on Motorcycle Manoevring. *SAE International*, p. 12.
Rice, R.S. and Kunkel, D.T. 1976. *Accident Avoidance Capabilities of Motorcycles - Lane Change Maneuver Simulation and Full-Scale Tests.* Buffalo, New York, USA.
Rowell, S. 2007. Modelling the Control Strategies for Riding a Motorcycle.
Schwab, A.L. and Meijaard, J.P. 2013. A review on bicycle dynamics and rider control. *Vehicle System Dynamics* 51(7), pp. 1059–1090. doi: 10.1080/00423114.2013.793365.
Sharp, R.S. 1971. The Stability and Control of Motorcycles. *Journal Mechanical Engineering Science* 13(5), pp. 316–329.
Sharp, R.S. 1978. A Review of Motorcycle Steering Behavior and Straight Line Stability Characteristics. *SAE Congress and Exposition*.
Sharp, R.S. 1985. The Lateral Dynamics of Motorcycles and Bicycles. . *Vehicle system Dynamics*, pp. 265–283.
Sharp, R.S. 1994. Vibrational Modes of Motorcycles and their Design Parameter Sensitivities. *Vehicle NVH and Refinement, Mechanical Engineering Publications,* pp. 107–121.
Sharp, R.S. 2001. Stability, Control and Steering Responses of Motorcycles. *Vehicle System Dynamics*, pp. 291–358.
Sharp, R.S. 2010. Rider Control of a Motorcycle near to its Cornering Limits. *Bicycle and Motorcycle Dynamics*.
Sharp, R.S., Evangelou, S. and Limebeer, D.J.N. 2004. Advances in the Modeling of Motorcycle Dynamics. *Multibody System Dynamics* 12, pp. 251–283.
Sharp, R.S. and Limebeer, D.J.N. 2001. A Motorcycle Model for Stability and Control Analysis. *Multibody System Dynamics* 6, pp. 123–142.
Slane, J., Timmerman, M., Ploeg, H. and Thelen, D. 2011. The influence of glove and hand position on pressure over the ulnar nerve during cycling. *Clin Biomech*.
Spalding, N. 2010. *MotoGP Technology*. 2nd ed. Haynes.
Styles, M.J. 2004. Predictive Engineering Processes for Motorcycle Dynamics.
Sugizaki, M. and Hasegawa, A. 1988. Experimental Analysis of Transient Response in Motorcycle-Rider Systems. *SAE Technical Paper Series 881783*.
Taguchi, M. 1975. Preliminary Test Report on the Controllability and Stability of the Experimental Safety Motorcycle. *Proceedings of the Second International Motorcycle Safety Conference.*
Torrado, P., Marina, M., Baudry, S. and Rios, M. 2021. Muscle Fatigue When Riding a Motorcycle: A Case Study. *Environmental Research and Public Health*.
Ueda, J. 2004. Equations of Motion to Describe Motorcycle Handling Torque Characteristic in Time of Steady-State Cornering Motion at a Large Bank Angle. *SAE 2004-32-0017 JSAE 20044304*, p. 11.
Vishay Measurements Group. 2011. *Surface Preparation for Strain Gage Bonding Instruction Bulletin B-129-8 Surface Preparation for Strain Gage Bonding*. Available at: www.micro-measurements.com.

Wahl, A., Kaut, F., Dikmenli, E., Klews, M. and Bosch GmbH, R. 2020. *Steering Torque Measurement on Motorcycles*.
Weir, D.H. and Zellner, J.W. 1978. Development of Handling Test Procedures for Motorcycles. *SAE Congress and Exposition*.
Weir, D.H. and Zellner, J.W. 1980. Experimental Investigation of the Transient Behavior of Motorcycles. *SAE 790266*, pp. 962–978.
Weir, D.H., Zellner, J.W. and Teper, G.L. 1979. Motorcycle Handling Volume II: Technical Report,. *System Technology, Inc.*, p. 25.
Williams, O. 2023. Gyroscopes - Mathematical Analysis.

9 Appendix

9.1 strain Gauge Setup Research

The chosen method for measuring the input force on the handlebars and footpegs is through Strain gauges installed directly on the handlebars and the footpegs. Different methods have been explored for torque or force measurement. Torque sensors for hollow shafts are available, these sensors are used in World Superbike, MotoGP, by manufacturers to measure the torque generated directly on the output shaft. The Torque sensor rotates with the output shaft and measures the amount of twist in the axle between certain points which can then be related to a torque (NCTE 2024). A torque sensor like this could theoretically be fitted within the steering stem if measurement accuracy is small enough. This would allow for measurement of the total steering torque, though not force input on each handlebar individually and in different axis, (Costa L 2017) have applied such method (Figure 68).

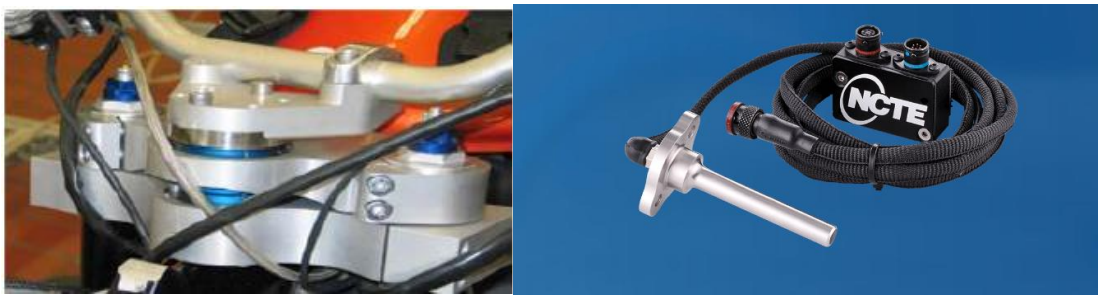

Figure 68: Steering Torque Measurement. (Wahl et al. 2020) (Left) – NCTE Internal Torque Measurement Sensor. (NCTE 2023) (Right)

(Wahl et al. 2020) have used force measuring bolts integrated in connection blocks between the top clamp and handlebar mount. The measuring bolt allows for uniaxial force measurement.

Figure 69: Force Measuring Bolts employed for Steering Torque Measurement (Wahl Et Al. 2020)

(Evertse 2010) has used two Bi-Axial Load Arms between the top triple clamp and handlebar mounts. In a similar fashion as Wahl et al. The Bi-Axial Arms are placed to measure force in the steering stem axis and axis perpendicular to that, which is then related to a steering torque through calculations.

(Biral et al. 2003) have applied a special method where they've constructed a cantilever beam connected to the triple clamp and a static part on the motorcycle, fitted with strain gauges to then relate to steering torque.

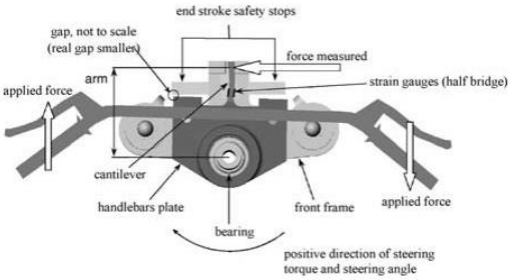

Figure 70: Cantilever Beam employed for Steering Force input measurement. (Biral et al. 2003)

The issue with the previously mentioned methods, in contrast to the current application, lies in the type of motorcycle used. Adventure/touring motorcycles generally have a steering assembly that, due to its bolting method to the top clamp Figure 69, allows more room for modifications and the installation of additional components. However, the sportsbike used in the current research employs a clip-on method which provides little to no space for applying these methods.

(Przibylla 2018; Bartolozzi et al. 2023b; Bartolozzi et al. 2023a) Have used strain gauges fitted on the handlebars, measuring two axis, 90° from each other, which measure strain generated by the bending moment. Steering torque is then calculated from the measurements.

Strain gauges are the most versatile and most used strain / force measurement method. Most Force sensing methods/ sensors are based on strain gauges (Vishay Measurements Group 2011).

The force input measurement method chosen in the current application is strain gauges applied to the handlebar tubes to measure direct strain. Due to the relatively small space requirement and low cost compared to previously mentioned methods.

(Evertse 2010) installed a load button on each footrest to measure the vertical load. (Bartolozzi et al. 2023a) used strain gauges on the footpegs to measure the vertical force and calculate the rolling torque. A force measurement bolt, as previously mentioned, would enable multi-axis measurement on the footpegs, which are bolted to the rearsets. However, considering space constraints and cost, strain gauges were chosen as the force measurement method. Four strain gauges were placed on each footpeg, positioned 90° apart, allowing for force input measurement in both the Y and X axes.

The electrical circuit in which the strain gauges are used, is based on a Wheatstone bridge, which allows the measurement of small changes in resistance (National Instruments 2016). A Wheatstone bridge is the electrical equivalent of two voltage divider circuits that are in parallel, with four resistive arms and an exciting voltage that is applied across the bridge, where the output voltage is measured between the middle nodes of the two voltage dividers. The configuration used is a half-bridge, in which the circuit has two active elements, a pair of strain gauges opposite each other, and two static resistors, as shown in figure.

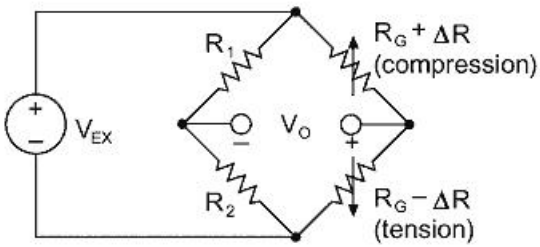

Figure 71: Graphical Representation of a Wheatstone Bridge. (National Instruments, 2016)

9.2 VI-Grade Model Setup

Following shows the setup of the Aprilia RS660's VI-Motorbike Model as setup and used in the simulations mentioned in the current work.

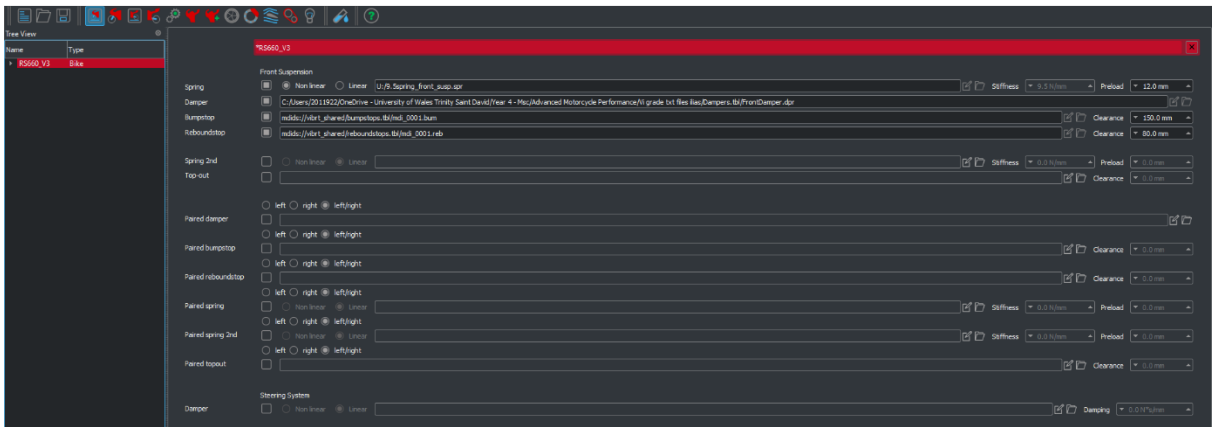

Figure 72: VI-Grade RS660 Front Suspension Setup Settings.

Figure 73: VI-Grade RS660 Front Suspension Physical Settings.

Figure 74: VI-Grade RS660 Rear Suspension Setup Settings.

Figure 75: VI-Grade RS660 Rear Suspension Physical Settings.

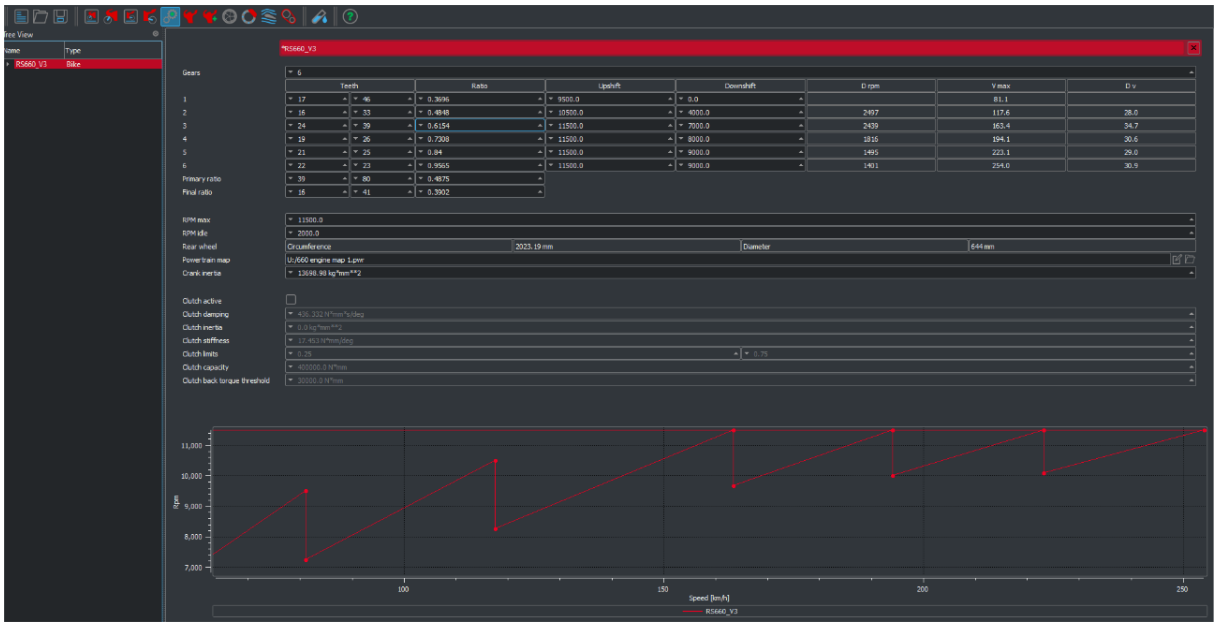

Figure 76: VI-Grade RS660 Powertrain Settings.

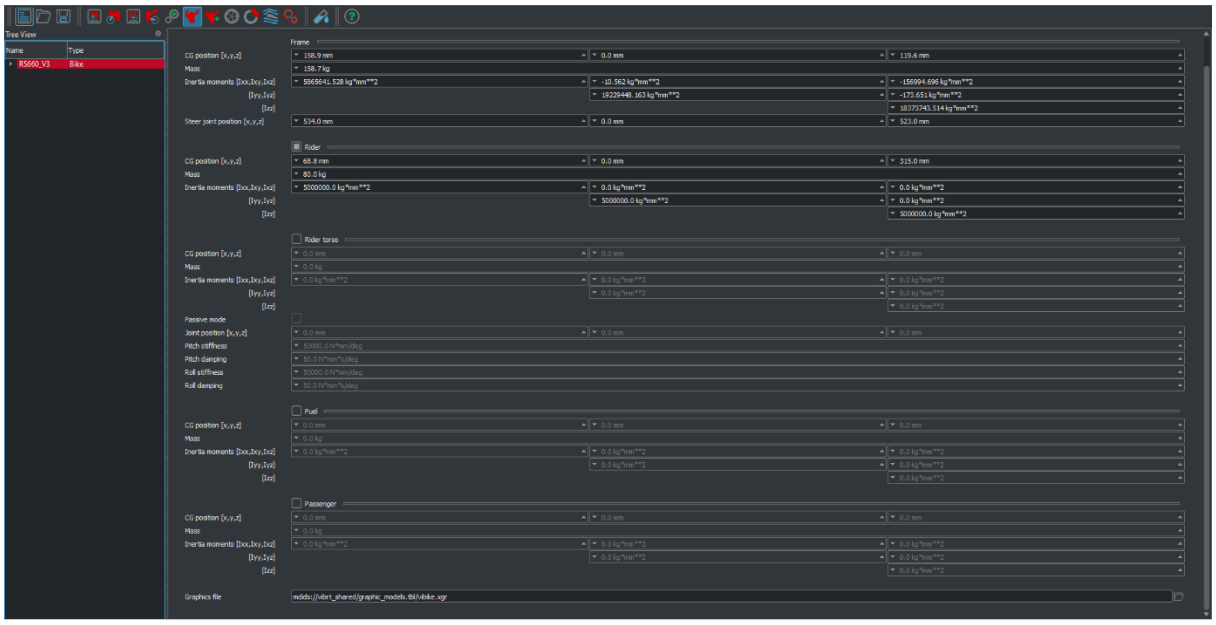

Figure 77: VI-Grade RS660 Frame Settings.

Figure 78: VI-Grade RS660 Wheels Settings.

As setting up the Spin Inertias in VI-BikeRealTime was not possible, altering the Spin Inertias in the .XBK Text File was required (Figure 79) in Line 18, the front wheel settings can be changed, Line 52 is used to alter the rear wheel settings.

Figure 79: VI-Grade RS660 Altering XBK Files for Spin Inertias.

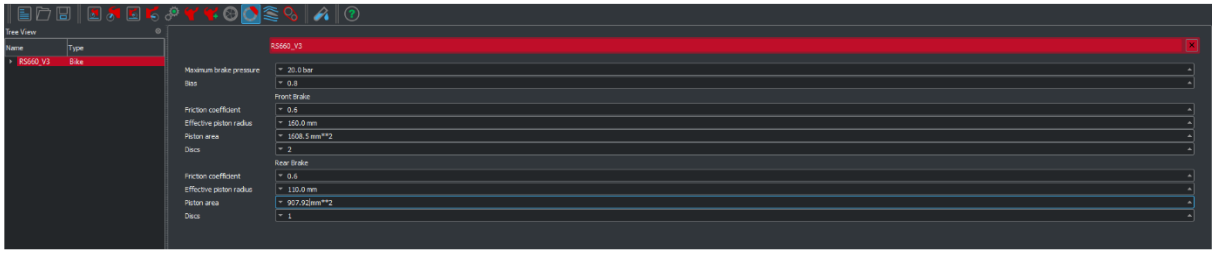

Figure 80: VI-Grade RS660 Brake Settings.

Figure 81: VI-Grade RS660 Aerodynamic Settings.

Figure 82: VI-Grade RS660 Chain Settings.

9.3 Problems and Failures

System building:

As the author had no experience in strain measurement and working with strain gauges, the fragility of the strain gauges and their wires posed issues during the building of the system with soldering, strain gauges braking breaking and posed a steep learning curve into insuring accuracy of the final constructed system. As previously mentioned, a strain gauge was short to complete both footpegs with the same strain gauge type, the previous could not be ordered anymore and a different type had to be used, due to the nature of the measurements and force calculations through the force input constants, this posed no issue in the final results.

Strain Gauge Amplifiers CAN Interference:

During the initial shakedown test of the measurement platform, where the motorcycle was ridden with the data system and only the handlebar strain gauges installed, the system appeared to function correctly and as expected. Following this successful test, the footpeg strain measurement system was installed. Initially, both strain gauge amplifier modules were connected to one of the two CAN IN lines on the logger via a shared CAN-Hub, while the other CAN IN line was used for the motorcycle's CAN connection, as the motorcycle was recording at a different baud rate. Calibration and bench testing, including loading scenarios, indicated that the complete system was performing as expected, with digit readings behaving as anticipated.

However, during a three-day race event at Cadwell Park—ideal for analysing riding data under various conditions—the strain measurements from all input channels were skewed and appeared to be affected by some form of interference. The cause of this issue was not immediately identified, and initial attempts to filter the channels to resolve the problem were unsuccessful.

Extensive bench testing was then conducted at the university workshop, using a Picoscope to test supply voltages, analyse the behaviour of different system components, and check connections. It was ultimately discovered that electronic interference occurred when both amplifier modules were connected to the same CAN IN line on the logger. Despite the 2D system being CAN-based and capable of recognizing both strain gauge modules as separate units, and advertised as being able to handle 'unlimited' offline CAN streams, this configuration led to the interference.

The issue was resolved by connecting a second CAN Hub to the same CAN IN line used for the motorcycle's connection and then connecting one strain gauge module to this separate hub, thereby placing the strain gauge amplifier modules on two separate CAN IN lines at the logger.

Significant effort was made to filter the recorded channels in an attempt to remove the interference. Various filtering techniques were employed, including offsetting channel jumps and sign switches, using FFT analysis, Matlab and a wide range of filters were tested. Although the channels were eventually filtered to reveal what

seemed like load variations. After the previously mentioned force input calculations, the results were not sensible, particularly when compared to later recorded data. Consequently, the force input data from the handlebars and footpegs, along with its interference from other channels, was deemed unsuitable for analysis. However, this experience provided valuable learning opportunities in data filtering, processing, and interference detection using an oscilloscope, contributing to the overall knowledge surrounding this subject.

Figure 83 shows a zoomed screenshot of raw strain gauge channels with the interference present.

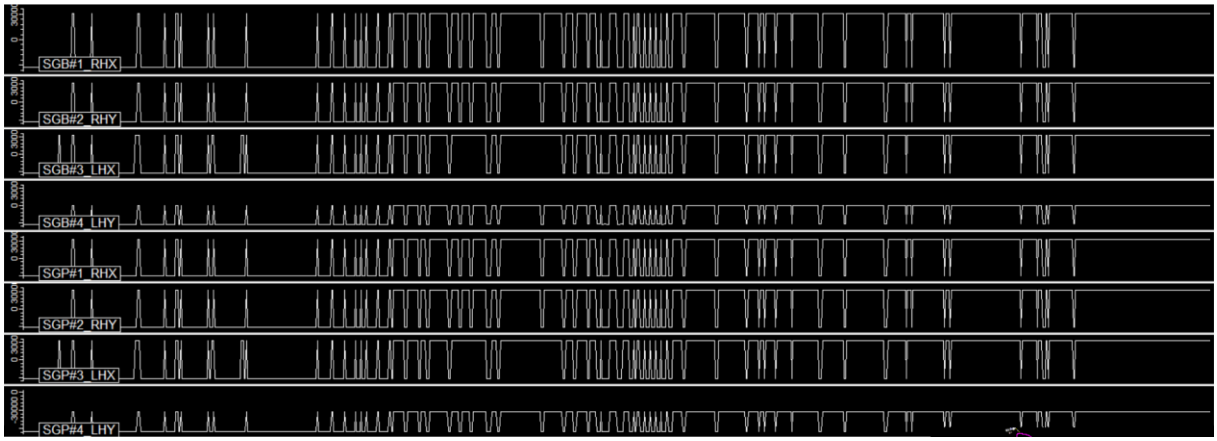

Figure 83: Raw recorded strain gauge channels with interference.

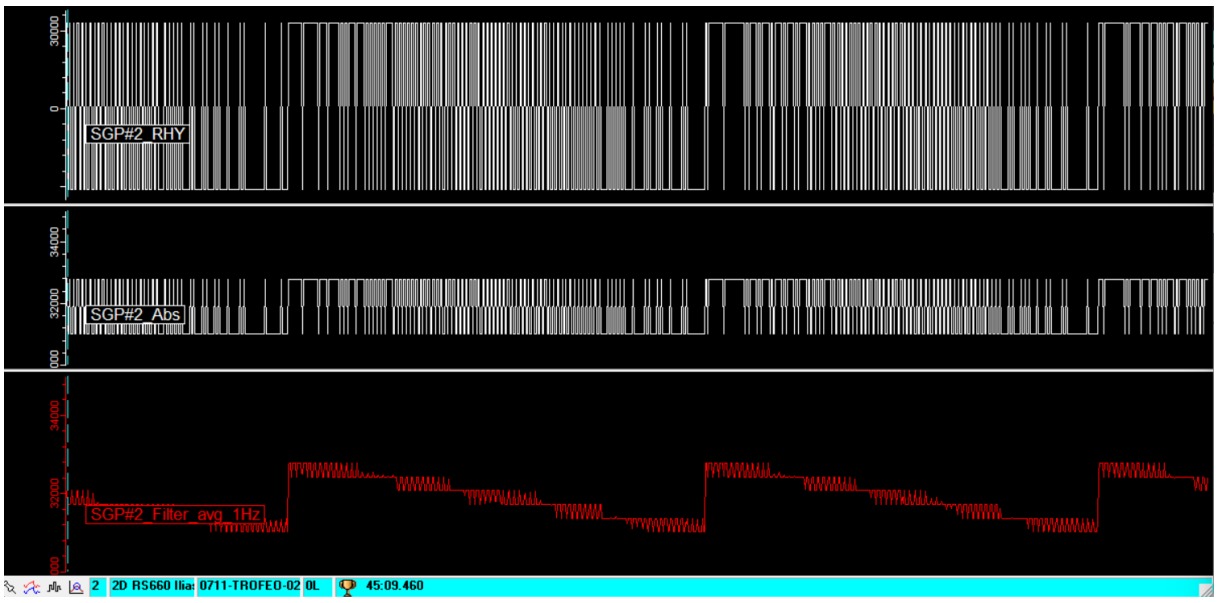

Figure 84: Filtered channel, showcasing gradual drift over period of time during unloaded conditions.

A bench test was conducted in the workshop, during which strain gauge signals were recorded for 45 minutes to check for irregularities. During this test, no load was applied to the handlebars or footpegs, and the motorcycle was neither touched nor moved. It was expected that the signal and strain values would remain constant or nearly so. However, as shown in Figure 84, this was not the case; the signal exhibited drifting, oscillating, and occasional resetting.

An investigation was carried out using a Picoscope to trace the voltage source from the motorcycle to the 5V feed for the strain gauges. Although some small voltage peaks were observed when comparing the motorcycle's power supply to a bench power supply, no significant influence was found. It is suspected that, due to the connection of two identical 2D strain gauge modules, the internal hardware or software may have difficulty keeping the two similar signal streams separate, potentially leading to recorded interference (PicoAuto 2023)

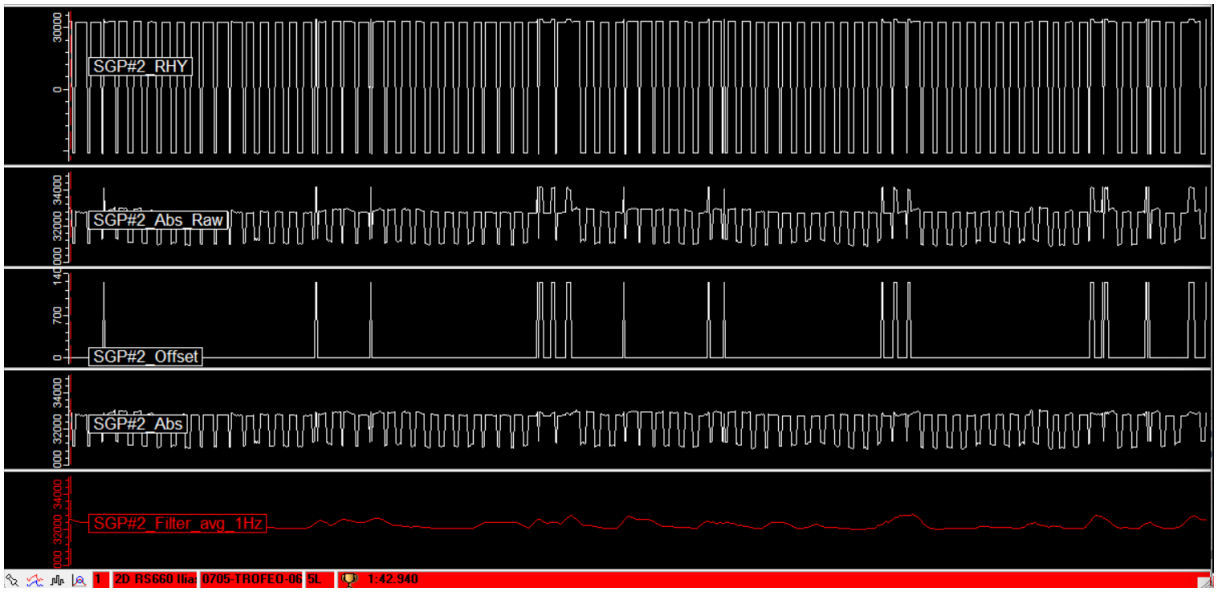

Figure 85: From Raw Channel to Filtered Channel.

Figure 85 shows a comparison between the raw channel data, the absolute value with a calculated offset to reduce peak occurrences, and the best filter identified for the specific channel. Although the filtered channel may appear reasonable at first glance, no meaningful data was ultimately retrieved. The channel still exhibited the gradual drift and resetting previously mentioned. As a result, while the data may seem acceptable at specific moments, the consistent variation means that a certain digit change at one point during the recording does not correspond to the same value at a different point thus cannot be used for force calculation or to indicate true loading conditions.

Steering angle sensor reading

During the initial calibration of the rotary angle sensor used to measure steering angle, the manufacturer's specifications were followed to correlate the variation in voltage with changes in the measured angle. Bench testing indicated that the calibration was correct; however, subsequent analysis revealed an issue. While the shape of the recorded data signal matched expectations, the change in angle values around the 0° point was smaller than anticipated. For instance, where a 2-3 degree steering angle is expected mid-corner (Cossalter 2006; Przibylla 2020), the sensor recorded only a 0.5° change.

It was ensured that the sensor's 'dead spot' was not within the motorcycle's physical 60° steering angle range. However, upon closer investigation (Figure 86) it was found that the sensor displayed a smaller angle change than was actually occurring, resulting in only a 10-degree difference at full range. This discrepancy is particularly significant for analysis at small angle changes, such as those occurring in the middle of a corner. To address this, calculation files were used to recalibrate and correct the real angle values from the measured data after testing. The sensor’s calibration was rectified for future testing.

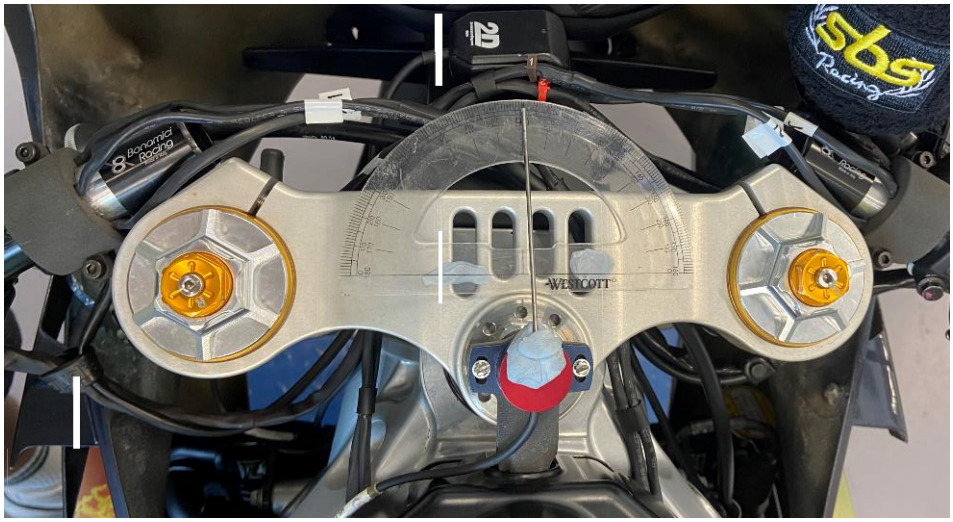

Figure 86: Protractor used with Pointer for Steering Angle Sensor Validation.

Testing Limitations

Although valuable testing and data were collected, particularly with regard to track riding, the author intended to conduct more controlled tests—such as figure-of-eight manoeuvres, controlled lane changes, and controlled radius corners—to further analyse different riding styles and rider inputs in a more controlled environment. These controlled tests would provide deeper insights into how rider inputs influence motorcycle response.

While the data gathered from the two riders involved in the current testing provided proof of concept for rider analysis, the plan was to include a rider with lap times closer to the author’s on the same day at Donnington for comparison.

Unfortunately, due to rain during that session and insufficient time to switch to wet wheels before the last session of the day, this testing could not take place. The wet conditions would have prevented the riders from pushing to achieve comparable lap times.

Analog input channel limitations

As previously mentioned, a limitation in the current work was the insufficient number of analog input channels available on the data logger, which prevented the recording of seat pressure on both sides along the Suspension travel potentiometers and steering angle sensor. For future work, a different data logger with CAN capability and a greater number of analog input channels will be required.

General Time, Cost Limitations

As is often the case in projects requiring testing and physical components, constraints related to budget and time presented certain limitations (sources). With unlimited funding, additional data loggers could have been acquired, enabling more comprehensive data collection. Similarly, with more time, further refinements could have been made, such as integrating tank pads and conducting additional test days with a broader range of riders.

However, considering the timespan and scope of this project, the work accomplished provides a solid foundation. Despite the challenges encountered, the results offer a functional basis for future research and development. This foundation allows for the expansion and improvement of areas that could not be fully explored in this initial phase.

31
aprilia
aprilia
UWTSD
MOTORSPORT
brembo
BERIK
Racing Team
CadwellPark